DEPARTMENT OF THE INTERIOR

U.S. GEOLOGICAL SURVEY

SURFACE FRACTURE NETWORK AT PAVEMENT P2001, FRAN RIDGE, NEAR YUCCA MOUNTAIN, NYE COUNTY, NEVADA

Administrative Report

for WM-11

Darlene Hoge

Prepared in cooperation with the
NEVADA OPERATIONS OFFICE,
U.S. DEPARTMENT OF ENERGY, under
Interagency Agreement DE-AI08-92NV10874

Draft

NM5502

DEPARTMENT OF THE INTERIOR

U.S. GEOLOGICAL SURVEY

SURFACE FRACTURE NETWORK AT PAVEMENT P2001, FRAN RIDGE, NEAR YUCCA MOUNTAIN, NYE COUNTY, NEVADA

by D.S. Sweetkind, E.R. Verbeek, F.R. Singer, F.M. Byers, Jr, and L.G. Martin

---

Administrative Report

Prepared in cooperation with the
NEVADA OPERATIONS OFFICE,
U.S. DEPARTMENT OF ENERGY, under
Interagency Agreement DE-AI08-92NV10874

Denver, Colorado

1995

U.S. DEPARTMENT OF THE INTERIOR
BRUCE BABBITT, SECRETARY

U.S. GEOLOGICAL SURVEY

GORDON P. EATON, Director

ADMINISTRATIVE REPORT

CONTENTS

PLATE

(in pocket)

1. Fracture trace map, Pavement P2001, Fran Ridge, Yucca Mountain, Nevada

FIGURES

TABLES

CONVERSION FACTORS AND ACRONYMS

Multiply	by	To obtain
micron (μ)	0.00003937	inch
millimeter (mm)	0.03937	inch
centimeter (cm)	0.3937	inch
meter (m)	3.281	foot
kilometer (km)	0.6214	mile

The following terms and abbreviations also are used in this report.

Ma	millions of years old
m.y.	millions of years ago

SURFACE FRACTURE NETWORK AT FRAN RIDGE, P2001, NEAR YUCCA MOUNTAIN, NYE COUNTY, NEVADA

by D.S. Sweetkind, E.R. Verbeek, F.R. Singer, F.M. Byers, Jr., and L.G. Martin

ABSTRACT

Detailed geologic mapping of the fracture network exposed at Pavement P2001 at Fran Ridge yields important constraints on the tectonic history and hydrologic parameters of the site of the proposed high-level nuclear waste repository at Yucca Mountain, Nevada. Pavement P2001 exposes the fracture network within the middle nonlithophysal and upper lithophysal zones of the Topopah Spring Tuff, immediately above the potential repository horizon. An early network of cooling joints, best developed in the middle nonlithophysal zone, consists of three mutually orthogonal joint sets: two subvertical sets trending northwest and northeast and one subhorizontal set. Three subsequent sets of tectonic fractures are all steeply dipping; the earliest tectonic fractures are oriented north-south, followed by northwest-trending and finally northeast-trending sets. At least some of the north-trending fractures have down-to-the-west normal displacement, and some of the northwest-trending fractures have right lateral displacement.

The sequential formation of fracture sets, documented through mapped termination relationships, inferred fracture origin (cooling or tectonic joint), and fracture reactivation and offset relationships, indicates that tectonic fractures formed as the

products of noncoaxial regional extension where extension directions changed from roughly E-W, to NE-SW and finally rotated to NW-SE. Many fractures experienced renewed growth or reactivation as faults during the formation of subsequent joint sets.

Fractures in the middle nonlithophysal zone of the Topopah Spring Tuff are large, continuous and form well-connected fracture networks similar to those exposed in pavements cleared previously in the Tiva Canyon Tuff. Fractures in the upper lithophysal zone of the Topopah are shorter, have a greater proportion of blind terminations and do not appear to form as well-connected a fracture network. The intensity of fracturing at P2001 is about half that seen at P1000 at the southern tip of Fran Ridge. The proximity of P1000 to major structures is probably responsible for the increase in fracture intensity. Brecciated fracture fill consists of predominantly Topopah Spring wallrock fragments cemented by calcite and silica.

INTRODUCTION

Study of the fracture network developed within the Topopah Spring Tuff provides important information regarding possible hydraulic and pneumatic pathways into and out of the potential repository at Yucca Mountain. The connectivity of the fracture network and overall fracture-related permeability are important components to be used in assessing the suitability and performance of a potential high-level nuclear waste repository at Yucca Mountain, Nevada. Connectivity of the fracture network is governed by fracture size and orientation distributions, fracture density, and the fracture system geometry, particularly the distribution of intersection types, all of which can be measured or described through detailed field observations. In addition to the hydraulic parameters,

the sequential development of the fracture network and possible subsequent reactivation of fractures serve as a sensitive indicator of the past stress history of the mountain. The determination of paleostress directions feeds the overall structural synthesis of the site area and can provide links between the genesis of the fracture network and major structural features. The spatial distribution of fractured blocks within the repository horizon is also important for understanding the overall structural integrity of the site from a mechanical and engineering standpoint.

Pavement P2001, located on the eastern flank of Fran Ridge, east of Yucca Mountain (fig. 1), exposes portions of the Miocene Topopah Spring Tuff immediately above the potential repository horizon and the fracture network developed there. The P2001 pavement is the largest of only two cleared exposures of the potential repository horizon available for detailed study and one of the largest exposures of any kind of this horizon within the site area. The fracture network at P2001 is exceptionally well exposed because in addition to the cleared pavement there are two vertical pits that penetrate the pavement, an adjacent box-cut, and a horizontal borehole that extends directly under the pavement. These various exposures provide three dimensional fracture network data that are free from sampling bias and also provide vertical control on the depth of fracture fillings and the vertical extent and importance of breccia bodies. In comparison with the only other cleared exposure of Topopah Spring Tuff, P1000 at the southern tip of Fran Ridge (see location map, pl. 1), pavement P2001 is located relatively far from major structures - this provides an important comparison of two possible structural situations that may be encountered at the repository horizon.

FIGURE 1. NEAR HERE

In addition to the geometric aspects of the fracture network, we have completed petrographic study of several samples of brecciated fracture fill material from pavement P2001. The study of fracture fillings in thin section includes a description of breccia clasts, fracture fill cementing materials, and alteration mineralogy. We have attempted to understand the origin of certain enigmatic brecciated fracture fillings at the pavement; whether the breccias are fault related, pedogenic in origin or formed by some other process. Petrographic study of fracture-filling materials also provides information regarding the reactivation of fractures and relative-age criteria for different fracture sets. Fracture fill paragenesis can provide evidence for fluid-flow history, flow pathways, fracture connectivity, and constrain the possible sources of the fluids.

HISTORY OF WORK AT FRAN RIDGE

The following background information and history of work at Fran Ridge is included to document the level of study in the area surrounding pavement P2001 and the amount of control on the fracture network at this site.

In late 1982 and early 1983, the horizontal drill hole UE 25-h#1 (collar location shown on pl. 1) was constructed under what is now the P2001 pavement (Norris and others, 1986). This borehole was drilled as part of a radionuclide transportation test in support of Exploratory Shaft testing in the Topopah Spring Tuff. Many problems were

Fig. 1. Location map, Fran Ridge, near Yucca Mountain, Nevada.

encountered during drilling, including collapse of uncased, fractured rock into the horizontal hole. Core recovery was moderate to poor over the first half of the hole (total drilling depth of 400 feet), but improved to greater than 80% in the interval between 209 to 388 ft with a change in drilling fluid. All core from this hole was unoriented, but improved core recovery for the lower portion of the hole did allow the calculation of fracture frequency in this interval.

A cleared pavement on the southern tip of Fran Ridge (P1000, approximately 1 kilometer south of P2001) was constructed in August, 1985 and mapped in late 1985 and early 1986 by Rick Page under the supervision of Chris Barton (both of the U.S. Geological Survey, Geologic Division). This pavement was constructed in the same rock unit that is exposed at P2001. A map of the pavement was included in a field trip guidebook by Barton and Hseih (1989), however data from P1000 have not been published to date.

In the late 1980's, two vertical pits were constructed at what is now the P2001 pavement; Pit 1 is located at the north end of P2001 and Pit 2 at the south end (pl. 1). These pits were constructed as test areas for mapping and drilling technologies to be developed for the Exploratory Shaft when it was planned as a vertical shaft. Soon after construction of the pits, the design of the Exploratory Studies Facility was changed to an adit and subhorizontal drift and no testing or mapping was ever conducted at the pits. Fractures within the pits and in the cleared areas immediately surrounding the pits were investigated in 1990-1991 (Throckmorton and Verbeek, 1995). Synoptic data from these pits were obtained including the general orientations and interrelationships for the various

fracture sets, but no map was created. The P2001 pavement was subsequently cleared of surficial debris between August and November of 1992, as an extension of the mapping and testing activities within the two test pits.

The most recent exposure in the vicinity of was created during the construction of the box cut surrounding Lawrence Livermore Laboratory's Large Block Experiment immediately to the north of the P2001 pavement. Fractures have been mapped on the three-dimensional, but the exposed walls of the box cut have not been mapped or described. During construction of the pit, Sandia National Laboratory conducted a series of infiltration tests that provide an indication of the degree of connectivity and fracture transmissivity that may exist for the pavement P2001 area (Mike Nichols, personal communication, 1995).

LOCATION AND SETTING

Fran Ridge is located east of the central block of Yucca Mountain, Nevada (fig. 1). The ridge is bounded to the west by the Fran Ridge fault, a splay off of the main trace of the Paintbrush Canyon fault (Scott and Bonk, 1984; Dickerson and Spengler, 1994). The Fran Ridge pavement is located on the eastern side of Fran Ridge, near the southern end, near the bedrock/alluvium contact. The pavement exposes 1300 square meters (14000 square feet) of Topopah Spring Tuff. The pavement is subhorizontal, with an average surface slope of about 20 degrees to the east.

STRATIGRAPHY

The rock units exposed at pavement P2001 include both the upper lithophysal (Tptul) and middle nonlithophysal zone (Tptmn) of the Topopah Spring Tuff (stratigraphic nomenclature and symbols follow the usage of Buesch and others, 1995) and the transition zone in between. The subdivision between the two units is based on multiple criteria including color, lithophysae content, fracture shape and fracture surface roughness. All of these features tend to change within a transitional zone some 5 to 10 meters in thickness (Byers, 1985; Byers and Moore, 1987; Buesch and others, 1995). The upper portion of the middle nonlithophysal zone is an orange-brown unit with no lithophysae, although abundant gray spots are present. Fractures tend to be planar or arcuate with very low surface roughness. The overall surface roughness is also low. The upper lithophysal zone is brownish-gray with abundant round lithophysae usually five to ten centimeters in diameter. Fractures tend to be planar but extremely rough. Overall surface roughness of natural outcrops is also high in the upper lihophysal zone. In between these two zones is a five- to ten-meter thick transitional zone where lithophysae begin to appear - most of these lithophysae are oblong to flattened. The gray spots that are prevalent within the middle nonlithophysal zone are still present. In addition, several subhorizontal partings appear in this transition zone. At pavement P2001, rocks that are unquestionably within the upper lithophysal zone are exposed at the extreme western edge of the pavement, in the vicinity of Targets 103, 104, 112 and 113 (shown as TGT103, TGT104, TGT112, and TGT13 on pl. 1). Based upon the multiple criteria discussed above, rocks of the middle nonlithophysal zone are exposed at the far northeast

end of the pavement in the vicinity of Pit 1 and in the wallrocks exposed in Pit 1 (pl. 1). The intervening areas are mostly in the transitional zone. The transitional nature of the contact is well exposed within test Pit 2, where no lithophysae are present at the bottom of the pit, but flattened, oblong lithophysae are present near the top. The transition zone forms a broad outcrop pattern across the pavement due to the low dip of the pavement surface. Due to the gradational nature of the contact and the fact that the transitional zone is wide, no line marking the contact has been put on plate 1. A line separating rocks that have properties most like the middle nonlithophysal zone from rocks that have properties most like the upper lithophysal zone could be drawn roughly along the long north-south fracture LMF39 (pl. 1), or roughly along a line drawn through targets TGT102, TGT106, TGT110, TGT115, and TGT120. It is along such a line that the pavement was divided for comparison of fracture properties between the upper lithophysal zone and the middle nonlithophysal zone (fig. 2). Pavement 1000, at the southern end of Fran Ridge (see location map, pl. 1) is constructed entirely within the middle nonlithophysal zone of the Topopah Spring Tuff.

FIGURE 2. NEAR HERE

METHODS AND DEFINITIONS

Fractures at pavement P2001 were mapped according to Technical Procedure USGS-GP-12, R1, "Mapping fractures on pavements, outcrops and along traverses". This procedure generally follows the field techniques outlined by Barton (Barton and Hsieh, 1989; Barton and others, 1993) and by the International Society for Rock

Fig. 2. Geologic map, Fran Ridge, near Yucca Mountain, Nevada. The middle nonlithophysal (Tptmnl) and upper lithophysal (Tptul) zones of the Topopah Spring Tuff are defined using the criteria discussed by Buesch and others (1995). Dashed lines represent the outcrop band of the transitional zone between the middle nonlithophysal zone and upper nonlithophysal zone of the Topopah Spring Tuff. The solid line represents the division used in this report to compare the two zones. The first appearance of lithophysae occur near the southern test pit. A contact based on the first appearance of lithophysae would occur approximately 10 m to the east of the cleared pavement.

Mechanics (ISRM, 1978). Each fracture on the pavement (pl. 1) has a label corresponding to an entry in the fracture data sheets which are tabulated as appendices to this report (appendices 1 and 2). The discussion below describes methods of data collection, the type of observations recorded, and the criteria that were used for distinguishing specific features.

No aerial photograph was available for this pavement; all pavement features were surveyed by hand from fixed location points. Raytheon Services, Nevada (RSN) surveyed the P2001 pavement in 1992 using 26 survey targets, labeled TGT101 through TGT126 and shown as large crosses on plate 1, that are affixed to the pavement at roughly 10 meter (33 foot) intervals. The RSN survey was carried out under a QA:NA directive, but the methods used at P2001 correspond to their standard QA:QA surveying techniques (i.e., they closed their survey loop). 45 intermediate location points were located during the mapping of P2001 using tape and compass triangulation from the RSN targets. These intermediate points are marked on the pavement with dark green paint and appear as small crosses on plate 1. Intermediate locations are labeled on the north half of pavement as N-1, N-2, etc., and on the south half as S-1, S-2, etc. The intermediate points are estimated to be located within 15 cm. of true location, based on triangulation error.

Pavement P2001 was mapped at a scale of 1:240 (1"=10'), and only fractures greater than 1.5 meters (5 feet) in trace length were mapped as individual fractures. Areas of rock breakage with abundant smaller fractures are displayed on the map, but no attribute data were collected in these areas nor were they used in any statistical analyses.

Most areas between the mapped fractures are relatively intact - there are few areas where a large number of fractures smaller than 1.5 meters in length exist and were not mapped. We believe the map presented on plate 1 is a fair representation of the true fracture fabric of this pavement and that a change to a smaller minimum cutoff length would not have resulted in a substantially different map pattern or interpretation. Pavements at Yucca Mountain mapped by Barton (Barton and others, 1993) were mapped using a minimum cutoff length of one foot. However, few fractures shorter than three feet appear on the maps of these pavements. The mapping at P2001 thus corresponds reasonably well to the level of detail and portrayal of fabric elements as displayed on other pavement maps at Yucca Mountain.

In accordance with technical procedure USGS-GP-12, R1, cooling joints and tectonic fractures are labeled separately at the Fran Ridge pavement. Tectonic fractures on the northern half of the pavement are labeled DSF1, DSF2, DSF3, and so on, and cooling joints labeled in a similar fashion DSJ1, DSJ2. Tectonic fractures on the southern half of the pavement are labeled LMF1, LMF2, LMF3, and so on, and cooling joints labeled in a similar fashion LMJ1, LMJ2. A feature was labeled as a cooling joint only if it was smooth (Roughness Coefficient (RC) less than six) and had tubular features (Barton and others, 1984; 1993) on at least a portion of the surface. Otherwise, rock discontinuities on the pavement were labeled as fractures. Subsequent to our mapping, we have interpreted some of these fractures to be cooling joints based upon their overall similarity to the known cooling features, as discussed below. A feature was called a fault only if it showed evidence of consistent, demonstrable displacement of other features

along its length and where the magnitude of separation was mappable. Minor offsets of fractures by other fractures were recorded in the remarks column of the attribute data sheets.

Confident distinction between cooling and tectonic joints in and near the proposed repository is a necessary first step in understanding the evolution of the fracture network and in modeling its properties. The distinction is easiest where tubular structures (Barton and others, 1984; 1993) are abundant, as in highly lithophysal zones of the Tiva Canyon Tuff. However, fractures identical to cooling joints in every respect may lack tubular structures, or have such structures exposed on only a portion of their area. For example, fracture DSF2, a NW-striking, steeply dipping joint exposed for 14 meters (46 feet) along its length, has visible tubular structures on its surface at only a single locality near its southeastern end. We interpret this feature to be a cooling joint, although we have retained the fracture designation in the label to maintain consistency with a data package that was submitted prior to completion of the mapping. Tubular structures are also exposed on only a small portion of the large, prominent, gently dipping cooling joints that lend to this pavement its pronounced step-like appearance. The surfaces of DSJ14 and DSJ15, near survey target TGT111, are exposed over a width of one to two meters for 12 meters (40 feet) or more, yet tubular structures are present over less than 10% of their surface. Other cooling joints nearby to the north and south exhibit similar properties. The absence of tubular structures on a given fracture, then, in no way disproves an origin by cooling even if such structures are present on other fractures nearby. Criteria for the recognition of cooling joints that lack tubular structures have been discussed by

Throckmorton and Verbeek (1995), and include low surface roughness (RC of five or less); smooth, continuous traces; appreciable length; parallelism with proven cooling joints nearby; and demonstrated early age as shown through abutting relations with fractures of other sets. In addition, where lithophysae are present in the rock, cooling joints intersect none or few of them. All of these criteria proved useful in distinguishing cooling from tectonic joints on Pavement 2001.

Fracture attitudes are listed as average values for a particular fracture (Appendix 1). Multiple measurements along individual fractures show that strike and dip may vary by five to 10 degrees over the length of the fracture. For curving fractures, where the change in strike or dip is greater than five to 10 degrees, multiple values or a range of values are given (appendix 1). In a few cases where the dipping surface of the fracture was not visible, the azimuth recorded was the azimuth of the fracture trace on the pavement surface - this approximates strike for steeply dipping fractures. The dip in these cases was assumed to be vertical.

Surface trace lengths were measured for all fractures (appendix 1). Height was only measured for steeply dipping fractures that intersected either of the test pits. The transition zone between the middle nonlithophysal zone and the upper lithophysal zone contains a number of subhorizontal cooling joints. These were mapped as surfaces; the explanation on plate 1 shows the line symbol used in depicting an exposed joint face on the map. For these subhorizontal cooling joints, the trace length was taken as the long dimension of the exposed fracture face, and the height the short dimension.

Surface roughness for each fracture was measured using the techniques described by Barton and others (1993) at what was thought to be a representative portion of the fracture surface. Roughness was typically taken approximately parallel to the fracture azimuth, as in many places only a few inches of the fracture were exposed above the pavement surface. Fracture roughness profiles were converted to a numerical roughness coefficient based upon the profiles shown in Barton and Choubey (1977).

A representative aperture (more properly called wall separation), or range of apertures if widely varying, was measured for fractures where both walls are in place and appeared undisturbed by weathering processes (appendix 2). Aperture is described in USGS-GP-12, R1 as the measured distance between the two fracture walls. However, true aperture refers to an actual opening and is not the same as wall separation. For example, any fracture filled with caliche has an aperture of zero. A fracture with walls 2 mm apart, each coated with opal 0.5 mm thick, has an aperture of 1 mm and a wall separation of 2 mm. In order to avoid confusion for later users, note that data collected as aperture in Appendix 2 are really wall separations and do not refer to open space, except where the fracture is specifically listed as open.

Several types of fracture fillings were noted (appendix 2). Almost all fractures were filled with calcite/caliche. Brecciated fracture fill material was of two types: clast or gouge supported breccia, and calcite- or caliche-cemented breccia, labeled as Type I and Type II, respectively, following the usage of A. Braun (A. Braun, written communication, 1995).

Particular attention was paid to how each fracture terminated as this information is critical to establish age relationships and to describe the connectivity of the fracture network. Termination of each fracture endpoint is described (appendix 2) as blind (fracture ends within unbroken rock or in a zone of small fractures not mappable at a scale of 1:240), T or Y termination (abutting relationship), X or intersecting relationship, or as covered.

Ten samples of fracture-fill material were collected for thin section analyses from three 3- to 8-centimeter wide north to northwest trending fractures using the aid of a hammer and chisel. Sample locations along fractures LMF107, DSF33, and DSF24 are shown on plate 1. Features observed in thin section were identified using both covered and polished thin sections with transmitted plane-polarized light and crossed-polarized light at low (25 X and 50 X), medium (100 X), and high (200 X and 400 X) magnifications. The scanning-electron microscope (SEM) was used on polished thin sections to determine the identities and chemical compositions of fracture-filling secondary minerals. Quantitative estimates of various constituents were made on 10X thin-section photo enlargements. The methods for collection and preparation are in accordance with Technical Procedures USGS-GP-01, R2, "Geologic Mapping", and USGS-GP-18. R1, "Petrographic Analysis of Volcanic Rocks".

FRACTURE CHARACTERISTICS

Fracture Orientation

Orientation data for all fractures mapped at P2001 are shown as a lower-hemisphere, equal area contour plot of poles to fracture planes (fig. 3). Fracture azimuths, dips and dip directions are tabulated in the appendix 1. The stereonet shows dominantly northwest, north-south and northeast trending fractures. The large proportion of the fractures are steeply dipping with a smaller number of fractures, mostly cooling joints, having low dips. Based on orientation, the following concentrations of poles that could correspond to fracture sets have been identified: three sets of high-angle fractures, including two sets or one bimodal set with clusters of poles in the northeast quadrant and one set of poles in the northwest quadrant, and a number of low-angle features that appear scattered through the center of the net.

FIGURE 3. NEAR HERE

Another representation of the different fracture sets is gained by plotting fracture azimuth vs. cumulative trace length (fig. 4). Fracture azimuth, from 270 to 090, are grouped in ten-degree bins and the cumulative length of all fractures for that azimuth bin are recorded. Only the azimuths of the tectonic joints are shown. Data from cooling joints were not included because many of the low-angle features with long trace lengths are undulatory and have variable strike directions. The bulk of the trace length

Fig. 3. Lower-hemisphere, equal area contour plot of poles to fracture planes, Fran Ridge pavement P2001. Total number of poles is 284. Open circles represent poles to tectonic joints, filled squares represent poles to joints with cooling tubes observed. Contours as percent of total per 1% area, contour intervals are 2, 4, 6, 8 and 10%.

distribution is made up of north-to northwest-trending fractures (fig. 4). Northeast-trending fractures, although abundant, add relatively little to the cumulative trace length distribution. The cumulative length of the long north- to northwest-trending fractures is only a minimum value because many of these fractures are censored (end of fracture not exposed) on at least one end. Most of the northeast-trending fractures terminate against other fractures and have both endpoints exposed. Thus, the cumulative lengths of the northeast-trending fractures are much closer to the actual value. A calculation of fracture intensity based on number of fractures per area would overemphasize the importance of the northeast fractures. A fracture intensity based on trace length per area, presented later in this report, would correctly weight the north- to northwest-trending fractures.

FIGURE 4. NEAR HERE

Identification of fracture sets

A more robust subdivision of fracture sets is obtained by sorting the fractures by surface roughness, to separate smooth cooling joints from generally rougher tectonic fractures (Barton and others, 1993). Cooling joints (fig. 5) were selected as having roughness coefficients of less than 5 (RC <5) in the middle nonlithophysal zone and RC<6 in the upper lithophysal zone; joint surfaces overall tend to be rougher in the upper lithophysal zone and joints with visible tubes commonly have RC of up to 6 in this zone.

FIGURE 5. NEAR HERE

Fig 4. Fracture azimuth vs. cumulative trace length. Data from cooling joints (listed as DSJ or LMJ in the Appendices) were not included, only the azimuths of tectonic joints are shown. Fracture azimuth, from 270 to 090, are grouped in ten-degree bins and the cumulative length of all fractures for that azimuth bin are recorded.

Fig. 5. Interpreted cooling joints at Fran Ridge pavement P2001. Fig. 4a shows the interpreted map distribution of C1, C2, and C3 cooling joints. This represents the appearance of P2001 prior to the formation of any tectonic fractures. Fig. 4b is a lower hemisphere, equal area projection of poles to these planes. Contours as percent of total per 1% area, contour intervals are 2, 4 6, and 8%. Cooling joint sets were selected as fractures with roughness coefficients of less than 5 (RC <5) in the middle nonlithophysal zone and RC<6 in the upper lithophysal zone. Only three of the C1 and C2 cooling joints have visible tubes; most C3 joints have cooling tubules over at least a portion of their area. Fractures lacking tubules were interpreted to be cooling joints based upon their overall similarity to the known cooling joints, including orientation, low roughness coefficient, gently curving fracture traces and long trace length.

Two sets of sub-vertical cooling joints, C1 and C2, are shown in fig. 5. Only two joints of the northwest-trending C1 set (DSF2 and DSJ8) and one of the northeast-trending C2 set (DSJ1) have visible tubes. The other fractures have thick caliche coatings and cooling tubes are not visible; these fractures were interpreted to be cooling joints based upon their overall similarity to the known cooling features, including orientation, low roughness coefficient, gently curving fracture traces and long trace length (Throckmorton and Verbeek, 1995). In the northern part of the pavement, fractures DSF1, DSF4, DSF7, DSF9, DSF10, DSF23, and DSF24 are all lengthy (5.2 to 13.1 m, 17-43 ft), steeply dipping joints of northwest strike and low surface roughness (RC of 2 to 4). Abutting relations prove they are among the oldest fractures present. For example, nine fractures terminate against fracture DSF9 and none cross it. The northwest-striking fractures southeast of Pit 1, near target TGT124, exhibit similar properties. The combination of these criteria, together with the parallelism of all these fractures to known cooling joints DSF2 and DSJ8 in the same area, provide strong evidence of a well-expressed set of northwest-striking cooling joints in this area (fig. 5). Farther south and west, in stratigraphically higher parts of the pavement surface where the rock becomes more highly lithophysal, the near lack of lithophysae on some joint surfaces was an additional useful criterion in the recognition of cooling joints belonging to this set. The median orientation of the C1 cooling joints is 322/77 SW, based on an average of 34 fractures.

Through similar means a second set of steeply dipping cooling joints, C2, was recognized on Pavement P2001; these strike east-northeast, approximately perpendicular

to set C1. The median orientation of the C2 cooling joints is 075/86 SE based on an average of 17 fractures. The resultant rectangular pattern of two steeply-dipping cooling joint sets, the joints of one set dominating in length and abundance over those of the other (fig. 5), is similar to that documented at other localities in the region (Barton and others, 1989; Throckmorton and Verbeek, 1995). Both sets of steeply dipping cooling joints appear to form more readily in the middle nonlithophysal zone (fig. 5).

A third set of cooling joints, C3, is represented by the widely scattered poles in the center of the net (fig. 5). These joints are generally shallowly dipping surfaces that have very long trace lengths and gently undulate. The median orientation of the C3 cooling joints is 084/21 S based on an average of 33 fractures. However, the C3 set has a very high dispersion and joints were given an average strike in order to portray them on the equal area nets. Thus, the median orientation is only approximate. These joints are concentrated in the transition from the middle nonlithophysal zone to the upper lithophysal zone (fig. 5). Most of these surfaces have cooling tubules over at least a portion of their area. Some of the joints dip more steeply and intersect each other in complicated ways, for example, LMF11 and LMF12, just west of test Pit 2.

Tectonic joints are defined on the basis of their greater surface roughness, generally shorter trace lengths and more irregular traces. The two clusters of poles in the northeast quadrant of the stereonet showing all P2001 data (fig. 3) are treated here as separate joint sets - a more northerly-trending set, T1 and a northwest-trending set, T2. The set T1 has a relatively high dispersion, with planes trending from north-northeast through north-northwest (fig. 6). The median orientation of the T1 tectonic joints is

354/86 W based on an average of 93 fractures. These fractures tend to be long and straight.

FIGURE 6. NEAR HERE

The T2 tectonic joints have almost identical strike directions to the northwest-trending cooling joints, but the cooling joints tend to dip mostly to the east whereas T2 joints have steep westward dips (fig. 7). The median orientation of the T2 tectonic joints is 329/84 W based on an average of 40 fractures. The seven degree difference in median strike between the T2 set and the C1 cooling joints is too small to be apparent in the field and underscores the need for consideration of fracture attributes other than orientation in the interpretation of the evolution of complex fracture networks. The tectonic joints are distinguished from northwest-trending cooling joints by being consistently rougher (roughness coefficients of 7 to 10 are typical), and having numerous lithophysal cavities pockmark their surfaces in the western part of the pavement, where the rock is highly lithophysal. Moreover, their relatively young age is evident locally where they cut through individual tubular structures on gently dipping cooling joints. T2 tectonic joints tend to link lithophysae and their traces are more irregular than those of the cooling joints. Fracture surface irregularity on the decimeter scale, which may not be recorded by the roughness coefficient, is a common difference between cooling and tectonic joints elsewhere on Yucca Mountain (Throckmorton and Verbeek, 1995). The T2 joints are commonly shorter than T1 joints, but in several cases the T2 joints form linear trends that

Fig. 6. Interpreted T1 tectonic joints at Fran Ridge pavement P2001. Fig. 5a is a lower hemisphere, equal area projection of poles to these planes. Contours as percent of total per 1% area, contour intervals are 10, 20 and 30%. Fig. 5b shows the interpreted map distribution of only T1 fractures. These fractures tend to be long, straight, and have blind terminations (fracture ends within unbroken rock). Fig. 5c represents the appearance of P2001 following the formation of the T1 set.

are en echelon or have incipient linkages between them. These fracture trends form a nearly throughgoing feature (Pollard and Aydin, 1988).

FIGURE 7. NEAR HERE

The third set of tectonic joints, T3, are northeast-trending fractures that have short trace lengths and usually truncate at both ends against the larger tectonic or cooling joints (fig. 8). The median orientation of the T3 tectonic joints is 055/87 SE based on an average of 39 fractures.

FIGURE 8. NEAR HERE

We emphasize that tubular structures provide the only unequivocal field evidence for cooling joints and that the other criteria mentioned above must be used in combination to provide effective distinction between cooling and tectonic joints. Some T2 joints, for example--particularly those that extend northwest and southeast from Pit 2--are 4 to 10 meters (12-30 feet) long and thus are of comparable dimension to some of the cooling joints of similar strike farther north, near Pit 1. The T2 joints near Pit 2 grew to such lengths because older joints that would otherwise have interfered with their lateral growth are less abundant here than in other parts of the pavement. Length by itself is not a reliable criterion to distinguish cooling from tectonic joints at this locality. Low surface roughness, absent or sparse lithophysal cavities intersecting the joint surface, and

Fig. 7. Interpreted T2 tectonic joints at Fran Ridge pavement P2001. Fig. 5a is a lower hemisphere, equal area projection of poles to these planes. Contours as percent of total per 1% area, contour intervals are 10 and 20%. Fig. 5b shows the interpreted map distribution of only T2 fractures. These fractures appear to have formed only where northwest-trending C1 cooling joints were absent (compare with fig. 4). Fig. 5c represents the appearance of P2001 following the formation of the T2 set.

Fig 8. Interpreted T3 tectonic joints at Fran Ridge pavement P2001. Fig. 5a is a lower hemisphere, equal area projection of poles to these planes. Contours as percent of total per 1% area, contour intervals are 10 and 20%. Fig. 5b shows the interpreted map distribution of only T3 fractures. Short trace lengths are the result of termination of T3 fractures against earlier cooling and tectonic joints. Fig. 5c represents the appearance of P2001 following the formation of the T3 set.

evidence of early formation as demonstrated through abutting relations are more important properties of cooling joints on this pavement and collectively are diagnostic of origin.

Throckmorton and Verbeek (1995) identified three sets of cooling joints and two major sets of tectonic fractures in their observations in and around the two test pits at Fran Ridge (fig. 9). A comparison of the median orientation for the fracture sets defined at each pit with the data from pavement P2001 is shown in table 1.

FIGURE 9. NEAR HERE

TABLE 1. NEAR HERE

These data differ from the P2001 data set in the following ways: 1) observations of the vertical walls of the two test pits are more likely to identify shallowly dipping surfaces. Observations made on the gently sloped pavement are biased against recognizing low-angle features (Terzaghi, 1965); 2) Throckmorton and Verbeek (1995) did not use a length cutoff in their observations; small fractures are better represented in their data set. In fact, due to the limited areal extent of their observation area, their data emphasize a different size range than the P2001 pavement data; 3) orientation of the fracture sets in the pits were measured subjectively - measurements were only taken on fractures that fit into sets previously identified by inspection. As such, the data from the test pits are much better clustered than data from the pavement surface where all fractures were measured; and 4) neither test pits expose the upper lithophysal zone of the Topopah

Fig. 9. Comparison of fracture data from the test pits to P2001 data. Fig. 9a is a lower-hemisphere, equal area contour plot of poles to fracture planes at the two test pits at the Fran Ridge site. Data are from Throckmorton and Verbeek (1995). Cooling joint sets are labeled C1, C2 and C3; tectonic joint sets are labeled T1, T3; subhorizontal joints are labeled SH. Total number of poles is 139. Contours as percent of total per 1% area, contour intervals are 2, 4, 6, 8 and 10%. Fig. 9b is a lower-hemisphere, equal area contour plot of poles to fracture planes at Fran Ridge pavement P2001 (symbols and contour intervals as in fig. 3). Cooling joint sets are labeled C1, C2 and C3; tectonic joint sets are labeled T1, T2 and T3.

Table 1. Median orientation of fracture sets, pavement P2001 and test pits.

[Orientation data from the to test pits from Throckmorton and Verbeek (1995). Subhorizontal joints, labeled SH, are foliation-parallel and have extremely rough surfaces. They were interpreted by Throckmorton and Verbeek (1995) as unloading joints. These features were not mapped at pavement P2001]

Location	Cooling Joints			Tectonic Joints			
	C1	C2	C3	T1	T2	T3	SH
Test pit 1	N28W/85SW	N80E/89SE	N62E/10SE	N01E/89NW	--	N50E/86SE	N49W/05NE
Test pit 2	N34W/84SW	N60E/67NW	--	N05E/79SE	--	--	N52W/05NE
Pavement P2001	N38W/77SW	N75E/86SE	N84E/21S	N06W/86W	N31W/84W	N55E/87SE	--

Spring Tuff. The northwest-trending T2 set is best exposed in the upper lithophysal zone and was not recognized in the pits.

Given the difference in the data sets described above, the overall orientation patterns between the pavement P2001 data and Throckmorton and Verbeek's (1995) observations at the two test pits are remarkably similar (fig. 9, table 1). The better clustering of points and the greater number of low-angle features in the data from the test pits can be explained by the reasoning presented above. Only one additional set of fractures, the T2 tectonic set, is apparent in the data from the pavement. These fractures predominate in the upper lithophysal zone, which was not observable in the test pits.

Fracture trace lengths

Histograms of fracture trace lengths by lithologic unit are presented in fig 10. These histograms show the frequency of trace lengths in 0.76 meter (2.5 foot) increments for both the upper lithophysal zone and the middle nonlithophysal zone. Data are also subdivided by the degree of trace length censoring where the censoring is zero for fracture traces with both ends observable, 1 for traces with only one end observable and 2 for traces with neither end observable. A 1.5 meter (five foot) length cutoff was employed during the mapping; only a few fractures shorter than this length were measured. As a result, these trace length distributions are not only censored but are truncated artificially to the left.

FIGURE 10. NEAR HERE

Fig. 10. Fracture trace length histograms, Fran Ridge pavement P2001. Upper and lower figures show trace length distributions in the middle nonlithophysal zone and upper nonlithophysal zone of the Topopah Spring Tuff, respectively. Data are subdivided by degree of censoring: zero for fracture traces with both ends observable, censoring is one for traces with only one end observable, and censoring is two for traces with neither end observable. Trace length distributions are not only censored but are truncated to the left due to the 1.5 m length cutoff that was employed during the mapping.

The shape of the trace length distributions for both units are similar and are consistent with a power-law or exponential model to these distributions. However, there are differences between the trace length distributions for the two zones. Trace length data from the middle nonlithophysal zone are skewed to longer trace lengths and median and mean trace lengths are significantly higher than those of the upper lithophysal zone. In addition, there are many more fractures with censored lengths in the middle nonlithophysal zone. Thus, trace lengths shown for the middle nonlithophysal zone (fig. 10) are only minimum lengths and the actual distribution would shift to even longer median trace length values. These trace length distributions are consistent with field observation that fractures within the upper lithophysal zone appear to have shorter trace lengths and a higher proportion of blind terminations than those within the middle nonlithophysal zone.

Fracture Style as a Function of Lithology

The overall style of fractures on Pavement 2001 differs markedly from place to place as a function of lithology. Fractures within the middle nonlithophysal zone tend to be planar or arcuate with low surface roughness (RC between 2 and 8). Fractures within the upper lithophysal zone tend to be planar but extremely rough (RC mostly greater than 10 and up to 20). One of the finest illustrations of this effect is a lengthy zone of T2 joints whose gradual change in properties from southeast to northwest parallels the gradation from sparsely lithophysal rock low on the pavement surface to the east, to highly lithophysal rock up section to the west. The fracture zone can be traced for more

than 40 meters (130 ft) from the southeastern edge of the pavement near survey target TGT108, through Pit 2, to the west edge of the pavement near survey target TGT119. Most of the T2 joints in the southeastern half of the zone, in the transition zone from sparsely to moderately lithophysal rock, are rather lengthy; sharply formed and visually prominent. In the more lithophysal rock higher in the section, the average length of the T2 joints decreases markedly; few can be followed as continuous surfaces for more than three meters (10 ft). The joints also become more difficult to follow visually, their surfaces become rougher and pockmarked by abundant lithophysal cavities, and their traces become more irregular. All of these changed properties reflect the difficulty of propagating a smoothly continuous fracture through a rock containing numerous large voids. Analogous decreases in joint length and continuity, and increases in surface roughness and trace irregularity, have also been noted in highly lithophysal portions of the overlying Tiva Canyon Tuff (Throckmorton and Verbeek, 1995, p. 27).

A related consequence of the presence of abundant lithophysae is that little movement was required to break the rock apart. Reactivation of joints in the western part of the pavement, resulted in locally marked brecciation. Some of the T2 joints pass laterally into zones of rubble through which a discrete fracture surface can no longer be recognized. The many fractures depicted on the map as dashed lines near survey target TGT119 reflect the difficulty in this area of tracing individual fractures through highly broken rock.

Spacing of Fracture Zones

T2 fractures appear to be clustered into northwest-trending zones that are spaced 6.1 to 7.6 meters (20 to 25 feet) apart. T2 fractures within these linear zones are en echelon or have incipient linkages between them. One such zone, described above, cuts the northeast side of test Pit 2 and trends northwest through survey targets TGT107 (at the southeast edge of the pavement), TGT110 (near the northwest corner of the fence surrounding test Pit 2), and TGT114. Several of the fractures in this zone, including LMF133 and LMF38, have documented right-lateral slip. A second northwest-trending zone extends from near the southwestern fence corner surrounding test Pit 2. This zone extends from TGT106 (just south of the southwestern fence corner), through TGT111, to TGT113 near the center of the western edge of the pavement. This zone consists of a linear succession of 2.1- to 3-meter (7-to 10-foot) long fractures that cannot be explicitly connected as a single feature. There is less evidence for a consistent sense of offset along this zone, although a dark gray breccia or rubble zone 2.4 meters (8 feet) south-southwest of TGT111 is offset in an apparent right-lateral sense along this zone. A third, less well defined zone is present in the southwest corner of the pavement in the vicinity of TGT112. Fractures along this zone are less continuous than the two zones described above and no definitive offset relationships could be found.

FRACTURE HISTORY

Formation of joint sets

Six fracture sets have been identified at the Fran Ridge pavement P2001: three sets of cooling joints and three sets of tectonic fractures. Previous fracture investigations at Yucca Mountain defined the cooling joints as the earliest formed fractures (Barton and others, 1993; Throckmorton and Verbeek, 1995). Evidence for the early formation of cooling joints at P2001 includes their long trace length, abutting relations with other fractures, presence of tubular structure and their relationship to lithophysae. In general, the cooling joints abut each other or have X intersections that are indicative of similar time of formation. However, in several places high angle cooling joints appear to terminate against the low-angle C3 surfaces. For example, the western end of LMJ9 and LMJ10 terminate against the low-angle joint DSJ16 to the west of Pit 2. Farther north, LMJ3 appears to terminate against gently-dipping cooling joint DSJ13. These abutting relationships, combined with the exceptional trace lengths of the low-angle C3 joints suggest that they may have formed slightly earlier then the two sets of steeply dipping cooling joints. Throckmorton and Verbeek (1995) found similar evidence for the early formation of the low-angle cooling set elsewhere at Yucca Mountain.

T1 joints appear to be the earliest-formed tectonic fracture set, because they are the longest tectonic fractures, have the largest percentage of blind terminations and are only truncated by preexisting cooling joints. The T2 fracture set was the next to form; in at least one case a T2 fracture offsets a T1 fracture. In other cases, north-south trending fractures appear to have renewed growth at their tips in the T2 direction, yielding a bent

or even sigmoidal overall fracture shape. In places the relationship between the T1 and T2 sets is not clearly defined, in part because T2 fractures predominate in the upper lithophysal zone where fracture trace lengths are short and intersections with other fractures are rare. However, the sequence of formation, T1 followed by T2, fits with the overall age relationships suggested by Throckmorton and Verbeek (1995) for other locations at Yucca Mountain. T3 fractures were the last to form and appear as short connectors between the earlier cooling and tectonic fracture sets.

Northwest-striking cooling joints on Pavement 2001 and later tectonic joints of the T2 set both constitute visually prominent fracture sets represented by abundant joints. The cooling joints are most abundant in the extreme northern part of the pavement, near Pit 1, but are of only scattered presence elsewhere (fig. 5). The later T2 tectonic joints, of similar orientation, show precisely the opposite pattern (fig. 7). That the T2 joints and the northwest-striking cooling joints are spatially almost mutually exclusive illustrates a common effect--that formation of new joints will be suppressed wherever existing fractures are favorably oriented to accommodate new increments of extensional strain. Similar examples are known from the Tiva Canyon Tuff on Yucca Mountain (Throckmorton and Verbeek, 1995).

Joints reactivated as faults

Slip or renewed growth of previously-formed surfaces are responsible for many of the ambiguous or indeterminate fracture termination relationships at P2001. There are only a few cases where apparent offset of fractures at P2001 can be proven as faults.

Evidence of down-to-the-west, predominantly dip-slip movement on a north-south joint is seen along fracture LMF39, a lengthy T1 joint reactivated as a normal fault. Offset segments of gently to moderately dipping cooling joints in several places along this fault can be matched from one side to the other, enabling the amount of slip and its direction to be determined. Those that dip northeast show a component of left strike separation, whereas those that dip southeast show right strike separation. Taken together these observations indicate that movement on fracture LMF39 was down-to-the-west with a calculated net slip of 18 centimeters (7 inches). Motion was oblique to the north - the slip line has a pitch of 34 degrees to the north in the plane of the fault (the slip line plunges 32 degrees towards N11W).

A second fault is the large northwest-trending T2 fracture that extends northwest from the north end of test Pit 2 (fractures LMF38, LMF133 and probably LMF98 southeast of Pit 2). This fracture offsets low-angle cooling joint LMJ6 with around 15 centimeters (6 inches) of right-lateral strike separation and offsets the T1 fracture LMF39, described above, by a similar amount. Because it offsets both high angle and low angle fractures with the same amount of strike separation, this fault must have almost purely strike-slip (right lateral) motion - the separations could not have been produced by a reasonable amount of dip-slip motion.

Striated fracture surfaces at P2001 also provide evidence of slip on previously formed joints. Among all joints at Pavement 2001 which bear evidence of reactivation, slickenside striae are most visually evident on the gently northeast- to southeast-dipping C3 cooling joints that divide the pavement into a series of low ledges. Observed bearings

of most of the striae on the subhorizontal surfaces fall within the fairly narrow range of 075 (N75E) to 103 (S77E), with an average of around 090 (N90E), very nearly perpendicular to the average strike of the T1 joints at this locality. Upon magnification with a hand lens, the striae are seen to occur on tiny *en echelon* planes cut either into the joint surface, or into the siliceous mineral coatings upon it, or both. Each of these striated surfaces dips at an angle slightly greater than that of the mean cooling-joint surface, and each is separated from the neighboring surface by a low, steep, non striated step that faces west. The resultant configuration is a common one among faulted joints (Petit, 1987) and indicates that the upper plate moved eastward with respect to the lower plate--that is, that the gently east-dipping cooling joints were reactivated as a series of low-angle normal faults. Good examples showing clearly the stepped morphology of the striated joint surfaces are visible in numerous places, particularly on cooling joints DSJ9 (immediately northeast of TGT115) and DSJ19 (east and south of survey target TGT118).

The time of slip on the C3 joints is problematical, but available evidence suggests that it occurred during or after formation of the T1 joint set and before formation of the T2 set. Geometrically, easterly slip on the C3 planes is most reasonably accommodated during east-west extension around the time of formation of the T1 fractures. East-west trending slickenside striae are developed on at least three minerals deposited within the gently dipping cooling joints, including (a) a thin, translucent film of vapor-phase quartz, (b) a thicker coating of white, granular quartz(?) that under magnification has a finely saccharoidal appearance; and (c) pale gray microbotryoidal opal. Although the timing of deposition for any of these mineral phases is unknown, the fact that slip postdated

precipitation of all three mineral phases suggests that it occurred well after cooling joints had already formed in the rock. Finally, we note that cooling joint DSJ9 east of fault LMF39 shows striae indicative of normal slip to the east, whereas the offset segment of the same joint west of the fault, DSJ10, shows none. Fracture DSJ10 dips toward the fault and appears to have been buttressed by it, implying that the fault--a reactivated T1 joint--must already have been present when slip occurred on the gently dipping cooling joints.

East-west extension appears to have predated the formation of the northwest-striking T2 joints. As described above, reactivated T2 joint LMF133 offsets T1 fault LMF39 at a point two meters (6 feet) north of survey target TGT110, north of Pit 2. This T2 joint forms a discrete, continuous surface between the offset segments of LMF39, and provides clear evidence of the relative ages of the T1 and T2 fractures.

Extensional strain during T1 time was expressed first in the formation of the north-striking T1 joints and, with continued extension, as localized normal faulting along the same joints. The relations described above tentatively bracket the time of east-west extension on low-angle C3 joints at Pavement 2001 to the time period between formation of the T1 and T2 joint sets. Because the measured slip vectors are fully compatible with the stress state during formation of the T1 joint set, we feel that some of the extensional strain was accommodated by slip along the C3 surfaces.

Fractures of northwest strike on Pavement 2001, mostly members of the T2 joint set but including some steeply dipping cooling joints, also occasionally show evidence of reactivation as faults. Where possible to demonstrate, reactivation appears as dominantly

right-lateral slip, as discussed above for fracture LMF133. Locally there is also a suggestion of small dip-slip movement where gently dipping cooling joints are offset by a few centimeters across T2 fractures. For example, near survey target S35, fractures LMF36 and DSF113, both reactivated T2 joints, appear to bound a downdropped trough 1.2 meters (4 feet) wide and 5.5 meters (18 feet) long. Observations of northeast-trending slickenside striae on some of the gently dipping cooling joints indicate that the C3 surfaces accommodated extensional strain during formation of the T2 joint set as well.

Faulted caliche-filled fractures

Caliche on Pavement 2001 completely fills most of the steeply dipping fractures and in many of them obscures all but small portions of their surfaces. The caliche in fractures striking north to northwest, including cooling joint set C1 and tectonic fracture sets T1 and T2, is 1 to 2 centimeters thick in many places, but that filling the east--northeast-striking joints of the T3 set is almost everywhere thinner. The thicker fillings commonly are crudely layered, and some layers are in part siliceous. Some of these fillings are striated.

Slickenside striae on surfaces within caliche were observed along four northwest-striking cooling joints, a T1 joint, a T2 joint, and a gently east-dipping cooling joint. The striae on all six of the steeply dipping joints rake steeply, 84 to 88 degrees, and are most prominently developed in the more siliceous parts of the caliche filling. In the four places where the sense of slip could be determined on these joints, that slip was consistently normal (Petit, 1987). The tectonic significance, if any, to be attached to these young

movements is uncertain. The slip vectors record exclusively dip slip on fractures of different strike, and appear kinematically incompatible with the present-day stress field as inferred from hydrofracture tests and borehole breakouts (Haimson and others, 1974; Rogers and others, 1983; Springer and others, 1984; Stock and others, 1985; Stock and Healy, 1988). These data suggest that the striae do not record continuing tectonic deformation in the Yucca Mountain-Fran Ridge area, but are more likely due to gravitational unloading as the rock mass was progressively decoupled from the regional stress field during erosion of overlying rock.

BRECCIAS AND BRECCIATED FRACTURE FILL

Occurrence at outcrop and hand-sample scale

Several types of brecciated material are observed at P2001. These are described macroscopically as clast or gouge supported breccia (Type I), matrix-supported breccia, usually as clasts "floating" in calcite matrix (Type II); and intensely fractured zones, often showing several directions of preferred fracture orientation and little clast rotation (Type III) (The labels Type I, II and III follow the usage of Braun (A. Braun, written communication, 1995). The type III breccias are clearly associated with intersections of large fractures; none of these areas was sampled. Many of the fractures at pavement P2001 are filled with Type II breccia, consisting of variable amounts of rock fragments with calcite or caliche matrix. The proportion of rock fragments varies from a few

percent up to as much as 50%. These matrix-supported (Type II) breccias appear to be similar in many respects to the authigenic-mineral cemented breccias (AMC) described by Levy and Naeser (1991) from fault zones on Busted Butte. Most of these breccias were interpreted to be the result of surficial, dominantly pedogenic, processes (Levy and Naeser, 1991). As a result, none of the matrix-supported breccias at P2001 was sampled.

For this study we sampled lenses of brecciated fracture fill material that we tentatively identified in hand sample as being a clast or gouge supported breccia (Type I). We anticipated that this fracture-filling material would be similar to Levy and Naeser's (1991) crushed tuff matrix (CTM) breccia. The breccia appears in hand sample as lenses up to 5 centimeters in width filled with small fragments contained in purplish-gray matrix that is very fine, having the appearance of crushed rock. Breccia fragments are usually small, around 5 mm, although larger fragments are present locally. Breccia fragments range from angular to subrounded and vary in color from gray, through orange-brown (the color of the wall rock), to light pink. In all, hand samples give the impression of a multi-lithologic clast assemblage.

In general, the fracture filling described above occurs as pods or lenses within fractures. The longest continuous exposure is within T1 fracture LMF107 at the southeast corner of the pavement. Here, brecciated fracture fill of this type extends for a horizontal distance of 3.7 meters (12 feet) before disappearing under cemented slope wash at the southern boundary of the pavement. Fill of this type occupies only the northern end of fracture DSF33. For most of its length, this fracture is a thin (1 cm), continuous caliche-filled fracture. Only at the northern end, near its intersection with a

number of large northwest-trending fractures, does DSF33 widen, become more broken and the brecciated fracture fill appear. Fracture fill of this type along fracture DSF24 can be traced into the Pit 1 but it cannot be traced for more than 35 centimeters below the pavement surface, although DSF24 continues as an open fracture (aperture around 1 mm) to the floor of the pit. Nearby fractures within the pit contain lenses of the same material at varying depths all the way to the bottom of the pit, at a depth of 8 meters (26 feet). A five to eight centimeter wide fracture filled with similar material extends nearly the entire height of the south wall of the Large Block Experiment box cut.

Petrographic Description

Detailed petrographic examination of the thin section suite revealed that the majority of rock fragments found in the fractures are locally derived from the surrounding Topopah Spring Tuff. However, there are minor constituents present that do not have the same petrographic composition and textures as the host rock. The abundance of the breccia and matrix constituents were estimated based on 10X photocopy enlargements of the thin sections (table 2). Described below are detailed textural descriptions of the host rock fragments, enveloping cementing material, and a matrix assemblage of phenocrysts of possible volcanic origin.

TABLE 2. NEAR HERE

Table 2. Estimated abundance of breccia constituents.

[Percentages of constituents estimated from photoenlargements of thin sections; percentages represent total abundance from 10 samples]

Constituent		Estimated abundance		
		Percent of whole rock	Percent of fragments	Percent of matrix
Breccia fragments:				
Topopah Spring Tuff[1]		70	99	--
Cognate rhyolite lava lithic clasts		<1	<1	--
Topopah Spring phenocryst fragments		<1	<1	--
	Subtotal	71	100	
Matrix filling:				
Silica (fine mosaic[2] and microgranular)		9.1	--	31.5
Very fine $CaCO_3$		18	--	62
Ash fall (silicic; very fine to fine)		0.6	--	2
Sepiolite (clay mineral)		0.1	--	0.5
Voids or holes		1.2	--	4
	Subtotal	29		100

[1] Mosaic quartz tends to replace the margins of the breccia fragments of Topopah Spring Tuff. This introduces some uncertainty in the identification of fragments and matrix.

[2] The fine-grained mosaic quartz resembles jasperoid, but we do not wish to infer a hydrothermal origin. Like the very fine-grained calcium carbonate (micrite), fine-grained mosaic and microgranular quartz can be deposited by ground water of meteoric origin, given sufficient time.

Breccia Fragments

The breccia fragments derived from the surrounding Topopah Spring host rock consist of the following: (1) devitrified, moderately to densely welded, middle nonlithophysal zone, (2) devitrified, moderately to densely welded upper lithophysal zone including aggregate intergrowths of vapor-phase quartz and sanidine feldspar, (3) minor cognate rhyolitic lava lithic fragments of the Paintbrush Group (Sawyer and others, 1994), and (4) fragments of primary (Topopah Spring) phenocryst mineralogy including plagioclase, sanidine, and biotite. The breccia fragments are angular to subangular and show considerable variation in grain size distribution (5 to 500μ) within the matrix (fig. 11). The margins of these breccia fragments have been modified by alteration.

FIGURE 11. NEAR HERE

The distinguishing microscopic features which characterize fragments derived from the host middle nonlithophysal zone include textures of relict, brown, flattened, formerly glassy shards. In places, former brown shards, probably once glassy, are outlined by thin (5 μm) colorless material, now very fine aggregates of silica minerals and alkali feldspar (fig. 12). Cryptocrystalline and axiolitic/spherulitc devitrification textures are typical of material derived from this zone (Byers and Moore, 1987).

FIGURE 12. NEAR HERE

Fig. 11. Character of breccia fragments, P2001. Breccia fragments are angular to subrounded and vary in size from 5 to 500 μ. Photo was taken using crossed nichols.

Fig. 12. Formerly glassy relict shards within fragments from the middle nonlithophysal zone. Fig. 12a. Flattened, formerly glassy brown shards are outlined by thin aggregates of silica minerals and alkali feldspar. Plane-polarized light. Fig. 12b. Moderately to densely welded fragment from the middle nonlithophysal zone that exhibits both cryptocrystalline and axiolitic/spherulitic devitrification textures. Photo was taken using crossed nichols.

Fragments derived from the upper lithophysal zone are easily recognized by the abundance of vapor phase crystallization. Vapor phase minerals are not only observed within and/or lining lithophysal and pumice cavities but are also observed within pores or vesicles throughout the matrix. Vesicles filled with tridymite are the most common (fig. 13). Overall, primary shard textures are less distinct than the underlying middle nonlithophysal zone owing to original vapor phase crystallization at the time of cooling of the Topopah Spring Tuff about 11 ma (Sawyer and others, 1994).

FIGURE 13. NEAR HERE

Cognate rhyolitic lithic fragments, probably originally contained within the Topopah Spring Tuff, must be older than the Topopah Spring Tuff, but their specific origin is difficult to determine.

Matrix

In addition to locally derived breccia fragments that constitute the major portion of the fractured material, other components have been introduced as a filling or matrix. These include very fine-grained calcium carbonate with sparse amounts of sepiolite and fine-grained to very fine-grained air-fall tuff. The matrix in these deposits consists mostly of very fine-grained calcite and quartz in the form of microcrystalline aggregates (resembling jasperoid), coarse crystalline mosaics, and comb structures. In addition to matrix fill, quartz and very fine-grained calcium carbonate are found to pervasively

Fig. 13. Tridymite-filled microvesicles within fragment from the upper lithophysal zone.

Fig. 13a. Crossed nichols. Fig. 13b. Photo was taken using plane-polarized light.

replace fragments and also occur as open-space fillings. The presence of very fine-grained calcium carbonate and silica was verified using the SEM.

Sepiolite, associated with very fine-grained calcium carbonate, appears as lamellar aggregates of thin elongate ribbons lining three fractures and in two areas as pore filling where it forms an elliptical pattern (fig. 14).

FIGURE 14. NEAR HERE

The reworked air-fall tuff has been identified on the basis of similar phenocryst mineralogy in three thin sections of samples collected at fractures LMF107 and DSF33. Modal analyses of two occurrences are shown in table 3. This reworked ash contains glass shards and pyrogenic phenocryst assemblage typical of ash-fall tuff (fig. 15). An attempt was made to correlate the phenocryst assemblage of the ash described here with late Tertiary and Quaternary ash-fall tuffs described by Izett (1981) and Izett and others (1988). Correct identification of the ash-fall tuff could provide critical information to help determine the minimum age of the fractures. However, Izett and others (1988) had much larger samples than the ones described here, and those authors were able to date the ashes radiometrically, mainly K/Ar dating of sanidine.

TABLE 3. NEAR HERE

FIGURE 15. NEAR HERE

Fig. 14. Sepiolite as pore-filling material. Photo was taken using crossed nichols.

Table 3. Modal analyses of areas containing reworked volcanic ash.

[Ash is fine- to very fine-grained; grain size ranges from 0.05 to 0.3 mm; dash in column, not applicable; ND, not determined]

Constituent	Thin section number 3742 (19.15 mm^2)				Thin section number 3748 (37.35 mm^2)			
	Number of points	Percent of rock	Percent of phenocrysts	Number of grains	Number of points	Percent of rock	Percent of phenocrysts	Number of grains
Total point count	766	100.0	–	–	1494	100	–	–
Groundmass (contains micrite)	602	78.6	–	–	1218	81.5	–	–
Lithic fragments[1]	59	7.7	–	–	83	5.6	–	–
Glass shards (minor zeolite)	13	1.7	–	–	28	1.8	–	–
Voids or holes in slide	48	6.3[2]	–	–	20	1.3	–	–
Phenocrysts:	44	5.7	100	–	145	9.7	101	–
Quartz	3	–	7	ND	10	–	7	ND
Sanidine	8	–	18	ND	43	–	30	ND
Plagioclase	30	–	68	ND	78	–	54	ND
Biotite	0	–	0	2	3	–	2	28
White mica (altered biotite?)	0	–	0	0	0	–	0	10
Hematite after magnetite	1	–	2	ND	4	–	3	8
Hornblende	0	–	0	5	4	–	3	31
Clinopyroxene	2	–	5	5	3	–	2	12
Sphene	0	–	0	2	0	–	0	3
Allanite	0	–	0	2	0	–	0	2
Zircon	0	–	0	2	0	–	0	1

[1] Lithics are dense (nonporous) rhyolite, which is mostly moderately to densely welded Topopah Spring Tuff.

[2] Some voids may represent phenocrysts plucked out of slide, principally sanidine.

Fig. 15. Volcanic ash as matrix between Topopah Spring Tuff breccia fragments. Ash consists of about 10 percent angular to subangular phenocrysts in a very fine-grained groundmass that includes volcanic glass shards. Gray to white phenocrysts are mostly feldspar, except as labeled above.

For comparison with the volcanic ash, several samples of surficial deposits collected by John Whitney (USGS) from the west side of Busted Butte were examined in thin section. A slide of a soil B zone from the west side of Busted Butte (provided by John Whitney, March 1995) contains mostly very fine-grained calcium carbonate with several scattered very-fine-textured (0.0625-0.125 mm), subangular to subrounded crystals of feldspar, mostly plagioclase and quartz. Also present are a few grains of rounded and corroded volcanic glass fragments (fig. 16a). Several slides of samples of wind-blown materials from "sand-ramps" on Busted Butte and Fran Ridge were found to contain well-sorted, medium-size, subangular to subrounded grains of quartz, feldspar, sparse volcanic glass, and rare mafic minerals (fig. 16b). These are late Pleistocene to Holocene fairly mature detrital assemblages whose grains have probably been recycled several times from the original volcanic source. These assemblages, which probably represent wind-transported impurities incorporated in the soil, only slightly resemble the pyrogenic assemblage observed in samples from P2001.

FIGURE 16. NEAR HERE

Overall, the fracture surfaces in contact with the breccia appears smooth, straight to sinuous, and in places, pinch and swell (dilated) (fig. 17). The wall rock, adjacent to the fracture, has an alteration selvage (0.5 to 2 mm) of mosaic and microgranular quartz and very fine-grained calcium carbonate.

FIGURE 17. NEAR HERE

Fig. 16. Samples of surficial and transported material from Busted Butte. Fig. 16a. Soil zone B, containing subangular to subrounded quartz, feldspar, volcanic glass, lithic fragments and opaque minerals. Photo was taken using crossed nichols.The feldspar and quartz appear light gray to white, glass and opaques appear black, and lithic fragments appear dark with light gray microlites. Fig. 16b. Windblown sand, containing subangular to subrounded quartz, feldspar, and lithic fragments (dark). Photo was taken using plane-polarized light.

Fig. 17. Examples of fracture surfaces in contact with brecciated fracture fill. Fracture surfaces in contact with breccia are smooth and straight to sinuous. Fracture wall separation is variable, resulting in pinches and swells. Light-colored fracture-filling material is quartz, dark-colored material is very fine-grained calcium carbonate. The wall rock adjacent to the fracture has an alteration selvage of mosaic and microgranular quartz 0.5 to 2 mm in width.

Timing of brecciation

Crystals of sanidine and plagioclase are commonly fractured. In one thin section (fig. 18), large plagioclase crystals are crushed and show some rotation as exhibited by their optical discontinuity. Locally, fragments may have a "jigsaw.puzzle" texture indicating that they have not been rearranged significantly from their original wall-rock positions. This observation indicates that the fracturing and brecciation occurred post crystallization and cooling of the Topopah Spring Tuff. Texturally, the matrix assemblage of interlocking crystals of microgranular quartz suggests that matrix filled in between the breccia after faulting.

FIGURE 18. NEAR HERE

It is very difficult to determine if there has been any displacement along these fractures. However, dilation of the fractures has occurred and is represented by the pinch and swell, voids, and open space fillings.

Genesis of quartz and very fine-grained calcium carbonate cement

The fine-grained quartz and very fine-grained calcium carbonate cement, in places, have interlocking textures and therefore probably have a common origin. The genesis of the very fine-grained calcium carbonate cement containing the sepiolite is almost certainly pedogenic, related to the desert soil profile. The horizontal drill hole

Fig 18. Crushed plagioclase phenocryst cut by veinlets of microgranular quartz. Photo was taken using crossed nichols.

into Fran Ridge, UE-25h#1, (Norris and others, 1986), contained "caliche", (which microscopically is very fine-grained calcium carbonate) a fine-grained, earthy form of calcium carbonate associated with desert soil formation. Caliche or very fine-grained calcium carbonate was observed for the first 24 m (80 ft) in the drill hole or about 9 m (30 ft) below the surface governed by the slope (a similar depth of caliche filling is seen in test pit 1). Beyond 24 m (80 ft) into the ridge, sporadic calcite was sparry, indicating longer, more stable conditions of crystallization. Although in many places the microscopic very fine-grained calcium carbonate is in the center of the veinlets and locally post-dates the comb quartz on the side of the veinlets, there are also many places where very fine-grained calcium carbonate and quartz are intergrown and seemingly were deposited together. From these relations, we would infer that the quartz is also pedogenic and related to the development of the soil profile, probably being deposited more slowly than the very fine-grained calcium carbonate, but both deposited as a result of transpiration of ground water (Stuckless and others, 1992). The genesis of the very fine-grained calcium carbonate cement is most likely authigenic.

DISCUSSION

Hydrologic Implications

Fluid flow through a fracture network depends in part on how well the fractures are interconnected. Fracture connectivity, in turn, is dependent upon fracture size and orientation distributions, fracture density, and the fracture system geometry, particularly the distribution of intersection types, all of which can be measured or described through

field observations and geometric analysis of the resulting pavement maps. Complex fracture networks, such as the one exposed at P2001, are typically well-connected since the development through time of multiple fracture sets promotes fracture interaction. Abundant cooling joints and early tectonic joints limited the amount of available area for subsequent fractures to propagate, thus many late fractures simply connect early-formed fractures. Fracture radii within the middle nonlithophysal zone must be quite large, judging from the long trace lengths and heights of the three sets of cooling joints and the T1 and T2 tectonic fractures at P2001. Many of the tectonic and cooling fractures exposed in Pit 1 and in the box cut around the Large Block Experiment extend the full height of the pits, at least 8 meters (26 feet). The subhorizontal C3 joints have exceptionally long trace lengths and probably act as important connectors between tectonic fractures and cooling joints in the two units, many of which terminate against the subhorizontal features or cross them.

The small portion of the upper lithophysal zone exposed at P2001 appears to be less well connected than the underlying middle nonlithophysal zone. High lithophysae density appears to interfere with fracture propagation. As a result, fracture trace lengths are shorter, fewer fractures from each set are present, and there are a greater proportion of blind fracture terminations. We do not know if the portion of the upper lithophysal zone exposed at P2001 is representative of the entire zone.

Geometric analysis of the P2001 pavement has yielded data on fracture intensity, fracture intersection intensity and termination probabilities (table 4, figs. 19 and 20).

TABLE 4. NEAR HERE

FIGURE 19. NEAR HERE

FIGURE 20. NEAR HERE

For comparison, we conducted a similar geometric analysis on the four published maps of pavements constructed elsewhere on Yucca Mountain and Fran Ridge (Barton and Hsieh, 1989; Barton and others, 1993). Fracture intensity can be displayed in a number of ways, one common way is to report the number of fractures per area. This measure of intensity is unsatisfactory, however, because it is scale-dependent; fracture intensity changes as the measuring region changes. A scale-independent measure of intensity, such as fracture trace length per unit area (units of 1/m) is a much more reliable tool for describing intensity and for comparison between pavements. Both intensity measures are reported in table 4 and fig 20. Fracture intensity varies for the P2001 pavement from a high of 1.7 m/m^2 in the middle nonlithophysal zone around Pit 1 to a low of 0.54 m/m^2 in the upper lithophysal zone. The average fracture intensity for the entire pavement is around 0.82 m/m^2. This average value compares favorably to fracture intensities from three pavements in the upper lithophysal zone of the Tiva Canyon Tuff (fig. 19). Fracture intensity in the middle nonlithophysal zone around Pit 1 appears to be slightly greater than that seen in the Tiva Canyon Tuff pavements; fracture intensity in the upper lithophysal zone is much less (fig. 19). Intersection intensity (fig. 20) is calculated as the number of fracture intersections per area ($\#/m^2$). As with fracture intensity, values for

Table 4. Geometric analysis of Yucca Mountain pavements

[Fracture intensities calculated as trace length per area, m/m^2, and number per area, #/m^2. Intersection intensity is calculated as number of intersections per area, #/m^2. Termination probability is the percentage of all fracture intersections that are T-terminations. Termination percentage is the percentage of all fracture endpoints, including blind or covered ends, that end in T-terminations]

Data Category	P2001			P1000	P100	P200	P300
	Pavement average	Upper lithophysal	Middle non-lithophysal				
Total number of map trace segments	527	527	527	1217	440	301	503
Number of traces used in analysis	395	91	102	709	338	158	377
Total length of all traces, meters	936.5	190.8	239.7	844.4	519.1	363.5	538.5
Mean trace length, meters	2.371	2.096	2.35	1.191	1.536	2.301	1.428
Trace length standard deviation, meters	2.706	1.645	2.379	0.7992	1.508	3.199	1.439
Region area, m^2	1140.5	353.5	138.82	280	425	513	528
Number of X intersections (Xs)	102	4	70	453	130	76	81
Number of T-terminations (Ts)	265	30	118	866	182	107	260
Fracture intensity, m/m^2	0.8211	0.5397	1.727	3.016	1.221	0.7087	1.02
Fracture intensity, #/m^2	0.3463	0.2574	0.7347	2.532	0.7953	0.308	0.714
Intersection intensity, #/m^2	0.3218	0.0961	1.354	4.711	0.7341	0.3567	0.6458
Termination probability (P[T/I]) %	72.21	88.24	62.77	65.66	58.33	58.47	76.25
Termination percentage (T%) %	39.26	20.41	79.73	70.18	28.62	39.63	38.35

Fig. 19. Comparison of fracture intensity, Yucca Mountain pavements. Fracture intensity is shown as number of fractures per square meter (upper figure) and as fracture trace length per square meter (lower figure). Upper and lower data points for each pavement define a range of intensitites derived from geometric analysis of several sub-regions of each pavement. Upper and lower data point for pavement P2001 define typical values for the middle nonlithophysal zone (Mnl) and upper lithophysal zone (Ul), respectively. Pavements 100, 200 and 300 (P100, P200 and P300) are within the upper lithophysal zone of the Tiva Canyon Tuff on Live and Dead Yucca ridges, Yucca Mountain. Pavement 1000 (P1000) is in the middle nonlithophysal zone of the Topopah Spring Tuff at the southern end of Fran Ridge.

Fig. 20. Comparison of fracture intersection intensity, Yucca Mountain pavements. Intersection intensity is shown as number of fracture intersections per square meter. Symbol ranges and pavement designations as in Fig. 19.

intersection intensity are similar to those for pavements in the Tiva Canyon Tuff.

Fracture and intersection intensity from P2001 may also be compared pavement 1000 (P1000) (figs. 19 and 20 and table 4). This pavement exposes the middle nonlithophysal zone of the Topopah Spring Tuff, the same rock unit that is exposed at P2001. P1000 is located at the southern tip of Fran Ridge, much nearer to the large splays of the Paintbrush Canyon Fault that bound Fran Ridge to the west (Scott and Bonk, 1984; Dickerson and Spengler, 1993). Pavement 1000 is much more intensely fractured and has more fracture intersections than P2001 (figs. 19 and 20 and table 4), probably as a result of proximity to these structures. Highly broken outcrops of lower lithophysal zone of the Topopah Spring Tuff at the southern end of Fran Ridge probably also reflect the zone of influence of the large faults. Pavements 2001 and 1000 may represent end-members in the possible range of fracture network properties within the middle nonlithophysal zone of the Topopah Spring Tuff. If fracture intensity is controlled by proximity to major faults, which of these pavements is used as an analog of the fracture intensity of the potential repository depends upon the number of faults projected through the repository horizon within the central block at Yucca Mountain.

Fracture intensities calculated from the horizontal borehole Ue25h#1 are not comparable to those reported here. Fracture frequencies in the cored intervals were calculated as fractures per linear meter, with a mean value of 22 fractures per meter (Norris and others, 1986). The linear fracture frequency, converted to a hypothetical set of fractures normal to the core axis for a unit cubic meter sphere (as in Scott and others, 1983), yields a calculated mean of 59 fractures per cubic unit meter (Norris and others,

1986). Conversion to the units displayed in Table 3 is difficult, but simple linear traverses across P2001 or even P1000 do not yield anywhere near this fracture intensity. In addition, the measure of the number of fractures per area is scale dependent and not good measure of intensity. The extreme fracture intensity reported for horizontal borehole Ue25h#1 may be the result of unrecognized drilling-induced fractures. Probably more important is the fact that there is no length cutoff when logging fractures in boreholes. Fracture trace length histograms at P2001 and for pavements in the Tiva Canyon Tuff (Barton and others, 1993) appear to follow power-law distributions. Fractures logged in the horizontal borehole undoubtedly include the very abundant fractures at the low end of the size range distribution that are not mapped on surface pavements. Thus, measured fracture intensity in the borehole is of little use in providing subsurface control for the fracture densities measured on the pavement.

Regional joint history and possible relations to faulting

The number, orientation and sequence of development of fracture sets at P2001 is similar in many respects to the development of the fracture network described for much of Yucca Mountain and Fran Ridge (Throckmorton and Verbeek, 1995). In addition to abundant cooling joints, four sets of steeply dipping tectonic joints in tuffs of the Paintbrush Group were recognized by Throckmorton and Verbeek (1995). Median strikes of these sets, listed in order from oldest to youngest, are N01W (T1), N31W (T2), N38E (T3), and N82W (T4). The first three sets are interpreted as products of noncoaxial regional extension during basin-range faulting; the fourth is a set of cross joints that

formed during erosional decompression and that strike at high angles to whatever older joints were already present. Observed properties of the joints of all four sets show that they originated as extension rather than shear fractures. Thus, for each set, two components of the stress field at the time of fracture can be defined: σ_3, perpendicular to the median fracture plane; and σ_{hmax}, parallel to fracture strike. The latter quantity refers to the maximum compression in the horizontal plane and is not necessarily equivalent to either of the principal stresses σ_1 or σ_2. Determining the orientations of these latter two components lies at the crux of integrating the joint history with known aspects of the faulting history of the area: for each episode of jointing, did fracture occur in a "normal" stress field (σ_1 vertical) or in a "strike-slip" stress field (σ_1 horizontal)? Partial resolution of this question can be derived from observation of slip directions on reactivated joints.

On the basis of slip directions observed on reactivated joints, two hypothetical end-member histories can be defined.

1) If σ_1 remained horizontal throughout the time span represented by the T1 through T3 episodes of extension, the stress field must first have rotated counterclockwise, from σ_1 about N-S to N31W, between the T1 and T2 events; and then clockwise, from N31W through north again and thence to about N38E, between the T2 and T3 events. The sequence of events might thus have been:

(a) formation of the T1 joint set with σ_1 oriented about N-S;

(b) counterclockwise rotation of σ_1 and initiation of left-lateral slip on

T1 joints as σ_1 assumed a northwest bearing;

(c) formation of the T2 joint set with σ_1 approximately N31W;

(d) right-lateral slip on T2 joints as the stress field began to rotate clockwise toward the T3 position;

(e) renewed growth of T1 joints and continued right-lateral slip on T2 joints as σ_1 rotated through N-S;

(f) waning of slip on T2 joints and initiation of right-lateral slip on T1 joints as the stress field continued to rotate clockwise; and

(g) formation of the T3 joint set, with σ_1 oriented approximately N38E.

This stress history could explain the down-to-the-west T1 fracture (LMF39) whose motion is oblique to the north and also explain consistent right lateral offsets along northwest-trending fractures at the Fran Ridge pavement.

2) Alternatively, if σ_1 remained vertical throughout this time span, slip on all reactivated joints would have been dominantly normal but would have included right-lateral and left-lateral components of slip, depending on the orientation of σ_3 with respect to the dip direction of the reactivated joint at any given time. Moreover, alternations between normal and strike-slip stress states are to be expected in this geologic setting, as explained by Minor (1989; and in press) and documented by him through fault-slip analysis in nearby areas to the north. A complex record of normal, oblique, and strike-slip events might thus arise from a relatively simple stress history.

The degree to which the structural record reflects either of the end-member histories mentioned above, or combinations of them, depends in large part on fluctuations in stress magnitudes through time. During the transition from the T1 to the T2 stress fields, for example, if the magnitude of the stress difference (σ_1-σ_3) remained too small in most places to overcome frictional resistance to slip on the T1 joints, little or no record of this transition might be preserved. Only a partial record of the total stress history is to be expected from any given locality, necessitating that correlations of detailed records from multiple localities be made before any pronouncements on regional histories be made. It is in this context that the history of reactivated joints on Pavement 2001 should be viewed.

Slip on steeply dipping joints at Pavement 2001 has occurred mostly on northwest-striking joints of the major cooling set and on early tectonic joints of the T1 and T2 sets. Nearly all of these faulted joints strike within the interval from due north to N35W. In addition, slickenside striae are common on gently northeast- to southeast-dipping cooling joints at this locality. Evidence of slip on the younger, ENE-striking T3 joints, in contrast, is rare despite the great numbers of these joints exposed on the pavement surface. The sole exception found to date is fracture LMF44, a short, N67E-striking T3 joint north of Pit 2, upon which local slickenside striae indicate left oblique slip. Although we believe that faulting on reactivated joints on Pavement 2001 dates mostly from the T1 through T2 events, the near absence of slickenside striae on the later T3 joints is of little help in interpreting the faulting history of this area. Most of the extension directions derived from measured slip vectors on reactivated joints at this

locality correspond to transtensional opening of the T3 joints, so that slickenside striae on their surfaces would be rare in any case.

Suggestions for further work

Although the geometry of the fracture network at P2001 is well described, it is unclear how representative this pavement is of the repository horizon as a whole or how well-connected the fracture network is throughout the Topopah Spring Tuff. Fracture data from additional pavements or additional outcrop surveys would help to determine how representative the pattern at P2001 is for the middle nonlithophysal zone of the Topopah Spring Tuff. Because of extreme sampling bias and small sample size, fracture intensity from boreholes cannot be properly extended to model the horizon. Similarly, fracture termination relationships can only be reliably obtained on a large mapped surface.

The vertical continuity of fracturing within the Topopah Spring Tuff is unknown, yet is critical in developing a fracture network model for this unit. The small amount of the upper lithophysal zone exposed at P2001 suggests that this unit may have fluid flow properties that are very different from the middle nonlithophysal zone. Presently, the character of the fracture network of each zone of the Topopah Spring Tuff, the connectivity between the zones and the fracture continuity between the Topopah Spring Tuff and overlying and underlying units are all unknown. Characterization of the vertical continuity of fracturing within the Topopah Spring Tuff would be a logical extension of current fracture network modeling of the Tiva Canyon Tuff and current surface mapping

of the vertical continuity of fractures within the bedded units that lie between the Tiva Canyon Tuff and the Topopah Spring Tuff.

The geometric analysis presented here for P2001 is only the first step towards understanding the hydrologic properties of the fracture network within the Topopah Spring Tuff. The critical element is to define the fractures that are important to flow. To this end, 3-D fracture network geometry must be combined with permeability testing to establish connected pathways. An integration of the geometric data from P2001 with the results of infiltration tests conducted in the box cut surrounding the Large Block Experiment would provide some useful information, but extensive permeability testing awaits penetration of the Topopah Spring Tuff by the ESF. In addition, the geometric aspects of the fracture network need to be combined with material properties of fracture-filling materials in order to asses the role of fracture-filling matrials in fracture flow.

Finally, geometric analysis of fracture data needs to be combined with past and ongoing structural mapping within the site area to evaluate the effect of major faults on the regional fracture pattern and to arrive at a regional paleostress history. Partial integration of the faulting and jointing histories from a single locality furnishes only a small part of the information needed for reconstruction of the regional paleostress history, as the prior results from Minor (1989; and in press) make clear. Moreover, our preliminary interpretations as presented here are based on unreduced data and have not yet received the benefit of computerized fault-slip analysis, from which stress states during any given episode of faulting can be more fully derived.

REFERENCES

Barton, C.C., Howard, T.M., and Larsen, E., 1984, Tubular structures on the faces of cooling joints - A new volcanic feature (abs.): Eos, Transactions of the American Geophysical Union, v. 65, p. 1148. (NNA.920814.0109)

Barton, C.C., and Hsieh, P.A., 1989, Physical and hydrologic flow properties of fractures: Field trip guidebook T385: International Geologic Congress, 28th, Washington, D.C., American Geophysical Union, 36 p. (HQX.890818.0028)

Barton, C.C., Page, W.R., and Morgan, T.L., 1989, Fractures in outcrops in the vicinity of drill hole USW G-4, Yucca Mountain, Nevada--Data analysis and compilation: U.S. Geological Survey Open-File Report 89-92, 133 p.

Barton, C.C., Larsen, E., Page, W.R., and Howard, T.M., 1993, Characterizing fractured rock for fluid-flow, geomechanical, and paleostress modeling: Methods and preliminary results from Yucca Mountain, Nevada: U.S. Geological Survey Open-File Report 93-269, 62 p. (GS940608314222.002)

Barton, N. R., and Choubey, V., 1977, The shear strength of rock joints in theory and practice: Rock Mechanics, v. 10, p. 1-54. (HQS.880517.2610)

Buesch, D.C., Spengler, R.W., Moyer, T.C., and Geslin, J.K., 1995, Revised stratigraphic nomenclature and macroscopic identification of lithostratigraphic units of the Paintbrush Group exposed at Yucca Mountain, Nevada: U.S. Geological Survey Open-File Report 94-469, *in press*.

Byers, F.M., Jr., 1985, Petrochemical variation of Topopah Spring Tuff matrix with depth (Stratigraphic Level), Drill hole USW G-4, Yucca Mountain, Nevada: Los Alamos National Laboratory Report LA-10561-MS, 38 pp.

Byers, F.M., Jr., and Moore, L.M., 1987, Petrographic variation of the Topopah Spring Tuff matrix within and between cored drill holes, Yucca Mountain, Nevada: Los Alamos National Laboratory Report LA-10901-MS, 72 pp.

Dickerson, R.P., and Spengler, R.W., 1994, Structural character of the northern segment of the Paintbrush Canyon fault, Yucca Mountain, Nevada: High Level Radioactive Waste Management, Proceedings of the Fifth Annual International Conference, vol. 4, pp. 2367-2372.

Haimson, B.C., Lacomb, J., Jones, A.H., and Green, S.J., 1974, Deep stress measurement in tuff at the Nevada Test Site: Advances in Rock Mechanics, v. IIa, National Academy of Sciences, Washington, D.C., p. 557-561.

ISRM, 1978, Suggested Methods for the Quantitative Description of Discontinuities in Rock Masses: International Journal of Rock Mechanics, Minerals Science and Geomechanics Abstracts, v. 15, pp. 319-368.

Izett, G.A., 1981, Volcanic ash beds; recorders of upper Cenozoic silicic pyroclastic volcanism in the Western United States: Journal of Geophysical Research, v.86, no. B11, p. 10200-10222.

Izett, G.A., Obradovach, J.D., and Mehnert, H.H., 1988, The Bishop ash bed (Middle Pleistocene) and some older (Pliocene and Pleistocene) chemically and mineralogically similar ash beds in California, Nevada, and Utah: U.S. Geological Survey Bulletin 1675, 37 p.

Levy, S.S. and Naeser, C.W., 1991, Bedrock breccias along fault zones near Yucca Mountain, Nevada: Los Alamos National Laboratory Report LA-UR-91-145, 25 p.

Minor, S.A., 1989, Paleostress investigation near Rainier Mesa, Nevada Test Site, *in* Olsen, C.W., and Carter, J.A. (eds.), Fifth Symposium on Containment of Underground Nuclear Explosions, Proceedings, v. 2, p. 457-482.

Minor, S.A., *in press*, Superimposed local and regional paleostresses--fault-slip analysis of Neogene Basin-and-Range faulting near a middle Miocene caldera complex, Yucca Flat, southern Nevada: Journal of Geophysical Research.

Norris, A.E., Byers, F.M., Jr., and Menson, T.J., 1986, Fran Ridge Horizontal Coring Summary Report, Hole UE-25#1, Yucca Mountain Area, Nye County, Nevada: Los Alamos National Laboratory Report LA 10859-MS, 78p.

Petit, J.P., 1987, Criteria for the sense of movement on fault surfaces in brittle rocks: Journal of Structural Geology, vol. 9, no. 5/6, p. 597-608.

Pollard, D.D., and Aydin, A., 1988, Progress in understanding jointing over the past century: Geological Society of America Bulletin, v. 100, p. 1181-1204.

Rogers, A.M., Harmsen, S.C., Carr, W.J., and Spence, William, 1983, Southern Great Basin seismological data report for 1981 and preliminary data analysis: U.S. Geological Survey Open-File Report 83-669, 243 p.

Sawyer, D.A., Fleck, R.J., Lamphere, M.A., Warren, R.G., Broxton, D.E., and Hudson, R., 1994, Episodic caldera volcanism in the Miocene southwestern Nevada Volcanic Field: Revised stratigraphic framework, $^{40}Ar/^{39}Ar$ geochronology, and implications for magmatism and extension: Geological Society of America Bulletin, v.106, p. 1304-1318.

Scott, R.B, Spengler, R.W., Diehl, S., Lappin, A. R., and Chornack, M.P., 1983, Geologic character of tuffs in the unsaturated zone at Yucca Mountain, southern Nevada: *in* Role of the unsaturated zone in radioactive and hazardous waste disposal; Mercer, J.W., Rao, P.S.C., and Marine, I.W., eds.,: Ann Arbor Science Publishers, Ann Arbor, Michigan, p. 289-335.

Scott, R.B., and Bonk, Jerry, 1984, Preliminary geologic map of Yucca Mountain, Nye County, Nevada, with geologic sections: U.S. Geological Survey Open File Report 84-494: scale 1:12000. (HQS.880517.1443)

Springer, J.E., Thorpe, R.K., and McKague, H.L., 1984, Borehole elongation and its relation to tectonic stress at the Nevada Test Site: Lawrence Livermore National Laboratory Report UCRL-53528, 43 p.

Stock, J.M., Healy, J.H., Hickman, S.H., and Zoback, M.D., 1985, Hydraulic fracturing stress measurements at Yucca Mountain, Nevada, and relationship to the regional stress field: Journal of Geophysical Research, v. 90, no. B10, p. 8691-8706.

Stock, J.M., and Healy, J.H., 1988, Stress field at Yucca Mountain, Nevada, *in* Carr, M.D., and Yount, J.C. (eds.), Geologic and hydrologic investigations of a potential nuclear waste disposal site at Yucca Mountain, southern Nevada: U.S. Geological Survey Bulletin 1790, p. 87-94.

Stuckless, J.S., Peterman, Z.E., Forester, R.M., Whelan, J.F., Vaniman, D.T., Marshall, B.D., and Taylor, E.M., 1992, Characterization of fault-filling deposits in the vicinity of Yucca Mountain, Nevada, Waste Management '92 Conference Proceedings, pp. 929-935.

Terzaghi, R.D., 1965, Sources of error in joint surveys: Géotechnique, v. 15, p. 287-304.

Throckmorton, C.K., and Verbeek, E.R., 1995, Joint networks in the Tiva Canyon and Topopah Spring Tuffs of the Paintbrush Group, southwestern Nevada: U.S. Geological Survey Open File Report 95-2, 179 pp.

APPENDIX 1 - ORIENTATION, SIZE AND ROUGHNESS DATA FOR FRACTURES AT PAVEMENT P2001

Appendix 1. Orientation, size and roughness data for fractures at pavement P2001.

[Location of numbered fractures shown on accompanying map. Azimuth and dip follow right-hand rule convention; dip direction is 90 degrees clockwise from strike. Reported orientation represents average fracture orientation, individual measurements may vary by 5-10 degrees for both strike and dip. A range of values is reported for curved fractures. Roughness coefficient (RC) follows Barton and Choubey (1977)]

Number	Azimuth	Dip	Dip Direction	Trace Length		Trace Height		RC	Remarks
				Feet	Meters	Feet	Meters		
DSF1	335 to 340	84	65	43	13.1	--	--	2	Does not offset cooling joint DSJ1. DSF1 may be offset at N end.
DSF2	315 to 328	70	58	46	14.0	--	--	1	Azimuth is near N30W at N and S ends, changes to N45W in central portion.
DSF3	336	80	66	16.5	5.0	--	--	8	--
DSF4a	325	72	235	34	10 4	--	--	4	DSF4 is a pair of parallel fractures 15 cm. apart. The western fracture dips west, the eastern fracture dips east. Fractures temporarily join near intersection with DSF33.
DSF4b	325	85	55	34	10.4	--	--	4	--
DSF5	344	75	74	15	4.6	--	--	4	May offset DSF114 with apparent right lateral separation.
DSF6	346	86	76	31	9.4	--	--	10	DSF6 is a brecciated zone (Type III) 15-30 cm. wide
DSF7	326	73	56	17	5.2	--	--	--	Fracture surface not well exposed.
DSF8	314	80	44	11	3 4	--	--	--	--
DSF9	325	82	55	32	9 8	--	--	3	--
DSF10	324 to 332	84	58	25	7 6	--	--	--	Azimuth is N28W at south end, N36W at north end
DSF11	60	62	330	13	4 0	--	--	8	--
DSF12	62	83	152	6.5	2.0	--	--	--	--
DSF13	60	90	150	7	2.1	--	--	8	--
DSF14	45	45	315	7.5	2 3	--	--	9	--
DSF15	21	90	111	9	2.7	--	--	--	--
DSF16	8	85	98	11	3.4	--	--	10	--
DSF17	326	72	236	6	1.8	--	--	--	--
DSF18	70 to 90	81	170	5	1.5	--	--	2	Azimuth for most of length is near N90E, azimuth is N70E where it curves towards DSF2.

Appendix 1. Orientation, size and roughness data for fractures at pavement P2001.

Number	Azimuth	Dip	Dip Direction	Trace Length		Trace Height		RC	Remarks
				Feet	Meters	Feet	Meters		
DSF19	55	81	325	9.5	2.9	--	--	5	--
DSF20	60	90	150	5	1.5	--	--	--	Mostly covered by caliche.
DSF21	300 to 340	54	230	17	5.2	--	--	16	Curving fracture with an azimuth of N20W at south end, N60W at north end
DSF22	325 to 340	86	243	16	4.9	--	--	18	--
DSF23	324	74	54	17	5.2	20	6.1	2	Extends from pavement surface to the bottom of northern test pit (Pit#1).
DSF24	338	80	248	17	5.2	20	6.1	--	Extends from pavement surface to the bottom of northern test pit (Pit#1).
DSF25	324 to 345	61	54	4.6	1.4	--	--	3	--
DSF26	5 to 45	90	108	7.8	2.4	--	--	12	Minor curved fracture; azimuth is N45E at the south end, N5E at north end.
DSF27	60 to 72	64	335	7.4	2.3	--	--	10	--
DSF28	352	72	262	20	6.1	10	--	5	Extends into northern test pit (Pit#1).
DSF29	318	77	48	12	3.7	--	--	9	--
DSF30	85 to 95	77	345	11	3.4	--	--	11	--
DSF31	83	79	350	7	2.1	--	--	--	--
DSF32	55	50	325	20	6.1	20	6.1	16	Extends from pavement surface to the bottom of northern test pit (Pit#1).
DSF33	007 to 013	79	280	71	21.6	--	--	10	Single fracture at south end near pit#2, becomes wider, more brecciated and increasingly associated with subparallel fractures northward.
DSF34	004 to 016	69	274	12 2	3.7	--	--	12	--
DSF35	290 to 299	73	201	5.2	1.6	--	--	9	--
DSF36	76	82	166	6.8	2.1	--	--	9	--
DSF37	290 to 309	75	219	17.5	5.3	--	--	11	--
DSF38	007 to 038	90	115	27	8.2	--	--	11	Curving fracture; azimuth near N38E at south end, subparallel to DSF33 (N10E) at north end.
DSF39	29	--	--	7	2.1	--	--	--	Dip cannot be measured.
DSF40	080 to 100	90	4	9.5	2.9	--	--	4	Curved fracture; azimuth is N80E at west end, N80W at east end.

Appendix 1. Orientation, size and roughness data for fractures at pavement P2001.

Number	Azimuth	Dip	Dip Direction	Trace Length		Trace Height		RC	Remarks
				Feet	Meters	Feet	Meters		
DSF41	040 to 045	90	133	14.5	4 4	--	--	8	Curved fracture.
DSF42	15	--	--	18	5 5	--	--	--	Dip cannot be measured
DSF43	075 to 084	77	170	18	5.5	--	--	3	Azimuth is N75E at east end, N84E at west end.
DSF44	57	--	--	13	4.0	--	--	--	Offset by DSF7, 2 cm apparent right lateral separation. No offset across DSF4.
DSF45	000 to 060	75-90	280	17	5 2	--	--	--	Curving fracture with variable dip; near vertical at south end, dips 75W at north end.
DSF46	24	90	114	6	1.8	--	--	--	Dip is difficult to measure accurately.
DSF47	335 to 350	80	250	9	2.7	--	--	--	Offset by DSF48, 2 cm apparent left lateral separation.
DSF48	024 to 035	75	120	7.5	2.3	--	--	--	At its SW end, DSF48 is a 20 cm wide zone of three anastamosing, very rough fractures. These fractures join to become a single, discrete fracture at the NE end.
DSF49	54	90	144	12	3.7	--	--	--	Offset by DSF1, 2 cm apparent right lateral separation. No offset across DSF62.
DSF50	005 to 055	68-80	125	5.5	1.7	--	--	--	Curving fracture with variable dip; attitude at SW end is N55E/80E, at NE end N5E/68E.
DSF51	272 to 286	90	2	6.5	2.0	--	--	--	Azimuth is N88W at east end, N74W at west end.
DSF52	335 to 355	90	76	8	2.4	--	--	--	DSF52 consists of two fractures with individual lengths less than 5 feet, joined by a possible hooking relationship near DSJ1. They do not offset DSJ1.
DSF53	355 to 015	56	288	12	3.7	--	--	3	Smooth, wavy fracture. Waviness has wavelength of 1 meter and amplitude of 10 cm
DSF54	000 to 026	85	103	15	4.6	--	--	--	Azimuth is N26E at north end, N-S at south end.
DSF55	000 to 025	90	101	23	7.0	--	--	6	Appears to be the dominant thoroughgoing fracture of the group DSF53, DSF54, DSF55.
DSF56	19	70	289	4.5	1.4	--	--	--	
DSF57	11	90	101	5	1.5	--	--	--	
DSF58	350 to 001	75	260	5.5	1.7	--	--	--	Azimuth is N10W for most of length, becomes north-south at south end.
DSF59	318	90	48	5.5	1.7	--	--	7	Wavy fracture. Waviness has wavelength of 0.3 meter and amplitude of 2 cm
DSF60	357	82-90	87	16	4.9	20	6.1	5	Extends from pavement surface to the bottom of northern test pit (Pit#1). Dip measured as 82E on pavement but steepens to near vertical within pit.
DFS61	358	77	268	10	3 0	--	--	5	Extends from pavement surface to the bottom of northern test pit (Pit#1).
DSF62	002 to 013	60-72	288	32	9.8	8	2.4	2	South end dips 72 to the west, north end dips about 60 to the west.

Appendix 1. Orientation, size and roughness data for fractures at pavement P2001.

Number	Azimuth	Dip	Dip Direction	Trace Length		Trace Height		RC	Remarks
				Feet	Meters	Feet	Meters		
DSF63	332	86	62	9	2.7	--	--	1	Possibly the continuation of DSF1. If so, DSF1 is offset by DSF62 with 30 cm. apparent right lateral strike separation.
DSF64	326	90	56	10 5	3.2	--	--	4	Parallel to DSF63 but crosses DSF62 with no offset.
DSF65	356	89	86	15	4.6	--	--	5	South end curves to N43W.
DSF66	044 to 051	90	140	17	5.2	--	--	3	Offset by DSF65 with 4 cm. apparent right lateral strike separation.
DSF67	3	90	93	13	4.0	--	--	--	
DSF68	52	90	142	15	4.6	--	--	9	Offset by DSF65 with 4 cm. apparent right lateral strike separation.
DSF69	10	80	100	17	5.2	--	--	6	Extends from pavement surface to the bottom of northern test pit (Pit#1).
DSF70	355	78	265	5.5	1.7	--	--	4	
DSF71	089 to 113	60-75	192	11	3.4	--	--	2	Very irregular fracture. Average attitude N78W/65S.
DSF72	157	77	247	10	3.0	--	--	3	No offset at DSF71.
DSF73	354 to 008	77	281	4.5	1.4	--	--	3	
DSF74	46	84	136	6	1.8	--	--	9	
DSF75	15	90	105	5	1.5	--	--	--	
DSF76	040 to 063	70	135	8	2.4	--	--	3	Irregular fracture, average strike is N45E.
DSF77	004 to 020	83	109	10	3.0	--	--	6	Irregular fracture, average strike is N19E.
DSF78	16	77	286	8	2.4	--	--	5	
DSF79	9	86	99	13	4.0	--	--	--	
DSF80	352 to 356	90	86	12	3.7	--	--	Very rough	Dip difficult to measure, but fracture is nearly vertical.
DSF81	341	75	251	9	2.7	--	--	Rough	
DSF82	342	90	72	15	4.6	--	--	--	Fracture walls at south end dips steeply toward each other, overall fracture is probably nearly vertical.
DSF83	348	90	78	6	1.8	--	--	Very rough	
DSF84	347	80	257	10	3.0	--	--	Rough	

Appendix 1. Orientation, size and roughness data for fractures at pavement P2001.

Number	Azimuth	Dip	Dip Direction	Trace Length		Trace Height		RC	Remarks
				Feet	Meters	Feet	Meters		
DSF85	352	80	262	12	3.7	--	--	Rough	
DSF86	338 to 348	87	68	13	4.0	--	--	9	
DSF87	353	90	83	5 5	1.7	--	--	Very rough	Dip difficult to measure, but fracture is nearly vertical
DSF88	76	--	--	6	1.8	--	--	--	Dip cannot be measured.
DSF89	343	89	253	5 5	1.7	--	--	Rough	
DSF90	358	88	88	18	5.5	--	--	8	
DSF91	336 to 352	80-85	262	11	3.4	--	--	14	Azimuth is N8W over most of length, curves to N23W at north end
DSF92	333 to 355	74	250	12	3.7	--	--	10	Azimuth is N5W at south end, N27W at north end.
DSF93	164	87	254	6	1.8	--	--	--	
DSF94	346	90	76	10 5	3.2	--	--	9	Dip difficult to measure, but fracture is nearly vertical.
DSF95	059 to 066	80	145	5 5	1.7	--	--	8	
DSF96	070 to 089	75	152	4	1.2	--	--	14	
DSF97	059 to 078	80	153	6	1.8	--	--	16	Average azimuth is N63E.
DSF98	332	80	62	7	2.1	--	--	Smooth	
DSF99	354	90	84	9	2.7	--	--	4	Dip difficult to measure, but fracture is nearly vertical.
DSF100	349	85	259		0.0	--	--	--	Near east end, fracture is the boundary between intact rock on the east and type II brecciated rock on the west
DSF101	353	--	--	8	2 4	--	--	--	Fracture is vertical to steeply west-dipping. Fracture separates intact rock on the east from type II brecciated rock on the west.
DSF102	320	75	230	7.5	2.3	--	--	Rough	
DSF103	335 to 345	90	70	5	1.5	--	--	--	Dip difficult to measure, but fracture is nearly vertical.
DSF104	340 to 355	89	80	9	2.7	--	--	--	Azimuth is N5W at south end, N20W at north end.
DSF105	2	89	272	4	1.2	--	--	7	Lens of type I breccia filling fracture. A second lens of this breccia 0.6 m in length occurs a few feet to the southwest.
DSF106	355	90	85	9	2.7	--	--	8	Does not offset cooling joint DSJ5. Appears to offset DSF107 with 2 cm. apparent right lateral strike separation.

Appendix 1. Orientation, size and roughness data for fractures at pavement P2001.

Number	Azimuth	Dip	Dip Direction	Trace Length		Trace Height		RC	Remarks
				Feet	Meters	Feet	Meters		
DSF107	020 to 050	90	140	12	3.7	--	--	8	Azimuth is N50E for most of length, curves to N20E at north end. Dip varies from 80NW south of intersection with DSF106 to vertical at the intersection, to 80SE north
DSF108	353	85	263	7	2.1	--	--	12	
DSF109	0	90	90	9	2.7	--	--	very rough	
DSF110	351	85	261	5	1.5	--	--	11	
DSF111	350	85	260	8	2.4	--	--	9	
DSF112	080 to 100	90	10	7	2.1	--	--	--	Dip difficult to measure, but fracture is nearly vertical.
DSF113	322	65	232	11	3.4	--	--	rough	
DSF114	73	90	163	11	3.4	--	--	8	Offset by DSF5 with 15 cm apparent right lateral separation.
LMF1	5	72	275	5.5	1.7	--	--	14	
LMF2	353	72	263	5	1.5	--	--	10	
LMF3	65	74	335	5 8	1.8	--	--	8	
LMF4	62	84	332	5	1.5	--	--	12	
LMF5	52	78	322	8.8	2.7	--	--	6	
LMF6	355	82	265	5.8	1.8	--	--	6	
LMF7	356	77	266	12.8	3.9	--	--	4	
LMF8	50	84	320	5	1.5	--	--	7	
LMF9	345	80	255	14.5	4.4	--	--	8	
LMF10	325 to 335	80	240	21 5	6.6	--	--	7	Azimuth is N35W at south end, N25W at north end.
LMF11	348	82	78	10	3.0	--	--	9	
LMF12	345 to 002	82	260	14.5	4.4	--	--	11	Azimuth is N2E at south end, N15W at north end.
LMF13	328	88	238	12.5	3.8	--	--	8	
LMF14	347	87	257	5	1.5	--	--	6	

Appendix 1. Orientation, size and roughness data for fractures at pavement P2001.

Number	Azimuth	Dip	Dip Direction	Trace Length		Trace Height		RC	Remarks
				Feet	Meters	Feet	Meters		
LMF15	345	87	255	5	1.5	--	--	10	
LMF16	334	88	244	21	6.4	--	--	4	
LMF17	324	82	234	6	1.8	--	--	5	
LMF18	332	76	242	10	3.0	--	--	8	
LMF19	334	76	244	10.5	3.2	--	--	7	
LMF20	354	74	264	6.3	1.9	--	--	15	
LMF21	(S-2)(N-15)	82	277	14.5	4.4	--	--	8	Azimuth is N2E at south end, N15E at north end.
LMF22	352	76	262	13.2	4.0	--	--	9	
LMF23	18	84	288	5.2	1.6	--	--	11	
LMF24	350	81	260	6.1	1.9	--	--	15	
LMF25	353	84	263	6.7	2.0	--	--	10	
LMF26	330	84	240	17.5	5.3	--	--	16	
LMF27	342	78	252	12.6	3 8	--	--	8	
LMF28	335	88	245	5.3	1.6	--	--	6	
LMF29	345	81	255	13 3	4.1	--	--	11	
LMF30	330	87	240	5.5	1.7	--	--	12	
LMF31	25	86	115	6	1.8	--	--	12	
LMF32	74	46	164	7.6	2.3	--	--	7	
LMF33	70	76	340	5.8	1.8	--	--	14	
LMF34	38	88	308	6 5	2.0	--	--	8	
LMF35	66	76	156	4.9	1.5	--	--	5	
LMF36	329	84	239	16.5	5.0	--	--	8	

Appendix 1. Orientation, size and roughness data for fractures at pavement P2001.

Number	Azimuth	Dip	Dip Direction	Trace Length		Trace Height		RC	Remarks
				Feet	Meters	Feet	Meters		
LMF37	305	77	215	6.5	2.0	--	--	10	
LMF38	330	86	240	29	8 8	--	--	7	
LMF39	355	74	265	69	21.0	--	--	9	Fault that offsets cooling joints near target 115. Appears to be offset by LMF133 with 15 cm. apparent right-lateral strike separation.
LMF40	290	76	200	5.2	1.6	--	--	10	
LMF41	75	80	165	9.8	3.0	--	--	10	
LMF42	294	88	204	4.2	1.3	--	--	9	
LMF43	340	81	250	6.6	2.0	--	--	10	
LMF44	67	88	337	4.2	1.3	--	--	8	
LMF45	327	82	57	7.5	2 3	--	--	8	
LMF46	24	75	294	5.8	1.8	--	--	14	
LMF47	30	84	300	9.4	2.9	--	--	12	
LMF48	65	87	155	20.5	6.2	--	--	14	
LMF49	335	88	245	25 2	7.7	--	--	8	
LMF50	42	86	132	7.7	2 3	--	--	9	
LMF51	50	81	320	15.6	4.8	--	--	11	
LMF52	330	70	240	9 8	3.0	--	--	12	
LMF53	357	88	267	6.8	2.1	--	--	15	
LMF54	330	78	240	5.5	1.7	--	--	11	
LMF55	30	79	349	5	1.5	--	--	14	
LMF56	14	78	284	3.5	1.1	--	--	15	
LMF57	70	88	160	4.5	1.4	--	--	12	
LMF58	28	76	298	8	2.4	--	--	9	

Appendix 1. Orientation, size and roughness data for fractures at pavement P2001.

Number	Azimuth	Dip	Dip Direction	Trace Length		Trace Height		RC	Remarks
				Feet	Meters	Feet	Meters		
LMF59	352	83	262	5.6	1.7	--	--	9	
LMF60	348	84	258	10	3.0	--	--	9	
LMF61	358	85	268	7 6	2.3	--	--	8	
LMF62	64	88	154	5	1.5	--	--	9	
LMF63	320	88	50	7.5	2.3	--	--	15	
LMF64	286	87	16	5	1.5	--	--	16	
LMF65	332	86	242	7.4	2.3	--	--	15	
LMF66	57	87	147	4.7	1.4	--	--	10	
LMF67A	60	85	150	6.5	2.0	--	--	15	
LMF67B	65	88	235	0 0		--	--	8	
LMF68	326	79	236	10.8	3 3	--	--	12	
LMF69	340	83	250	12.5	3.8	--	--	7	
LMF70	332	87	242	9	2.7	--	--	9	
LMF71	344	79	254	7 2	2.2	--	--	5	
LMF72	72	89	342	7.4	2.3	--	--	5	
LMF73	25	88	295	5.2	1.6	--	--	16	
LMF74	14	82	284	6.7	2.0	--	--	16	
LMF75	330	82	240	7.4	2.3	--	--	14	
LMF76	285	86	195	4.5	1.4	--	--	12	
LMF77	358	79	268	8	2.4	--	--	8	
LMF78	325	77	235	11.5	3.5	--	--	7	
LMF79	50	75	140	7	2.1	--	--	5	

Appendix 1. Orientation, size and roughness data for fractures at pavement P2001.

Number	Azimuth	Dip	Dip Direction	Trace Length		Trace Height		RC	Remarks
				Feet	Meters	Feet	Meters		
LMF80	54	86	144	6	1.8	--	--	5	
LMF81	62	87	152	5	1.5	--	--	12	
LMF82	352	86	262	8.7	2.7	--	--	10	
LMF83	359	87	269	8	2.4	--	--	8	
LMF84	11	89	281	7	2.1	--	--	10	
LMF85	350	86	260	5.8	1.8	--	--	10	
LMF86	325	87	235	23 2	7.1	--	--	8	Extends from pavement surface to the bottom of pit#2.
LMF87	44	79	314	6.6	2.0	--	--	8	
LMF88	65	89	155	12.6	3 8	--	--	8	
LMF89	347	89	77	20.4	6.2	--	--	9	
LMF90	10	79	280	5.8	1.8	--	--	12	
LMF91	18	84	108	9.3	2.8	--	--	7	
LMF92	19	87	109	7	2.1	--	--	9	
LMF93	359	86	269	8 2	2.5	--	--	8	
LMF94	8	88	278	6.6	2.0	--	--	8	
LMF95	30	79	300	13 8	4.2	--	--	8	
LMF96	20	86	290	9	2.7	--	--	8	
LMF97	59	87	149	15.8	4.8	--	--	9	
LMF98	318	75	48	11.3	3.4	10	3	10	Appears to be the southward continuation of LMF133. Extends from pavement surface to the bottom of pit#2
LMF99	329	76	239	11.4	3.5	--	--	7	
LMF100	50	84	320	5 2	1.6	--	--	5	
LMF101	316	83	46	5	1.5	--	--	6	

Appendix 1. Orientation, size and roughness data for fractures at pavement P2001.

Number	Azimuth	Dip	Dip Direction	Trace Length		Trace Height		RC	Remarks
				Feet	Meters	Feet	Meters		
LMF102	315	89	45	18.6	5.7	10	3	7	Appears to be the southward continuation of LMF137. Extends from pavement surface to the bottom of pit#2.
LMF103	333	76	63	7	2.1	--	--	5	
LMF104	68	87	158	12 3	3.7	--	--	6	
LMF105	45	76	135	8.6	2.6	--	--	5	
LMF106	10	83	100	5.6	1.7	--	--	6	
LMF107	355	75	265	16.1	4.9	--	--	7	
LMF108	4	84	94	13.4	4.1	--	--	8	Extends from pavement surface to the bottom of pit#2.
LMF109	60	87	330	6	1.8	--	--	6	
LMF110	78	77	168	6.3	1.9	--	--	4	
LMF111	341	81	251	8.3	2.5	--	--	8	
LMF112	54	84	144	6.3	1.9	--	--	1	
LMF113	350	78	260	18.2	5.5	--	--	15	
LMF114	50	88	140	6.6	2.0	--	--	11	
LMF115	300	72	210	7.3	2.2	--	--	7	
LMF116	320	76	230	5.2	1.6	--	--	6	
LMF117	344	72	254	9.2	2.8	--	--	9	
LMF118	356	76	266	5.6	1.7	--	--	6	
LMF119	47	87	137	12.9	3.9	--	--	12	
LMF120	59	86	149	9.8	3.0	--	--	10	
LMF121	74	84	164	9.5	2.9	--	--	4	
LMF122	322	74	232	18	5.5	--	--	9	
LMF123	50	86	140	7.2	2.2	--	--	12	

Appendix 1. Orientation, size and roughness data for fractures at pavement P2001.

Number	Azimuth	Dip	Dip Direction	Trace Length		Trace Height		RC	Remarks
				Feet	Meters	Feet	Meters		
LMF124	349	72	259	10.8	3 3	--	--	9	
LMF125	2	88	272	20	6.1	--	--	5	
LMF126	74	86	344	4.8	1.5	--	--	10	
LMF127	58	88	328	6.9	2.1	--	--	6	
LMF128	305	79	215	6 8	2.1	--	--	6	
LMF129	309	84	39	4.5	1.4	--	--	4	
LMF130	325	71	235	7.8	2.4	--	--	4	
LMF131	72	85	342	4.4	1.3	--	--	8	
LMF132	332	81	242	11.5	3 5	--	--	8	
LMF133	322	85	232	13	4.0	--	--	8	
LMF134	61	87	151	5.3	1.6	--	--	9	
LMF135	320	85	50	6.2	1.9	--	--	10	
LMF136	2	88	92	11.8	3.6	--	--	7	
LMF137	324	89	54	13 2	4.0	--	--	5	
LMF138	328	74	238	5.4	1.6	--	--	6	
LMJ1	350	37	260	14	4.3	--	--	4	
LMJ2	260	15	350	10	3.0	--	--	9	
LMJ3	310	28	220	19	5.8	--	--	6	Attitude at south end, 345/50W, at north end, 326/44W
LMJ4	86	41	176	4 6	1.4	--	--	6	
LMJ5	285	34	15	6.7	2.0	--	--	6	
LMJ6	76	52	346	12.8	3.9	--	--	5	
LMJ7	60	25	330	8.7	2.7	--	--	8	

Appendix 1. Orientation, size and roughness data for fractures at pavement P2001.

Number	Azimuth	Dip	Dip Direction	Trace Length		Trace Height		RC	Remarks
				Feet	Meters	Feet	Meters		
LMJ8	310	17	220	8.8	2.7	--	--	6	
LMJ9	85	29	175	8 8	2.7	--	--	9	
LMJ10	275	28	5	8	2.4	--	--	6	
LMJ11	305	31	215	6 5	2.0	--	--	5	Attitude at southeast end, 088/29S; at north end, 005/27W
LMJ12	50	34	320	6.6	2.0	--	--	8	
DSJ1	65	74	155	20.5	6.2	--	--	1	
DSJ2	60	7	330	28	8.5	--	--	6	
DSJ3	10-350	8-14	291	18 5	5.6	--	--	6	
DSJ4	347-002	14-21	290	15.7	4.8	--	--	6	
DSJ5	72	52	162	11.5	3.5	--	--	4	
DSJ6	140	25	230	31	9 4	--	--	6	
DSJ7	0	25	90	4	1.2	--	--	1	
DSJ8	136	62	226	22	6.7	--	--	2	
DSJ9	328	25	58	8	2.4	--	--	2	
DSJ10	346	32	76	11	3.4	--	--	1	
DSJ11	331	23	61	6	1.8	--	--	3	
DSJ12	219	11	309	14	4.3	--	--	6	
DSJ13	230	10	320	7	2.1	--	--	6	
DSJ14	329-50	1-20	59-140	21	6.4	--	--	6	Gently arcuate; attitude at N end, 059/8W; near Tgt111, 000/2E; S end, 050/20S
DSJ15	5	9	95	50	15.2	--	--	6	
DSJ16	140	12-14	230	12	3.7	--	--	6	
DSJ17	0	5-10	90	33	10	--	--	6	

Appendix 1. Orientation, size and roughness data for fractures at pavement P2001.

Number	Azimuth	Dip	Dip Direction	Trace Length		Trace Height		RC	Remarks
				Feet	Meters	Feet	Meters		
DSJ18	333	8	63	20	6.1	--	--	6	
DSJ19	359-011	7-10	89-101	62	18.9	--	--	6	

APPENDIX 2 - FRACTURE ATTRIBUTES AND TERMINATIONS, PAVEMENT P2001

Appendix 2. Fracture attributes and terminations, pavement P2001.

[Fracture apertures in millimeters. Types of fracture fill described in text.]

Number	Aperture	Fill Type	Termination Relationships	Remarks
DSF1	10	Caliche	South end extends off pavement. At north end, DSF1 either terminates against DSF62 or is offset by it and continues as DSF63. If offset, the fracture is offset by DSF62 with 15 cm. right lateral strike separation.	Does not offset cooling joint DSF1. Does not offset large fracture DSF32.
DSF2	20	Caliche	North end extends off pavement. South end horsetails into three 2 meter-long fractures.	A 1 m2 zone of Type II breccia lies between DSF2 and DSF10, near their intersection with DSF6.
DSF3	2 to 10	Caliche	North end terminates against a 1 meter fracture, south end terminates against DSF55, partially covered by caliche.	
DSF4	0.1 to 15	Caliche, minor type I breccia	South end extends off pavement. North end mostly covered by caliche, fractures do not cut cooling joint DSJ2.	Typical aperture is 5 mm.
DSF5	2 to 12	Pearly calcite	South end extends off pavement. N end has low-angle termination with DSF33, with local Type II breccia near intersection.	
DSF6	150 to 300	Type II breccia	South end extends off pavement. North end terminates against DSF2 or extends into Type II breccia between DSF2 and DSF10.	This fracture forms the eastern boundary of the complicated Type II breccia mass bounded by DSF6, DSF8 and DSF9
DSF7	10	Caliche, some banded pearly calcite	North end mostly obscured by thick caliche, does not appear to be continuous with DSF98. Fracture dies out to south into several small fractures, some of which may curve into DSF5.	
DSF8	15	Caliche	North end is a low-angle Y termination with DSF7. South end extends into Type II breccia west of DSF6, possibly continues and joins with DSF6 near target 117.	
DSF9	18	Caliche, some banded pearly calcite	North end extends off pavement. South end terminates in the breccia zone west of DSF6.	
DSF10	10	Caliche, type I breccia at north end	North end extends off pavement. South end is a T termination against DSF11.	North end of fracture has a number of splays of similar orientation.

Appendix 2. Fracture attributes and terminations, pavement P2001.

Number	Aperture	Fill Type	Termination Relationships	Remarks
DSF11	--	Caliche	West end curves into a Y termination with DSF2. East end terminates against DSF52.	This is a minor, nonsystematic fracture.
DSF12	1	Open	West end is a T termination with DSF9. East end terminates against a small fracture near DSF6.	
DSF13	4	Caliche	West end is a T termination with DSF9. East end is a T termination against DSF2.	
DSF14	5	Caliche	West end is a T termination with DSF9. East end is a T termination against DSF2.	
DSF15	5	Caliche	West end is a Y termination with DSF9. East end is a Y termination against DSF2.	
DSF16	9	Caliche, some banded pearly calcite	West end is a Y termination with DSF9. East end is a Y termination against DSF2.	
DSF17	2	Open, partial caliche	North end is a Y termination against DSF12 and DSF16. South end terminates against a fracture at the edge of the breccia zone west of DSF6.	DSF12-DSF17 are minor cross-fractures between DSF9 and DSF2 and are probably younger than these two systematic fractures
DSF18	15	Caliche	East end extends off pavement. West end appears to curve into a T termination with DSF2.	
DSF19	3	Caliche	Southwest end is a Y termination with DSF6, northeast end is a Y termination with DSF2.	Offset by DSF21 with 3 cm. right lateral strike separation.
DSF20	1	--	Southwest end is a T termination with DSF6, northeast end is a probable T termination with DSF2.	Fracture mostly covered by caliche.

Appendix 2. Fracture attributes and terminations, pavement P2001.

Number	Aperture	Fill Type	Termination Relationships	Remarks
DSF21	10	Caliche	South end terminates against a small fracture near edge of pavement. North end is a Y termination with DSF6.	
DSF22	1	Caliche	South end terminates against a small fracture near edge of pavement. North end extends to the breccia west of DSF6. Small fractures within the breccia have a similar alignment to DSF22 and DSF17.	
DSF23	1	Open, partly covered	North end extends into test pit#1. South end merges with DSF24.	
DSF24	10 to 25	Type I breccia	North end extends into test pit#1. South end merges with DSF23.	From observation in pit, breccia filling only extends 0.6 m below pavement surface. However, other nearby fractures have similar fill deeper in the pit
DSF25	1	Open	Merges (low angle termination) with DSF24 at both ends.	
DSF26	1	Open, partial caliche	North end is a Y termination against DSF23. South end is a T termination with DSF29.	Minor curved fracture, partly covered by caliche
DSF27	3	Open, partial caliche	East end is a T termination with DSF23. West end is a T termination with DSF28.	Minor cross fracture.
DSF28	1	Open, partial caliche	North end extends into pit#1. South end has complicated low-angle termination with DSF55.	
DSF29	--	Open, partial caliche	Ends as an open face on north end (Blind termination). South end extends off of pavement.	
DSF30	2	Open, partial caliche	East end is a T termination with DSF29. West end T terminates against minor fractures near DSF31.	

Appendix 2. Fracture attributes and terminations, pavement P2001.

Number	Aperture	Fill Type	Termination Relationships	Remarks
DSF31	2	Open, partial caliche	East end connects with DSF30 through minor fractures. Fracture is deflected southward as it crosses DSF32 and has a low-angle termination with DSF62.	
DSF32	5	--	North end extends into pit#1. South end has a Y termination with DSF62.	
DSF33	10 to 20	Caliche, Type I breccia	North end terminates within the Type II breccia between DSF8 and DSF6. South end connects with LMF123 through minor fractures.	For most of length, fracture is caliche filled. Type I breccia occurs at north end near intersections with the large, northwest-trending fractures.
DSF34	1 to 5	Caliche	Blind termination at south end. T termination with DSF35 at north end.	May extend 15 cm. beyond DSF35
DSF35	2	Caliche	East end extends off of pavement. West end is a Blind termination.	Does not continue to DSF33.
DSF36	2	Open	Northeast end extends off of pavement. West end is a Y termination with DSF34.	Fracture mostly covered by caliche.
DSF37	1 to 2	Caliche, Type II breccia	West end is covered by caliche. East end is a horsetail of minor fractures of similar orientation.	West of DSF33, fracture is a 5 cm. zone of Type II breccia . East of DSF33, fracture is only 1-2 mm wide and filled with caliche.
DSF38	5 to 15	Caliche, pearly calcite	South end is a T termination with DSF37. North end is subparallel to DSF33 for several meters, eventually merges with DSF33.	A zone of Type II breccia exists near the intersections between DSF33, DSF38, DSF39 and DSF41.
DSF39	5 to 40	Minor type I and II breccia	South end covered by caliche. North end terminates in Type II breccia adjacent to DSF33.	
DSF40	0.1 to 3	Caliche/partially open	West end covered by caliche. East end is a T termination with DSF33.	

Appendix 2. Fracture attributes and terminations, pavement P2001.

Number	Aperture	Fill Type	Termination Relationships	Remarks
DSF41	0.1 to 30	Caliche, minor type I breccia	South end is a Y termination with DSF40. North end merges with DSF39 near intersection with DSF33.	Average aperture 10 mm.
DSF42	1 to 20	Caliche	South end is a Y termination with DSF41. North end crosses DSF43 and appears to curve into DSF33.	Average aperture 10 mm
DSF43	1 to 3	Caliche/partially open	West end covered by caliche. East end is a T termination with DSF6.	Crosses DSF33 and DSF5 with no offset. Slight southward deflection in vicinity of DSF4.
DSF44	3	Caliche	West end covered by caliche. East end is a T termination with DSF8.	Offset by DSF7 with 2 cm. right lateral strike separation. No offset at intersection with DSF4.
DSF45	10 to 25	Caliche/type I breccia	N end is a T termination with DSF31. Southwest end is a T termination against DSF10.	Type II breccia is continuous from intersection at DSF1 to the termination at DSF10.
DSF46	10	Caliche	South end is a Y termination with DSF10. North end is a Y termination with DSJ1 and DSF47.	Minor cross fracture.
DSF47	2 to 4	Caliche	South end T termination at DSJ1. North end is a Y termination DSF49.	Offset by DSF48 with 2 cm. left lateral strike separation.
DSF48	1 to 8	Caliche	Northeast end is a Y termination against DSF1. Southwest end horsetails to terminate against both DSJ1 and DSF10.	DSF48 is a 20 cm. wide zone composed of at least three anastamosing, very rough minor fractures. This zone becomes a single discrete feature at the northeast end.
DSF49	3	Caliche	Northeast end is a Y termination with DSF31. Southwest end appears to terminate against DSF10.	No offset where DSF49 crosses the large fracture DSF1.
DSF50	--	Open face	South end is a T termination with DSF1. North end curves into a low angle Y termination with DSF11.	

Appendix 2. Fracture attributes and terminations, pavement P2001.

Number	Aperture	Fill Type	Termination Relationships	Remarks
DSF51	2	Caliche	West end is a Y termination with DSF1. East end is a T termination with DSF55.	Fracture is an open face over most of its length. No offset at X intersections with DSF50 or DSF11.
DSF52	3	Caliche	Y terminations with DSF53 at south end and DSF3 on the north.	DSF52 is composed of two fractures each less than 5 feet long. They join (hook?) south of DSJ1. No offset of DSJ1.
DSF53	3	Open face	South end is a Y termination with DSF1. North end is mostly obscured under caliche, but appears to be a low angle Y termination against DSF55.	
DSF54	12	Caliche	South end is a Y termination with DSF1and DSF53. North end is mostly obscured under caliche, but appears to be a low angle Y termination against DSF55.	
DSF55	2 to 12	Caliche	South end extends off edge of pavement. North end is a complicated splay of minor fractures that have Y terminations with DSF28 and DSF29.	Aperture is 2-3 mm. at north end, 10-12 mm. at south end. North of DSJ1, this is 20 cm. wide zone of at least four subparallel, 2-3 mm. wide fractures.
DSF56	20	Caliche	North end is a Y termination with DSF1. South end terminates against DSF2.	
DSF57	35	Open	Extends off pavement on both ends.	Appears to be a minor fracture.
DSF58	10	Caliche	Extends off pavement at south end. North end terminates in complicated low angle zone with DSF28 and DSF55.	
DSF59	2 to 3	Caliche	Northwest end is a Y termination with DSF30. Southeast end is a Y termination against DSF55.	
DSF60	--	Open	North end extends into test pit#1. Blind termination on the south end.	

Appendix 2. Fracture attributes and terminations, pavement P2001.

Number	Aperture	Fill Type	Termination Relationships	Remarks
DFS61	5	Caliche	North end extends into test pit#1, intersects DSF32 within pit. T termination on the south end against DSF30.	
DSF62	2	Caliche	Y-termination against DSF10 at south end. Northern end bound the west wall of test pit#1.	
DSF63	2	Caliche	T-termination against DSF66 on north end. Y-termination against DSF62 on south end.	
DSF64	5 to 10	Open	T-termination against DSF66 on north end. Y-termination against DSF32 on south end.	
DSF65	10 to 15	Caliche	North end covered. South end is a Blind termination.	
DSF66	3 to 5	Caliche	Northeast end extends into test pit#1 and appears to truncate against a low-angle parting about 1 m below the pavement surface. Southwest end is a Y-termination against DSF10.	
DSF67	20	Caliche	North end is a Y-termination against DSF10. South end is a Blind termination near DSF68.	
DSF68	3 to 5	Caliche	Northeast end is a Y-termination against a small northeast-trending fracture. Southwest end is a Y-termination against DSF10.	
DSF69	--	Caliche	South end is a Y-termination against DSF1 and DSF31. North end extends into test pit #1.	
DSF70	1	Caliche, partly open	T-termination against DSF71 on north end. Y-termination against DSF24 on south end.	

Appendix 2. Fracture attributes and terminations, pavement P2001.

Number	Aperture	Fill Type	Termination Relationships	Remarks
DSF71	2	Caliche	West end is a blind termination - does not intersect DSF24. East end partially covered but probably Y termination with DSJ6.	
DSF72	1 to 3	Caliche	Southern termination covered, probable Y termination with a small northeast-trending fracture. Northern end is a Y-termination with DSF74, may extend 10-15 cm. beyond.	No offset at intersection with DSF71.
DSF73	1	Caliche	T-termination against DSF71 on south end. Low angle Y-termination against DSF72 on north end.	
DSF74	4	Caliche	T-termination against DSJ8 on northeast end. Y-termination against DSF24 on southwest end.	
DSF75	3 to 5	Caliche	Y terminations with DSF2 on the north, DSF9 on the south.	
DSF76	3	Caliche	Y terminations with DSF2 on the north, DSF9 on the south.	Connection to DSF9 is through small fractures of similar orientation to DSF76.
DSF77	1 to 3	Caliche	Y terminations with DSF2 on the north, DSF9 on the south.	
DSF78	1 to 3	Caliche	Y terminations with DSF2 on the north, DSF9 on the south.	
DSF79	--	Caliche	Y terminations with DSF2 on the north, DSF9 on the south.	Connection to DSF9 is through small fractures of similar orientation to DSF79.
DSF80	70 to 100	Type II breccia	Northern termination indistinct, possibly blind. Fracture widens at southern end into a fan of minor fractures.	DSF80-DSF85 form a northwest-trending zone of fractures. All are filled by type II breccia. Terminations at both ends are difficult to determine; fractures don't appear to extend north of target 119 or south of the

Appendix 2. Fracture attributes and terminations, pavement P2001.

Number	Aperture	Fill Type	Termination Relationships	Remarks
DSF81	10	Type II breccia	Northern termination indistinct, splits into two subparallel fractures due east of target 119. Possible Blind termination at southern end.	
DSF82	15 to 50	Type II breccia	Northern termination indistinct, possibly blind Fracture continues across small gully at southern end as a fan of minor fractures, does not cut DSJ11.	
DSF83	20 to 30	Type II breccia	North end, possible Y termination with DSF80. Blind termination into lithophysae at south end.	
DSF84	10 to 20	Caliche	Both terminations indistinct, possibly blind.	
DSF85	50 to 60	Type II breccia	Northern termination indistinct, possibly blind. Fracture widens at southern end into a fan of minor fractures.	North end is a discrete, breccia-filled fracture. Due west of intermediate survey point N4, it is a 15 cm. wide zone of parallel fractures.
DSF86	2 to 3	Partial open face	Both terminations indistinct, possibly blind.	
DSF87	3	Caliche	Northern end extends off pavement. Southern end is a T-termination against DSF88.	This fracture possibly extends 1.5 m south of DSF88 as expressed by an erosional trough.
DSF88	5	Caliche	Blind eastern termination; does not intersect DSF86. Western end appears to be a T-termination against DSF89.	This fracture possibly extends west of DSF89 as expressed by an erosional trough
DSF89	3 to 5	Caliche	North end is a low-angle Y termination with DSF90. Southern termination possibly blind.	Cannot prove that small fracture cutting LMJ2 is the southern extension of DSF89, although it has a similar trend.
DSF90	–	Open face	Southern termination covered, does not appear be continuous with LMF77. Blind northern termination.	

Appendix 2. Fracture attributes and terminations, pavement P2001.

Number	Aperture	Fill Type	Termination Relationships	Remarks
DSF91	15 to 20	Caliche	Northern termination against a minor east-northeast trending fracture. Southern end unknown - ends at open face of topographic ledge above DSJ10.	North end of fracture on trend with zone of closely spaced northwest trending fractures. South end does not appear to cut DSJ10, see DSF94 below.
DSF92	8	Caliche	Same as DSF91, see above.	Same as DSF91, see above.
DSF93	10	Open, partial caliche	North end, Y termination against DSF92. Southern end unknown - ends at open face of topographic ledge above DSJ10.	South end does not appear to cut DSJ10, see remark for DSF94 below
DSF94	10 to 15	Open, partial caliche	North end, T termination against DSF95. Southern end unknown - ends at open face of topographic ledge above DSJ10.	Fractures south of DSJ10 have similar trends to DSF91, 92 and 93 but continuity is difficult to establish due to heavy caliche. Undulations of caliche surface may indicate throughgoing fractures.
DSF95	--	Open face	West end is a T termination with DSF92. East end is a blind termination or against a minor fracture.	
DSF96	12	Open face	West end is a Y termination with DSF95. East end is a T termination with LMF39.	
DSF97	25	Open face, disturbed	West end is a T termination with LMF39. East end stops at topographic bench, termination unknown.	
DSF98	10	Type I breccia	North end extends off pavement. South end covered by caliche, but does not appear to be continuous with DSF7.	Brecciated fracture fill at north end has purplish-gray matrix containing 1 mm. wallrock? fragments.
DSF99	--	Open face	North and south ends covered by caliche and cemented slope wash.	Discontinuous fractures of the same trend as DSF99 can be traced as far south as DSF96.
DSF100	1 to 3	--	Southern termination covered, no clear intersection with LMF39. Northern end appears to terminate in a zone of many small fractures and broken rock.	At northern end, fracture is a boundary between intact rock on the east and broken rock on the west.

Appendix 2. Fracture attributes and terminations, pavement P2001.

Number	Aperture	Fill Type	Termination Relationships	Remarks
DSF101	–	–	Northern end covered in caliche. Southern termination blind or against minor fracture.	Fracture is a boundary between intact rock on the east and cemented broken rock on the west. Broken rock is at least in part fractured, unrotated pieces of wall rock, although some is cemented slope wash.
DSF102	3 to 4	Caliche	Northern end extends off pavement. Southern end is a V-termination with DSF104, covered SE of DSF104.	If small, shallowly west-dipping cooling joint south of target 120 is a part of DSJ4, then DSF102 offsets it with 1 m. right lateral strike separation
DSF103	1 to 2	Caliche	Northern end extends off pavement. Southern end is a Y-termination with DSF102.	
DSF104	3 to 4	Caliche	Northern end extends off pavement. Southern end is covered.	
DSF105	130	Type I breccia	Terminations at both ends of this breccia lens are indistinct, possibly blind.	
DSF106	3 to 5	Caliche	Northern end is a Y-termination against a minor northeast-trending fracture. Southern end is a Blind termination 20 cm. south of DSF107.	Cooling joint DSJ5 is not offset by this fracture. DSF106 appears to offset DSF107 with 2 cm. of right lateral strike separation.
DSF107	3	Caliche	Northern end terminates into a zone of closely spaced small fractures that parallel LMF39. Southern end terminates into the zone of closely spaced fractures that are on trend with DSF91 and 92.	Does not offset cooling joint DSJ3.
DSF108	3 to 5	Caliche	Southern end is a T-termination with DSF96. Blind northern termination - this fracture is not continuous with DSF106.	
DSF109	3 to 8	Caliche	Southern end is a T-termination with DSF95. Blind northern termination - this fracture is not continuous with DSF106.	
DSF110	2		Blind southern termination. North end terminates against a minor east-trending fracture.	Does not cut cooling joint DSJ10.

Appendix 2. Fracture attributes and terminations, pavement P2001.

Number	Aperture	Fill Type	Termination Relationships	Remarks
DSF111	2 to 20	Type III breccia	Blind southern termination, rock is broken into a network of small fractures in this area. North end covered.	Aperture is 2 mm. at south end, 20 mm. at north end. Linear ridges in caliche covering DSJ10 may be the northern extension of DSF111.
DSF112	3 to 4	Caliche	Terminations are lost in rubble at both ends.	
DSF113	5	--	Blind northern termination, does not extend to DSF112. Southern end mostly covered by caliche, probable extension cuts cooling joint near marker S-35.	
DSF114	0.1 to 15	Caliche	West end is a T termination with DSF38. East end extends off pavement.	DSF114 appears to be offset by DSF5 with 15 cm. of right lateral strike separation, but may not be the same fracture on either side of DSF5.
LMF1	3 to 4	Minor type II breccia	Blind termination on south end. North end T-terminates into small breccia-filled fracture.	Fracture cuts lithophysae
LMF2	4	Minor type II breccia	South end terminates into small breccia-filled fracture. North end is a T termination against LMF3.	Fracture cuts lithophysae
LMF3	6 to 30	Type II breccia	East end terminates at a zone of small fractures, west end is covered by caliche.	Possibly continuous with LMF4
LMF4	7 to 10	Type II breccia	Both ends blind, terminate into zones of small fractures.	Fracture cuts lithophysae
LMF5	1 to 10	Type II breccia	Blind termination at west end. East end terminates against LMF-6.	1 mm. caliche fill over most of length.
LMF6	3 to 5	Caliche	South end terminates into small breccia zone. North end terminates at LMF5.	

Appendix 2. Fracture attributes and terminations, pavement P2001.

Number	Aperture	Fill Type	Termination Relationships	Remarks
LMF7	45 to 70	Type I and II breccia	Both ends covered by caliche.	
LMF8	1 to 2	Caliche	West end covered by caliche, Blind termination at east end.	Fracture connects lithophysae, fairly smooth between lithophysae.
LMF9	40 to 90	Type II breccia and caliche	South end covered by caliche, north end blind, terminates into small fractures.	
LMF10	1 to 20	Caliche	South end blind. Blind termination at north end.	Fracture cuts lithophysae
LMF11	4 to 7	Caliche	South end terminates into slightly broken rock. North end terminates against LMF10.	Fracture cuts spot.
LMF12	25 to 40	Caliche	South end blind. Blind termination at north end.	Fracture cuts lithophysae
LMF13	1	Caliche, partially open	Blind termination at south end. North end covered by caliche.	Fracture cuts lithophysae
LMF14	1 to 20	Caliche	Both ends blind.	
LMF15	5 to 10	Caliche	Both ends blind.	
LMF16	4 to 12	Type II and caliche	Blind termination at south end North end extends off pavement.	Fracture cuts lithophysae

Appendix 2. Fracture attributes and terminations, pavement P2001.

Number	Aperture	Fill Type	Termination Relationships	Remarks
LMF17	2 to 5	Caliche	South end is a Y-termination against LMF16. Blind termination at north end	
LMF18	2 to 6	Type II and caliche	Blind terminations at both ends.	Breccia is discontinuous, fracture cuts lithophysae.
LMF19	1 to 4	Type II and caliche	South end blind, partly covered. North end is a blind termination.	Breccia is discontinuous, fracture cuts lithophysae.
LMF20	6	Caliche	South end terminated by LMF10, north end terminated by LMF13.	
LMF21	2 to 27	Caliche, partially open	South end is a blind termination, north end covered by caliche.	Aperture at south end is 2 to 3 mm , at north end 20 to 27 mm.
LMF22	1 to 4	Caliche	South end is a blind termination, north end covered by caliche.	Fracture cuts lithophysae
LMF23	6 to 12	Caliche	South end is a blind termination, north end terminated by LMF22.	
LMF24	1 to 6	Caliche	South end covered by caliche, north end terminated by LMF25.	Fracture cuts lithophysae
LMF25	2 to 4	Caliche	South end covered by caliche, north end terminated by LMF24.	Fracture cuts lithophysae
LMF26	8 to 12	Mostly Type II breccia, some Type I.	Both ends terminate into small breccia zones.	Offsets small breccia zone with 3" right lateral strike separation.

Appendix 2. Fracture attributes and terminations, pavement P2001.

Number	Aperture	Fill Type	Termination Relationships	Remarks
LMF27	4 to 15	Type II breccia and caliche	Both ends terminate into small breccia zones.	
LMF28	1 to 4	Caliche	South end terminated by LMF27, north end is a blind termination.	
LMF29	1 to 5	Caliche	South end terminates into breccia, north end is a blind termination	
LMF30	10 to 30	Type II breccia	South end terminates into breccia zone, north end is covered.	
LMF31	2 to 12	Caliche	South end terminates into zone of minor fractures. North end against LMJ1	
LMF32	6 to 15	Banded Calcite	Both ends terminate into small breccia zones.	Does not offset cooling joint LMJ7.
LMF33	5 to 12	Caliche	East termination unknown, ends at topographic ledge. West end terminated by LMF39.	
LMF34	5 to 7	Caliche	East termination unknown, ends at topographic ledge. West end terminated by LMF39.	
LMF35	4 to 7	Caliche	East termination unknown, ends at topographic ledge. West end terminated by LMF39.	
LMF36	4 to 12	Type I breccia	South end terminates into breccia zone. North end is a blind termination.	

Appendix 2. Fracture attributes and terminations, pavement P2001.

Number	Aperture	Fill Type	Termination Relationships	Remarks
LMF37	2 to 4	Caliche	South end terminates into breccia zone. North end is a blind termination	
LMF38	20 to 45	Caliche	South end continues as LMF133 to test pit#2. North end terminates into breccia zone.	Offsets the fault LMF39 with 7 inches right lateral strike separation. Offsets LMFJ6 with same magnitude and sense of offset.
LMF39	7 to 47	Mostly caliche and banded calcite, some type II breccia	South end terminates into zone of minor fractures south of test pit#2. North end dies out into several minor fractures at the north end of pavement.	Offsets pair of cooling joints near Tgt115. Net slip is 7 inches.
LMF40	20 to 30	Caliche	East end terminated by LMF39. West end terminates into zone of minor fractures.	
LMF41	4 to 10	Caliche	East end mostly covered by caliche, probable termination against LMF38. West end terminates into small breccia zone.	
LMF42	1 to 5	Caliche	East end is a blind termination. West end terminates against LMF39.	
LMF43	5 to 10	Open	South end terminates in fractured zone, north end terminated by LMF33.	
LMF44	2 to 4	Caliche	East end covered by caliche, west end terminated by LMF39	
LMF45	5 to 20	Caliche	South end terminates in fractured zone, north end terminates into breccia.	
LMF46	2	Caliche	South end is a blind termination, north end is a blind termination.	

Appendix 2. Fracture attributes and terminations, pavement P2001.

Number	Aperture	Fill Type	Termination Relationships	Remarks
LMF47	1 to 2	--	South end terminated by LMF49, north end terminates into small breccia zone.	
LMF48	2	Caliche	East end terminated by LMF39. West end terminates into zone of small fractures.	Does not offset the two large subhorizontal cooling joints that it crosses. Fracture cuts lithophysae.
LMF49	4 to 25	Caliche and type II breccia	South end terminates into breccia zone, north end covered by caliche, probably blind.	
LMF50	1	Caliche	East end is a blind termination, west end terminated by LMF49	Does not offset the three cooling joints it crosses, fracture cuts spots.
LMF51	3 to 7	Caliche	West end terminates into small breccia zone, east end terminated by LMF39.	Does not offset the two cooling joints it crosses.
LMF52	1 to 2	Caliche	South end terminated by LMF72, north end terminates in zone of small fractures.	
LMF53	2 to 20	Caliche	South end is a blind termination, north end covered by caliche.	
LMF54	0.5 to 2	Caliche	South end is a blind termination, north end crosses cooling joint LMJ7, blind termination in fractured rock.	
LMF55	7 to 40	Type I breccia with banded Calcite	Both ends terminate into minor breccia zones.	
LMF56	2 to 7	Caliche	South end terminated by LMF57, north end terminates into minor breccia zone.	

Appendix 2. Fracture attributes and terminations, pavement P2001.

Number	Aperture	Fill Type	Termination Relationships	Remarks
LMF57	3 to 10	Caliche	West end terminated by LMF58, east end is a blind termination.	
LMF58	5 to 12	Banded Caliche	Both ends terminate into minor breccia zones.	
LMF59	15 to 50	Type II breccia, banded calcite	Both ends covered by caliche.	
LMF60	15 to 25	Type II breccia and caliche	Both ends terminate into minor breccia zones.	
LMF61	12 to 22	caliche	Both ends covered by caliche.	
LMF62	4 to 7	Caliche	East end terminates into minor breccia zone. West end is a blind termination.	
LMF63	10 to 20	Caliche	Both ends terminate into minor breccia zones.	
LMF64	4 to 10	caliche	East end terminates at cooling joint. West end terminates into minor breccia zone.	
LMF65	4 to 9	Caliche	South end terminates at cooling joint. North end is a blind termination.	
LMF66	1 to 3	Caliche	East end terminated by LMF70, west end is a blind termination.	

Appendix 2. Fracture attributes and terminations, pavement P2001.

Number	Aperture	Fill Type	Termination Relationships	Remarks
LMF67	12 to 24	Banded calcite, type II breccia, caliche	East end terminated by LMF86, west end terminated by LMF70.	Aperture at southwest end ranges from 12 to 24 mm., fill is banded calcite and type II breccia. Aperture at north end ranges from 2 to 6 mm., fill is caliche.
LMF68	2 to 6	--	Southern termination unknown, ends at open face. North end terminated by LMF66.	Smaller fractures with similar trend appear to link LMF68 with LMF65.
LMF69	4 to 20	Caliche	Southern termination unknown, ends at open face. North end covered by caliche	
LMF70	5 to 34	Type II breccia, caliche	Southern termination unknown, ends at open face. North end terminated by LMF66.	
LMF71	9 to 30	Type II breccia, caliche	South end covered by caliche. North end terminates into minor breccia zone.	
LMF72	7 to 10	Caliche	East end is a blind termination, west end terminates into minor breccia zone.	
LMF73	2 to 7	--	South end terminated by LMF74. North end is a blind termination.	
LMF74	7 to 25	Caliche	Both ends terminate into minor breccia zones.	
LMF75	0.5 to 5	Caliche	Both ends terminate into minor breccia zones.	
LMF76	5 to 11	Type II breccia, caliche	East end terminates against cooling joint. West end covered by caliche.	

Appendix 2. Fracture attributes and terminations, pavement P2001.

Number	Aperture	Fill Type	Termination Relationships	Remarks
LMF77	2 to 7	Caliche	South end is a blind termination. North end terminates into minor breccia zone.	
LMF78	4 to 12	Caliche	South end terminates into breccia. North end extends off pavement.	Fracture cuts lithophysae
LMF79	4 to 8	Type II breccia, caliche	East end terminated by LMF-21. West end terminated by LMF-9.	
LMF80	3 to 15	–	East end terminates in a zone of minor fractures. West end is a blind termination.	
LMF81	15 to 32	Type II breccia, caliche	East end terminates against LMF36. West end covered by caliche.	
LMF82	2 to 10	Caliche	South end covered by caliche. North end terminates in zone of minor fractures.	
LMF83	20 to 30	Caliche	Both ends terminate into minor breccia zones.	
LMF84	2 to 16	Caliche	South end terminates in minor fractured zone. North end terminated by LMF110.	
LMF85	2 to 10	Caliche	South end is a blind termination, north end terminated by LMF86.	
LMF86	1 to 22	Caliche	South end is a blind termination, north end extends into test pit#2.	Fracture does not appear to extend across test pit.

Appendix 2. Fracture attributes and terminations, pavement P2001.

Number	Aperture	Fill Type	Termination Relationships	Remarks
LMF87	5 to 12	Caliche	East end terminated at LMF89, west end terminates into breccia	
LMF88	5 to 9	Caliche, Type II breccia	East end covered West end terminated by LMF86.	
LMF89	1 to 15	Caliche	South end terminates in minor fractured zone. North end terminated by LMF98.	
LMF90	5 to 8	Caliche	South end terminated by LMF97, north end terminated by LMF88	
LMF91	7 to 20	Type II breccia, caliche	South end terminated by LMF97, north end terminated by LMF 86.	
LMF92	1 to 4	Caliche	South end is a blind termination, north end terminated by LMF97.	
LMF93	2 to 22	Type II breccia, caliche	South end terminated by LMF104. North end terminated by LMF97.	
LMF94	2 to 7	Caliche	South end is a blind termination. North end terminated by LMF97.	
LMF95	2 to 18	Caliche	South end terminated by LMF104, north end terminated by LMF97	
LMF96	3 to 7	Caliche	South end terminated by LMF103, north end is a blind termination.	

Appendix 2. Fracture attributes and terminations, pavement P2001.

Number	Aperture	Fill Type	Termination Relationships	Remarks
LMF97	2 to 52	Type II breccia, caliche	East end terminated by LMF115, west end terminated by LMF113.	Type II breccia occurs at east end of fracture.
LMF98	3 to 27	Banded calcite with minor clasts	South end covered by caliche. North end extends into test pit #2.	Possible continuation of LMF133 from northwest side of test pit #2.
LMF99	2 to 25	Caliche	South end terminates into breccia zone. North end is a blind termination.	
LMF100	3 to 8	Caliche	East end terminated by LMF102. West end terminated by LMF99.	
LMF101	2 to 7	Caliche	South end covered by caliche. North end terminates in fractured zone.	
LMF102	2 to 10	Caliche	South end extends off pavement. North end extends into test pit#2.	Possible continuation of LMF137 from northwest side of test pit #2.
LMF103	1 to 22	Caliche	South end covered. North end terminated by LMF95.	
LMF104	1 to 18	Caliche, banded Calcite	West end mostly covered by caliche, hooks into LMF113. East end terminates in breccia	
LMF105	1 to 9	Type I breccia	East end terminates against LMF107. West end terminates into minor breccia zone.	LMF107 widens abruptly at intersection with LMF105.
LMF106	1 to 8	Caliche	North end terminated by LMF115. South end terminated by LMF105.	

Appendix 2. Fracture attributes and terminations, pavement P2001.

Number	Aperture	Fill Type	Termination Relationships	Remarks
LMF107	50 to 70	Type I breccia	South end covered, probably extends off of pavement. North end covered by caliche.	Clasts of wallrock and possibly other lithologies up to 1 cm. In fine rock matrix and calcite cement.
LMF108	10 to 12	Caliche	South end blind or terminated by LMF67. North end extends into test pit#2 where it terminates against LMF86 1 foot below pavement surface.	
LMF109	2 to 4	Caliche	East end is a blind termination, west end blind.	
LMF110	1 to 3	--	East end terminated by LMF86, west end terminated by LMF83.	
LMF111	10 to 22	Minor Type I breccia midway along fracture	South end terminated by LMF112. North end terminates into minor breccia zone.	
LMF112	7 to 24	Caliche	East end terminated by LMF104. West end extends off pavement.	
LMF113	3 to 30	Caliche	South end mostly covered by caliche, hooks with LMF104. North end terminated by LMF67.	
LMF114	2 to 5	Caliche	East end terminated by LMF99. West end terminated by LMF86.	
LMF115	1 to 7	Caliche	East end extends off pavement, west end is a blind termination	Offsets LMF107 with 2.5" of left-lateral strike separation
LMF116	4 to 21	Caliche	South end covered by caliche. North end terminates against LMF117.	

Appendix 2. Fracture attributes and terminations, pavement P2001.

Number	Aperture	Fill Type	Termination Relationships	Remarks
LMF117	2 to 22	Caliche	South end terminates into breccia zone. North end terminated by LMF102.	Fracture with type I breccia, similar to LMF107 lies about 1 m to the east.
LMF118	4 to 6	Caliche, type II breccia	South end terminated by LMF97. North end terminates in zone of minor fractures.	
LMF119	1 to 3	Caliche	East end extends off pavement. West end extends into test pit#2.	Fracture does not appear to extend across test pit
LMF120	1 to 12	Caliche	East end extends off pavement. West end extends into test pit#2.	Fracture does not appear to extend across test pit.
LMF121	0.5	Caliche	East end terminates against LMF122. West end is a blind termination.	Possibly offset by LMF122 and continues on east side to pavement edge.
LMF122	2 to 7	Caliche	South end covered. North end terminates into minor breccia zone.	Possibly offsets LMF121 with 15 cm. right lateral strike separation.
LMF123	2 to 5	Caliche	Both ends are blind terminations or terminations into zones of small fractures.	
LMF124	5 to 9	Caliche	South end terminated by LMF132. North end terminates into minor breccia zone.	
LMF125	4 to 22	Caliche	South end extends into test pit#2. North end terminates into zone of minor fractures.	Possible continuation of DSF33. The endpoints of the two fractures are separated by a narrow zone of minor fractures.
LMF126	1 to 3	Caliche	East end terminates into breccia zone. West end terminated by LMF125.	

Appendix 2. Fracture attributes and terminations, pavement P2001.

Number	Aperture	Fill Type	Termination Relationships	Remarks
LMF127	1 to 2	Caliche	East end terminated by LMF128, west end is a blind termination.	
LMF128	1 to 8	Caliche	East end terminates in fractured zone. West end terminates into LMF123.	
LMF129	0.5 to 2	Caliche	South end terminates into breccia zone. North end terminated by LMF120.	
LMF130	0.5 to 6	Caliche	North end terminated by LMF121. South end covered by caliche.	
LMF131	1 to 2	Caliche	East end is a blind termination, west end terminated by LMF132.	
LMF132	2 to 7	Caliche	South end joins LMF137 and extends into test pit#2. North end terminated by LMF124.	
LMF133	5 to 22	Type II breccia, caliche	South end extends into test pit#2. North end probably continuous with LMF38.	Possible continuation of LMF98 from southeast side of test pit #2. Offsets the fault LMF39 with 15 cm. right lateral strike separation.
LMF134	5 to 15	Type II breccia, caliche	East end terminated by LMF133. West end terminated by LMF39.	
LMF135	1 to 5	Caliche	South end terminated by LMF48. North end is a blind termination.	
LMF136	2 to 8	Caliche	South end terminated by LMF51. North end terminated by LMF38.	Does not offset the two cooling joints it crosses.

Appendix 2. Fracture attributes and terminations, pavement P2001.

Number	Aperture	Fill Type	Termination Relationships	Remarks
LMF137	1 to 3	Caliche	South end merges with LMF132 and extends into test pit#2. North end terminates against LMF39.	Possible continuation of LMF102 from southeast side of test pit #2.
LMF138	2 to 32	Caliche	South end extends off pavement. North end terminates into minor breccia zone.	
LMJ1	2 to 4	Caliche	South end terminated by LMF31, north end terminated by LMF32	
LMJ2	2	Caliche	East end terminates into breccia, west end terminates into flat plane	
LMJ3	1	Caliche	South end covered by caliche, north end terminates into flat plane	
LMJ4	10 to 15		East end terminated by contact, west end terminated by LMF39	
LMJ5	1 to 2	Caliche	East end terminated by contact, west end terminated by LMF39	
LMJ6	1		West end terminates in fractured zone, east end terminates in fractured zone	
LMJ7	1	Caliche	East end covered by caliche, west end terminates into flat plane	
LMJ8	1 to 2	Caliche	South end terminated by LMF48, north end terminates in fractured zone	

Appendix 2. Fracture attributes and terminations, pavement P2001.

Number	Aperture	Fill Type	Termination Relationships	Remarks
LMJ9	4 to 7	Caliche	East end terminates in fractured zone, west end terminates into DSJ16	
LMJ10	5		East end terminates in fractured zone, west end terminates into DSJ16	
LMJ11	1	Caliche	East end terminates in fractured zone, west end terminated by small fractured zone	
LMJ12	4 to 12		East end terminates near fractured zone, west end is blind	
DSJ1	5	Caliche	East end extends off pavement, W end probably truncated by DSF10, may extend farther W	
DSJ2		Caliche	West end truncated by LMF39, east end eroded	
DSJ3	6	Caliche	Both ends blind	This joint is not truly continuous with DSJ4 - there is a short gap near DSJ5.
DSJ4	10	Caliche	Both ends blind	
DSJ5	12	--	Both ends blind	
DSJ6	10	Caliche, partially open	South end blind, north end blind or truncates against DSF86.	

Appendix 2. Fracture attributes and terminations, pavement P2001.

Number	Aperture	Fill Type	Termination Relationships	Remarks
DSJ7	3	Caliche	Both ends blind	
DSJ8	2	Caliche	Extends off pavement to SE, N end extends into test pit #1	J8 seen on north wall of test pit #1, extends the full height of the pit.
DSJ9	--	Open face	West end truncated by LMF39, east end eroded	
DSJ10	--	Open face	Both ends eroded	
DSJ11	--	Open face	Both ends eroded	
DSJ12	3	--	Both ends blind.	May be continuous with DSJ3
DSJ13	3	--	Both ends blind.	
DSJ14	--	Open face	N end blind, S end plunges under DSJ15, covered.	
DSJ15	--	Open face	N end blind or against LMJ7, S end blind or covered.	DSJ15 or a similar cooling joint can be traced, with a few minor breaks, to the south edge of the pavement.
DSJ16	2	--	Both ends blind.	

Appendix 2. Fracture attributes and terminations, pavement P2001.

Number	Aperture	Fill Type	Termination Relationships	Remarks
DSJ17	--	Open face	Both ends blind.	
DSJ18	--	Open face	Both ends blind.	DSJ17,18 and 19 form the large, low angle surface on the eastern side of the pavement. Most of actual joint surface is eroded, only present along west edge.
DSJ19	--	Open face	Both ends blind.	

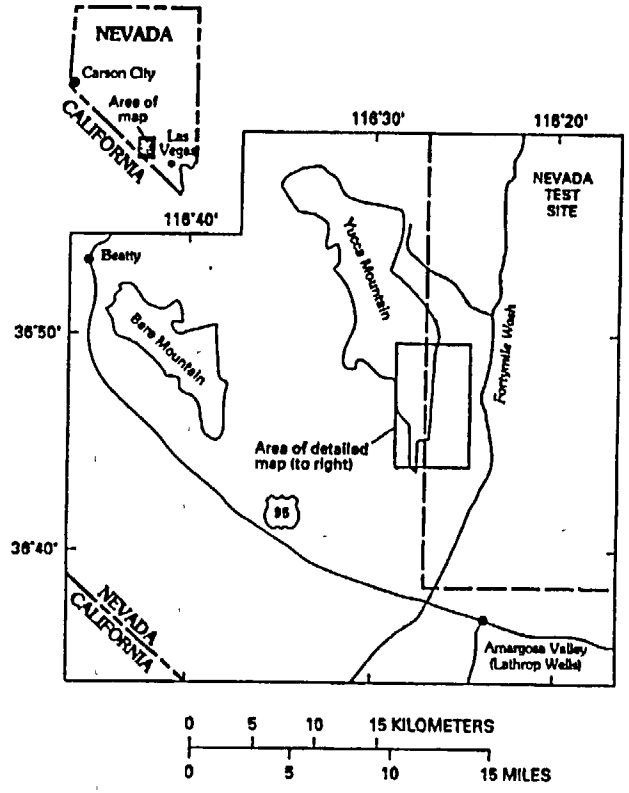
NEVADA
Carson City
Area of map
Las Vegas
CALIFORNIA
116°40'
116°30'
116°20'
NEVADA TEST SITE
Beatty
Yucca Mountain
Bare Mountain
Fortymile Wash
36°50'
Area of detailed map (to right)
95
36°40'
NEVADA
CALIFORNIA
Amargosa Valley (Lathrop Wells)
0 5 10 15 KILOMETERS
0 5 10 15 MILES

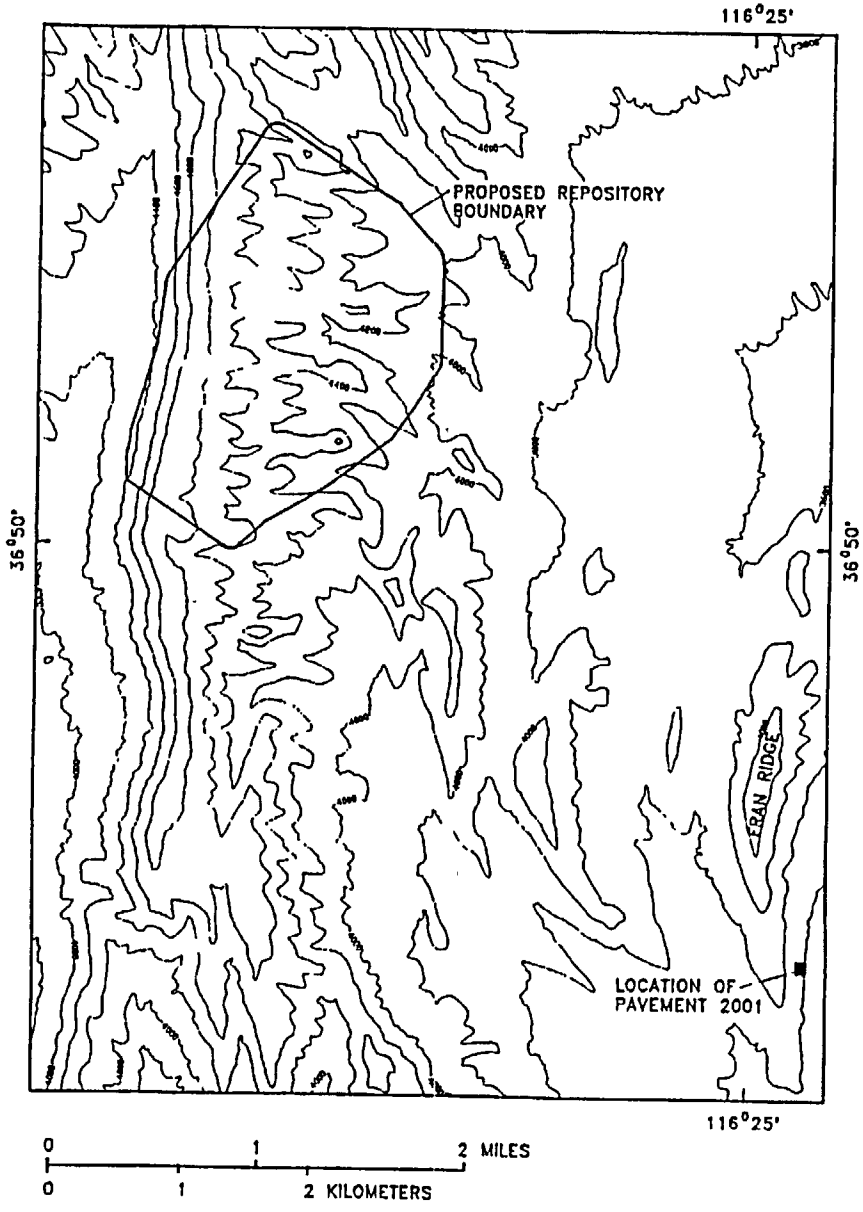
116°25'
PROPOSED REPOSITORY BOUNDARY
36°50'
FRAN RIDGE
LOCATION OF PAVEMENT 2001
116°25'
0 1 2 MILES
0 1 2 KILOMETERS

1-69

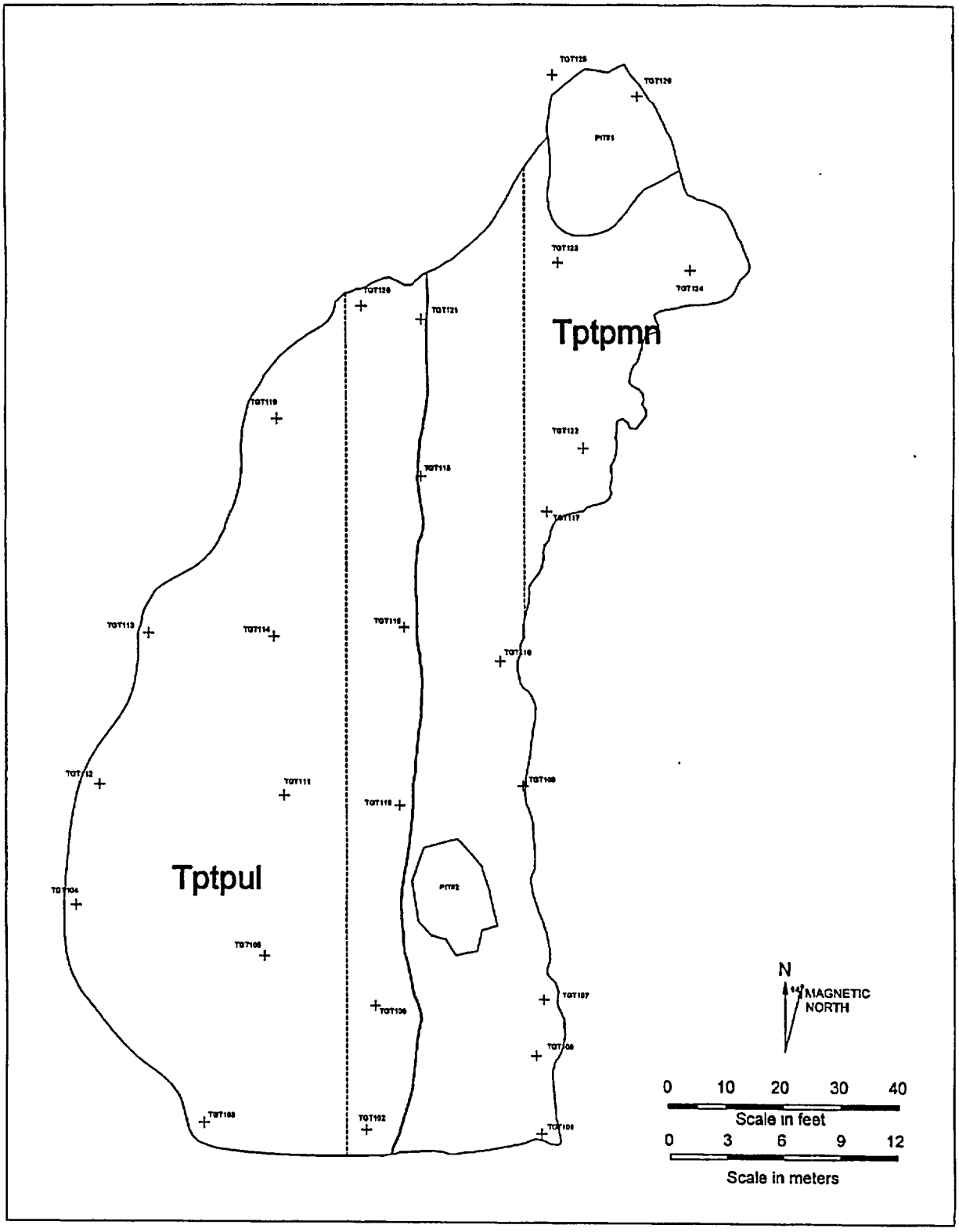
Tptpmn
Tptpul
N
MAGNETIC NORTH
0 10 20 30 40
Scale in feet
0 3 6 9 12
Scale in meters

fig 2

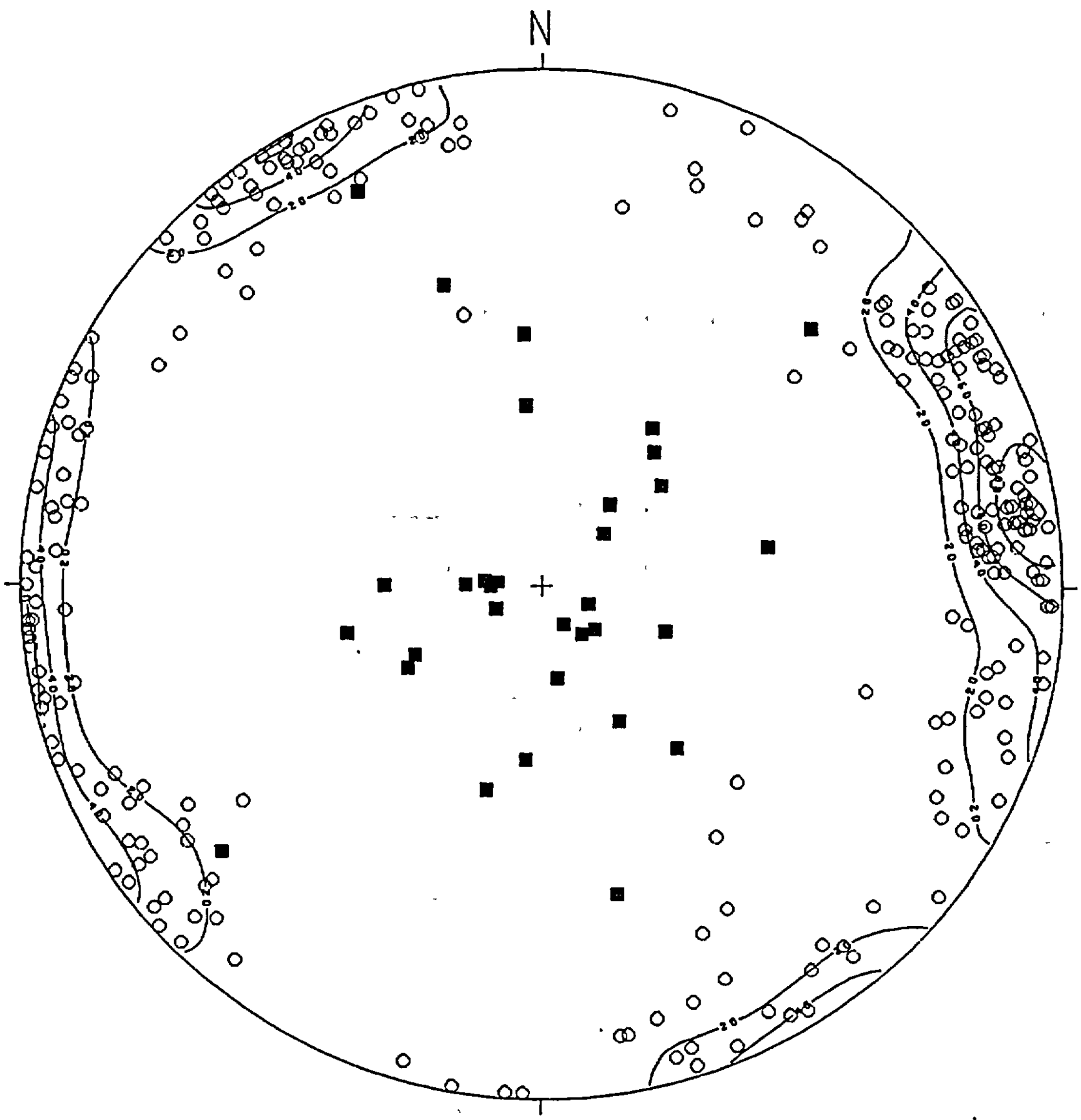

Fig 3

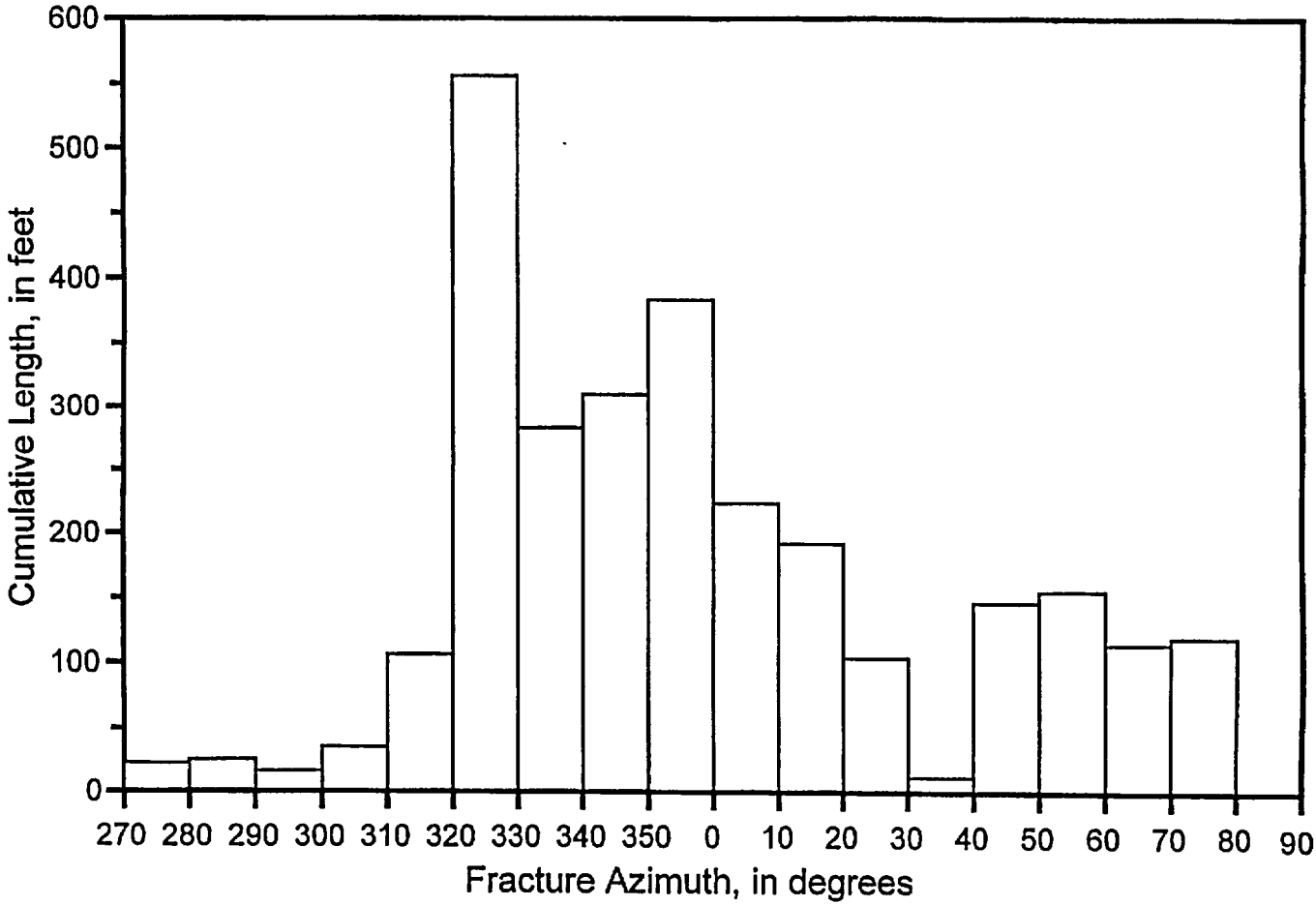
600
500
400
300
200
100
0
Cumulative Length, in feet
270 280 290 300 310 320 330 340 350 0 10 20 30 40 50 60 70 80 90
Fracture Azimuth, in degrees

Fig 4

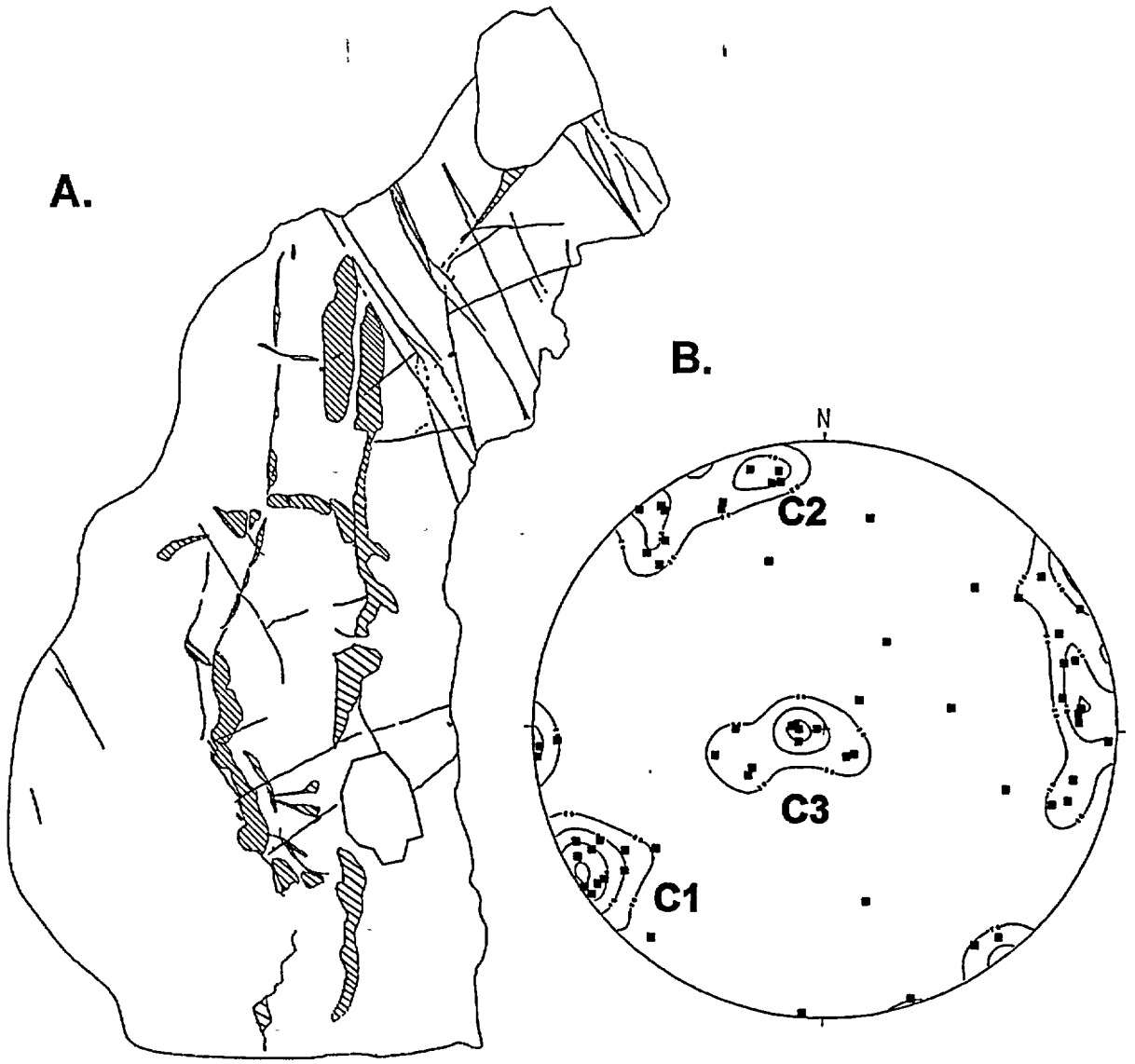

Fig 5

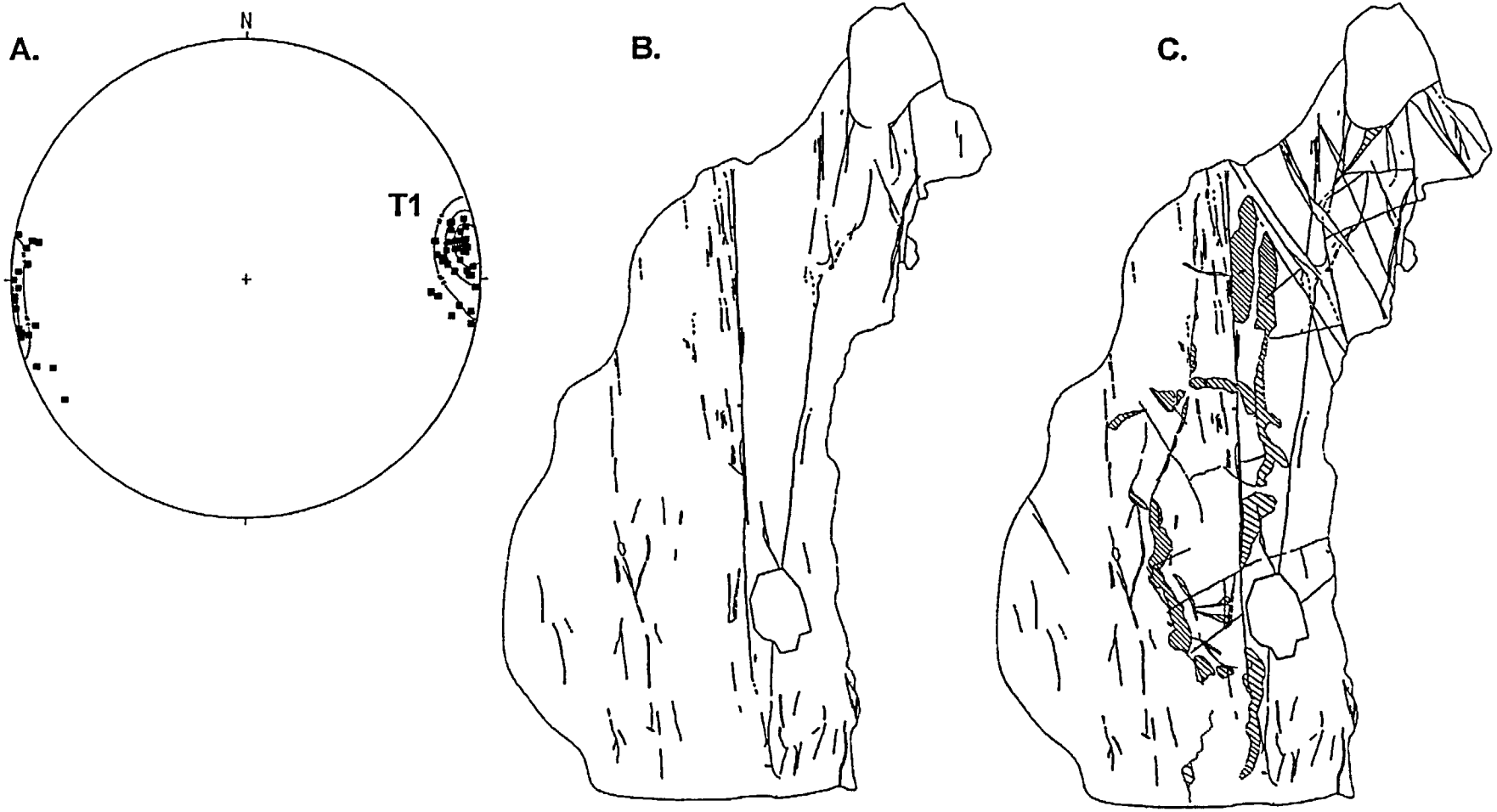

Fig 9

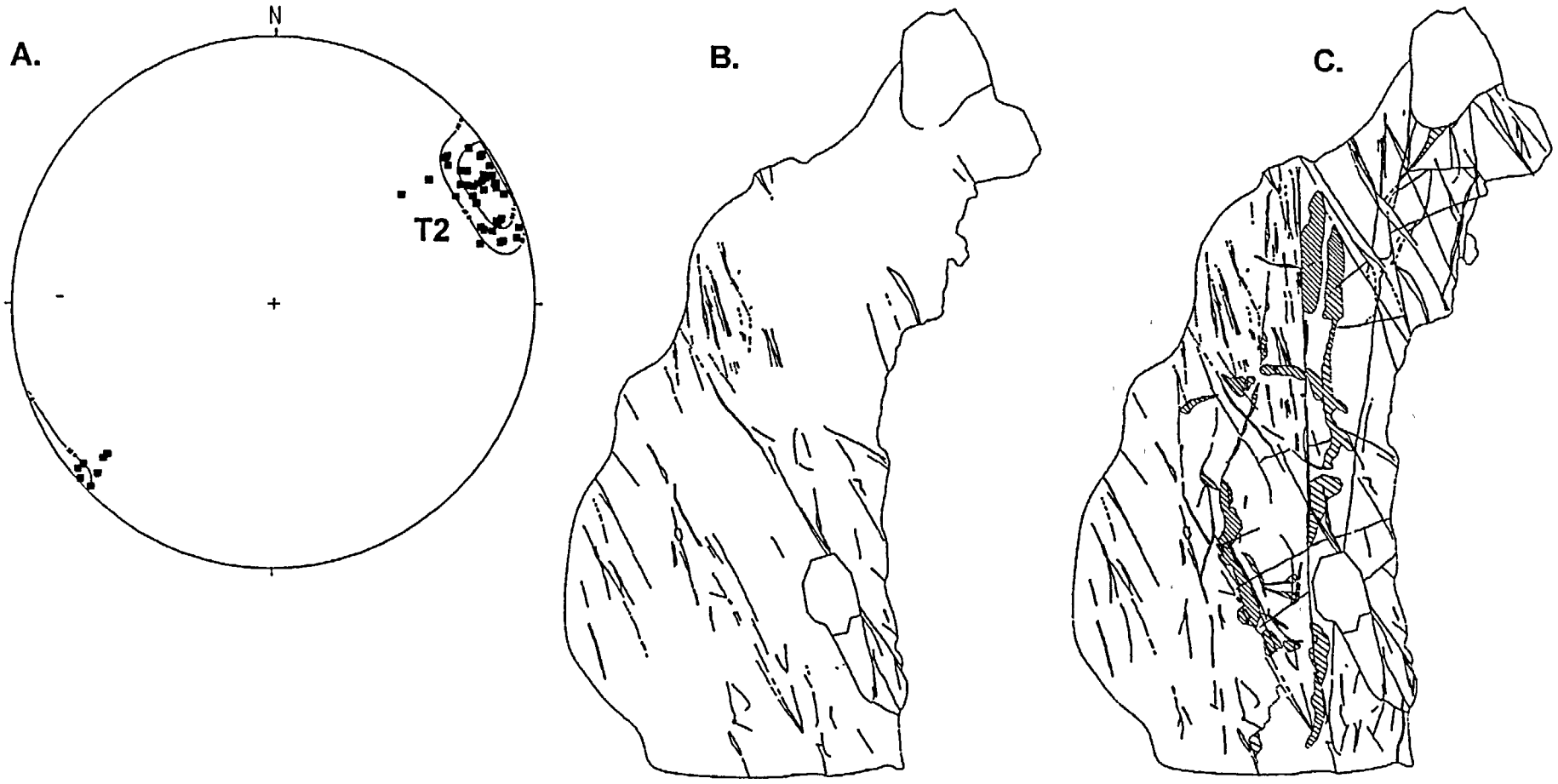

Fig 7

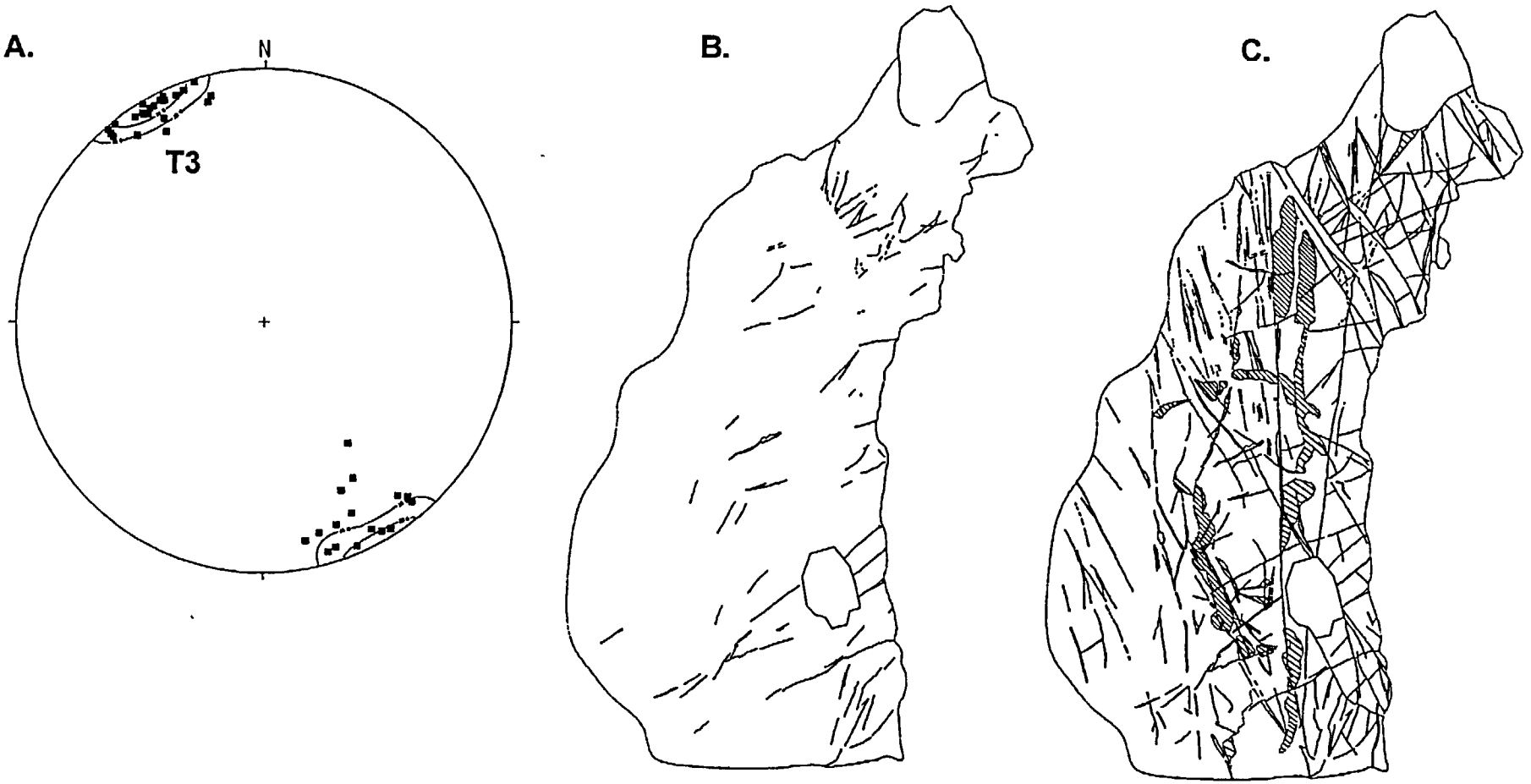

Fig 8

A. TEST PIT DATA

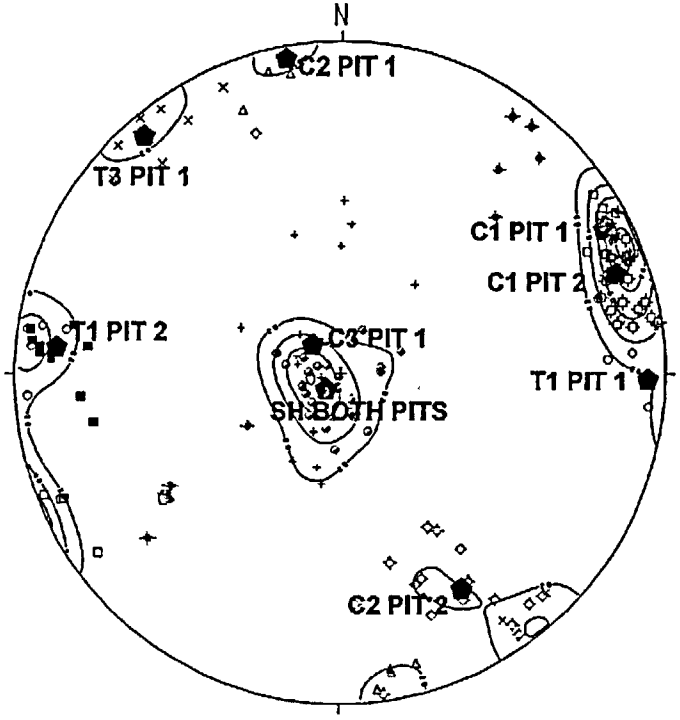

SYMBOL LEGEND, FIG 9A

COOLING JOINT SETS

- C1 Pit 1
- C2 Pit 1
- C3 Pit 1
- C1 Pit 2
- C2 Pit 2
- C3 Pit 2

TECTONIC JOINT SETS

- T1 Pit 1
- T3 Pit 1
- T1 Pit 2
- SH, both pits
- Median set orientation, test pits

SYMBOL LEGEND, FIG 9B

- Mapped tectonic joints, P2001
- Mapped cooling joints, P2001
- Median set orientation, P2001

B. PAVEMENT DATA

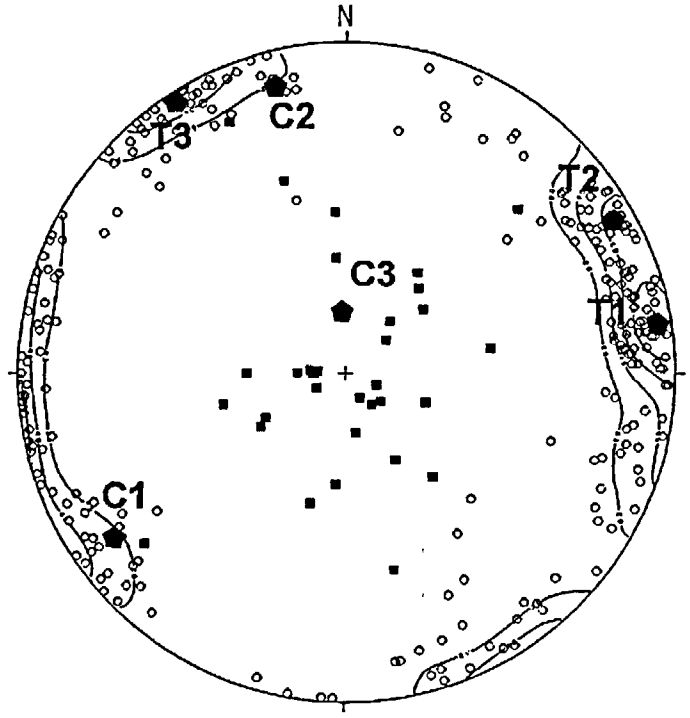

Fig 9

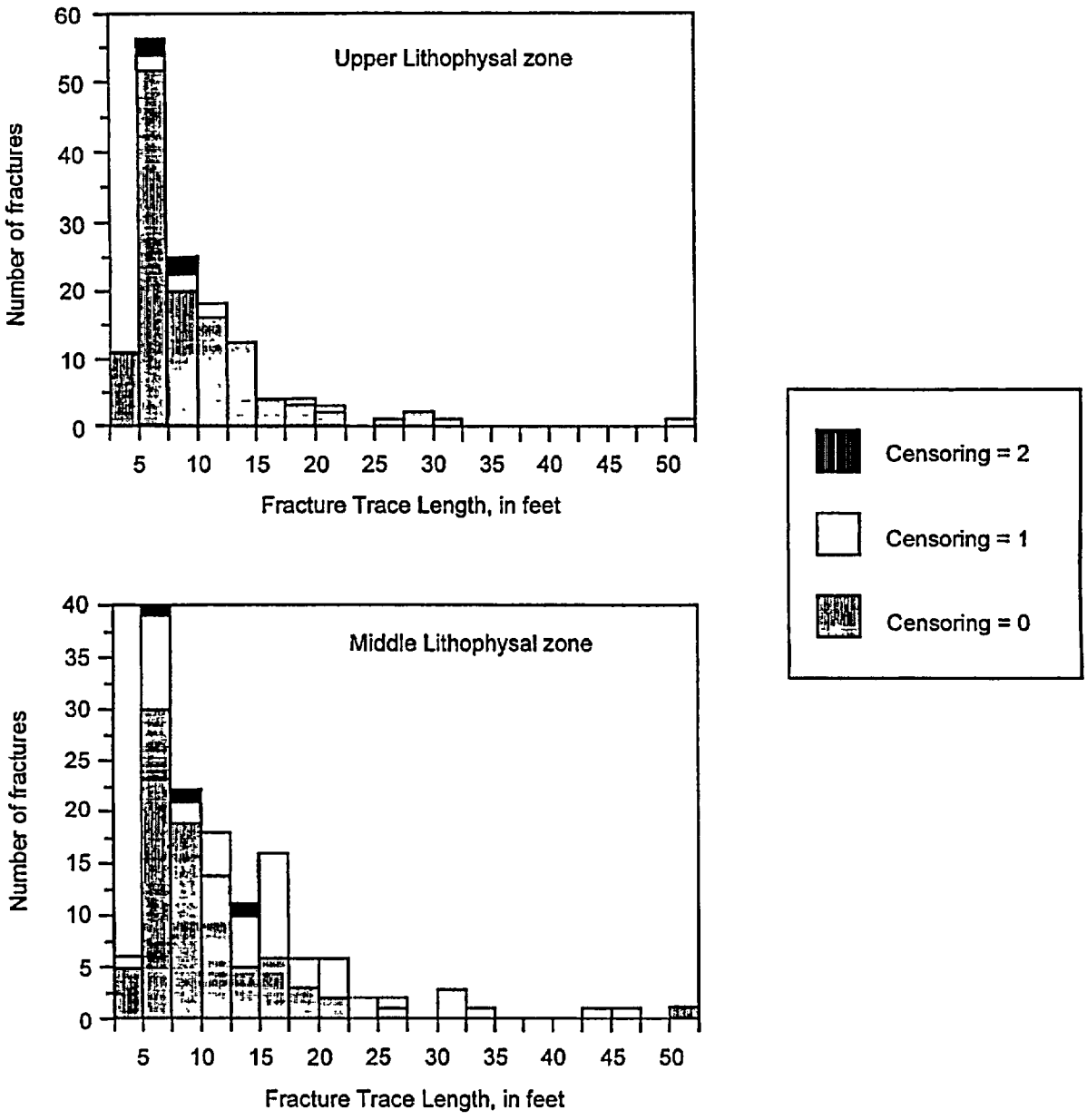
Upper Lithophysal zone
Number of fractures
60
50
40
30
20
10
0
5
10
15
20
25
30
35
40
45
50
Fracture Trace Length, in feet
Middle Lithophysal zone
Number of fractures
40
35
30
25
20
15
10
5
0
5
10
15
20
25
30
35
40
45
50
Fracture Trace Length, in feet
Censoring = 2
Censoring = 1
Censoring = 0

Fig 10

Fig 11

a)

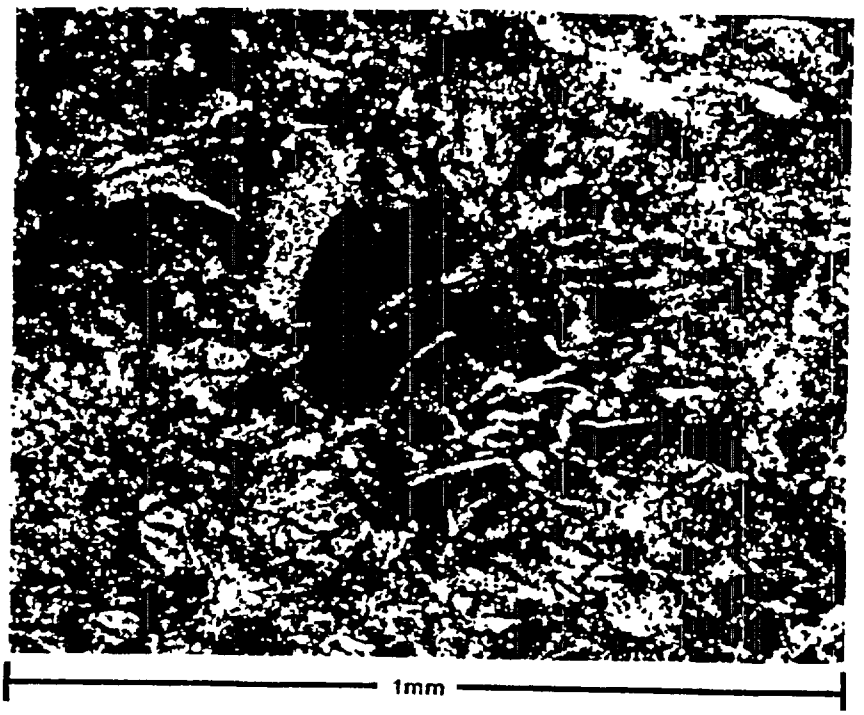

b)

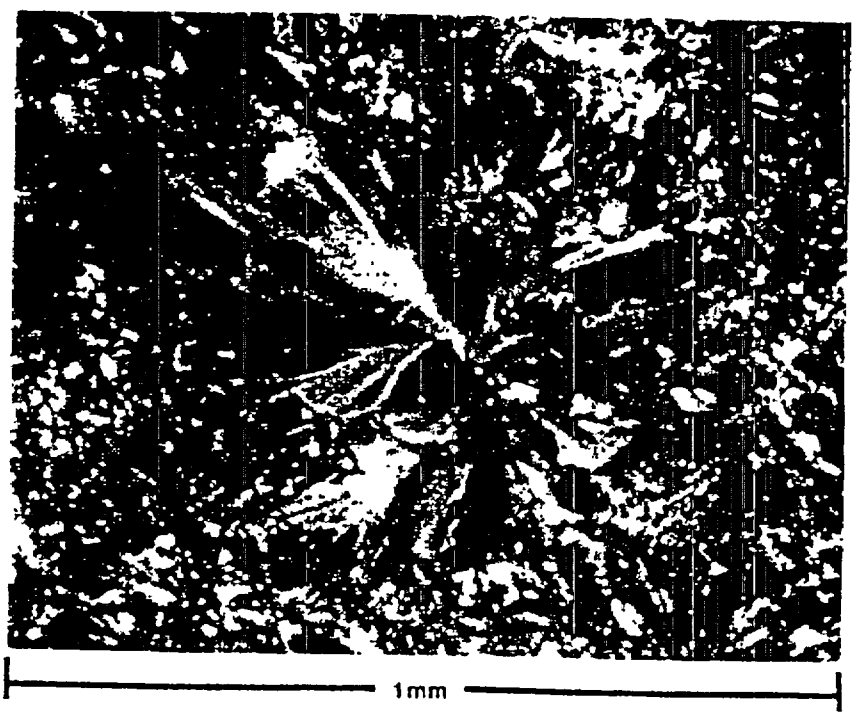

Fig 12

a)

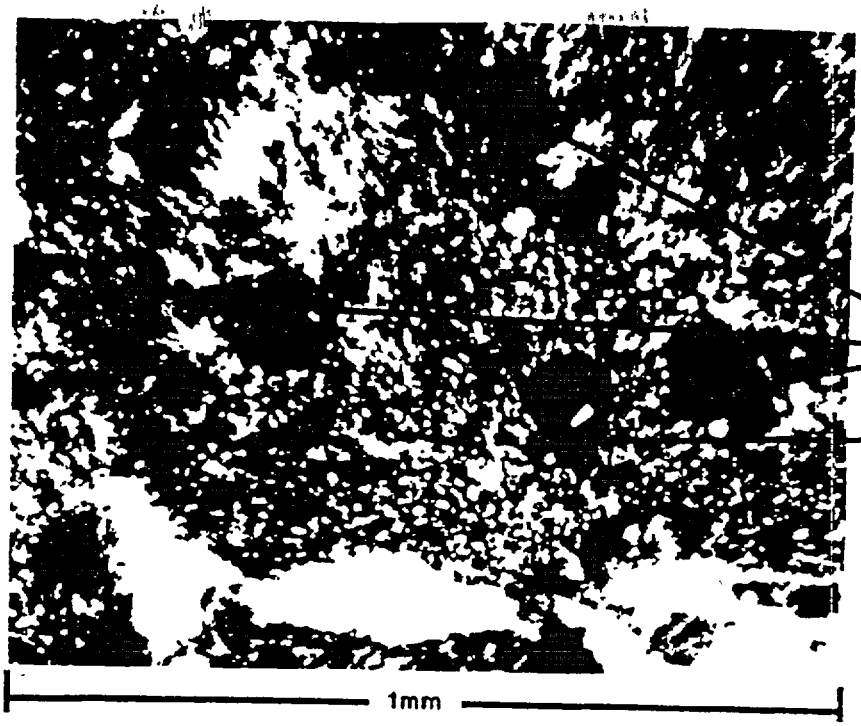

Crossed Nichols

b)

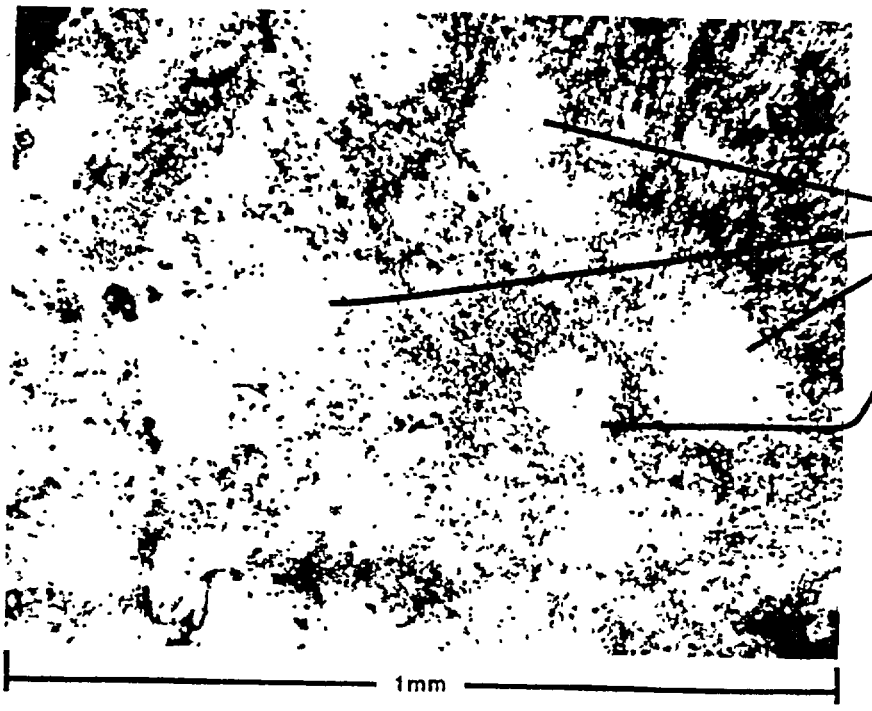

Plane-Polarized Light

Fig 13

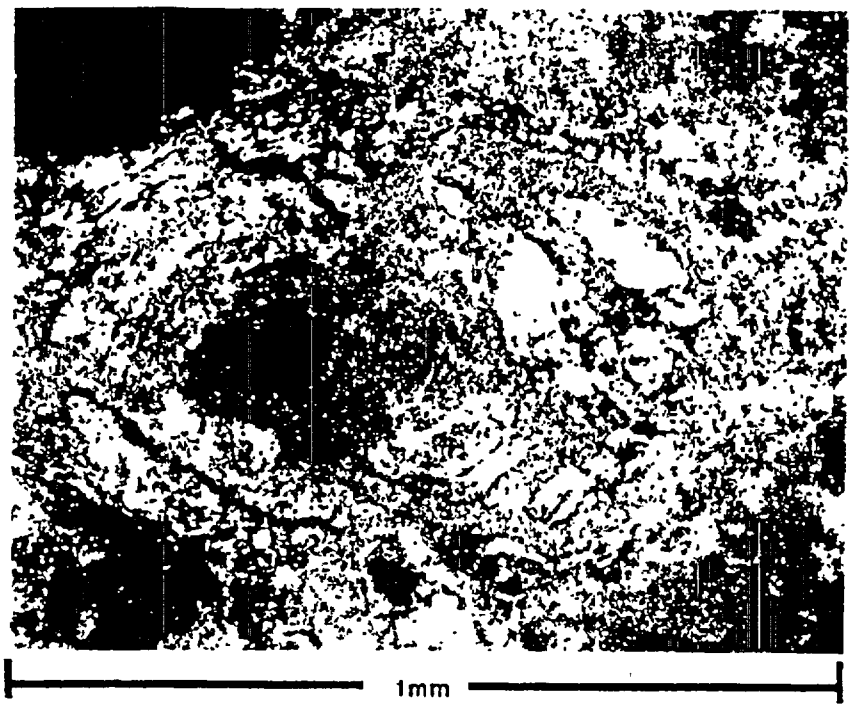

Fig 14

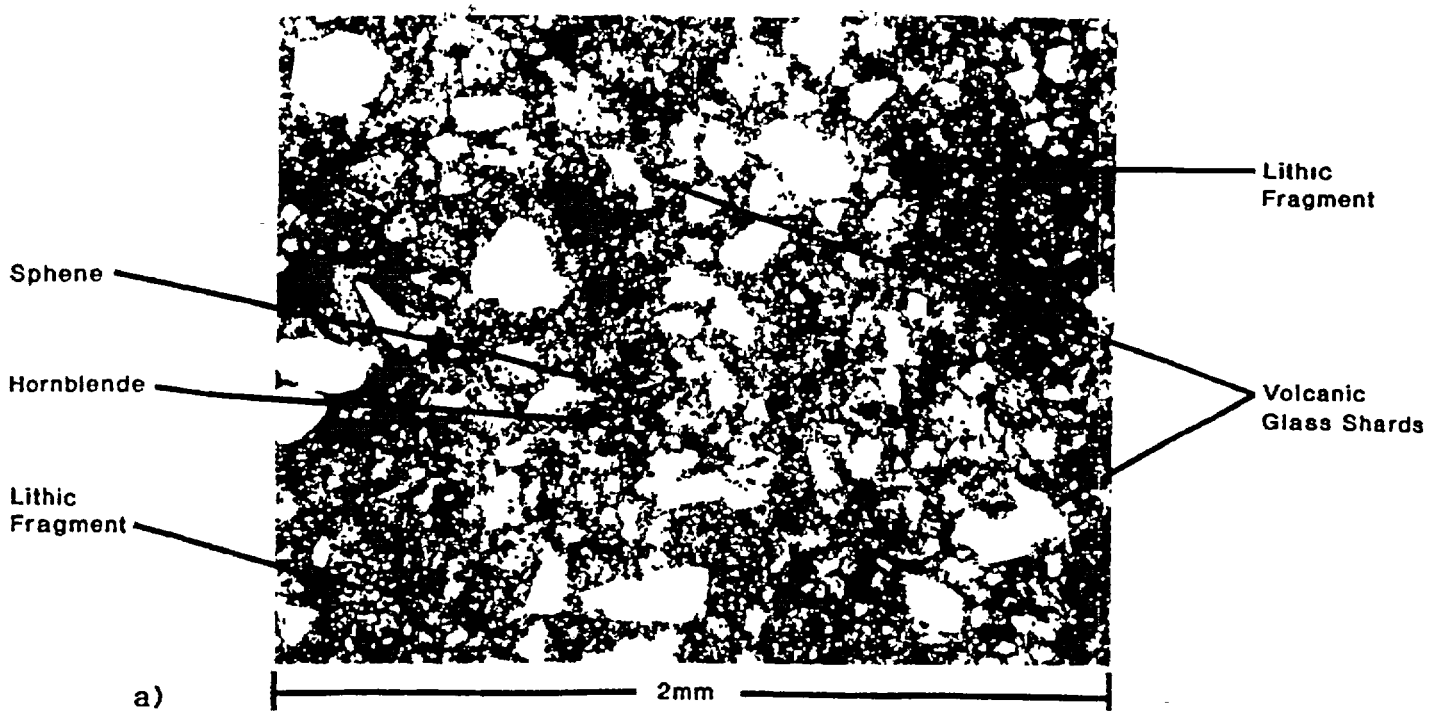
Lithic Fragment
Sphene
Hornblende
Volcanic Glass Shards
Lithic Fragment
a)
2mm
Plane-Polarized Light

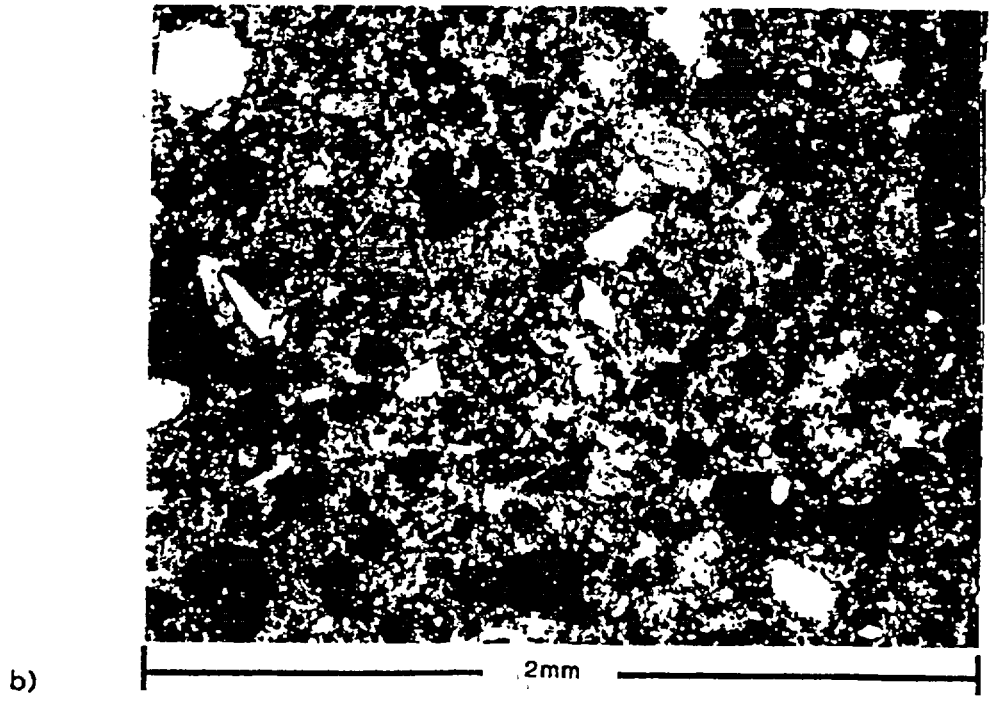
b)
2mm
Cross Nicols

Fig 15

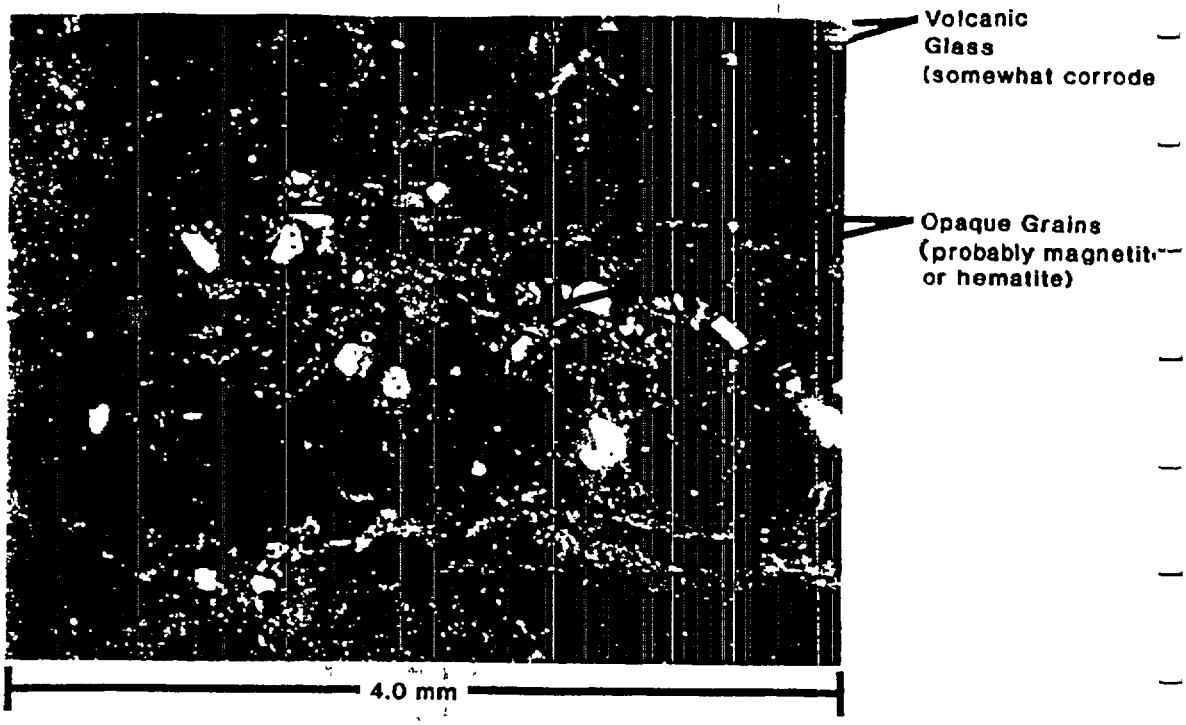
Volcanic
Glass
(somewhat corrode
Opaque Grains
(probably magnetit
or hematite)
4.0 mm

a)

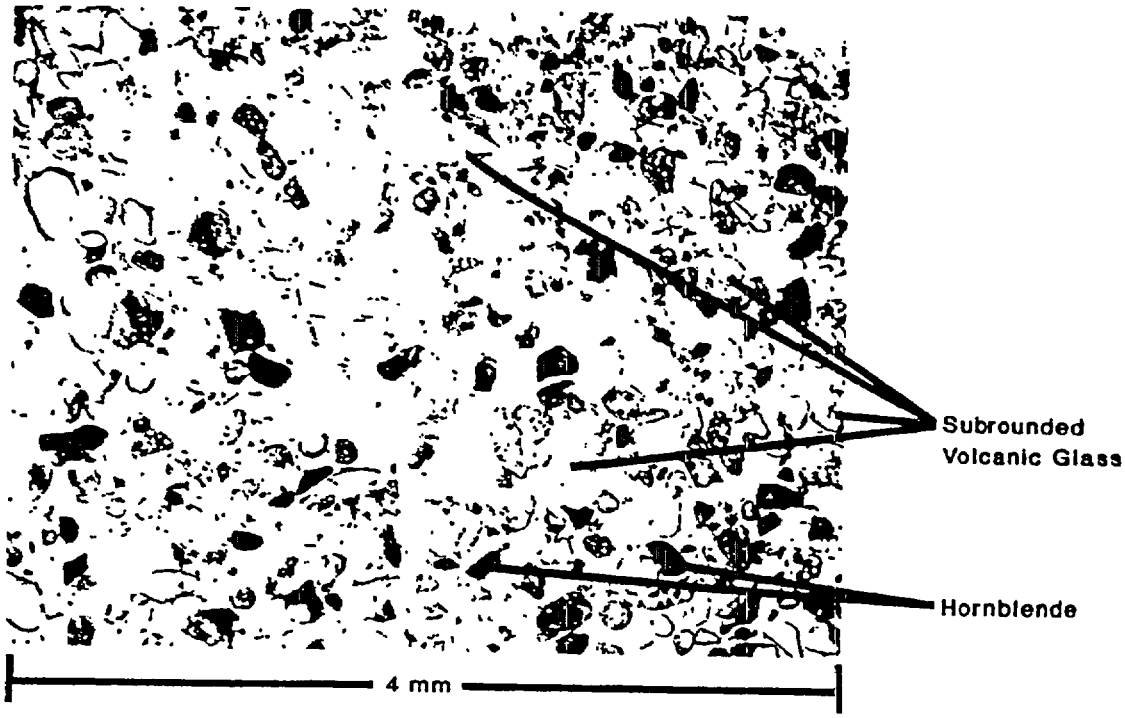
Subrounded
Volcanic Glass
Hornblende
4 mm

b)

Fig 16

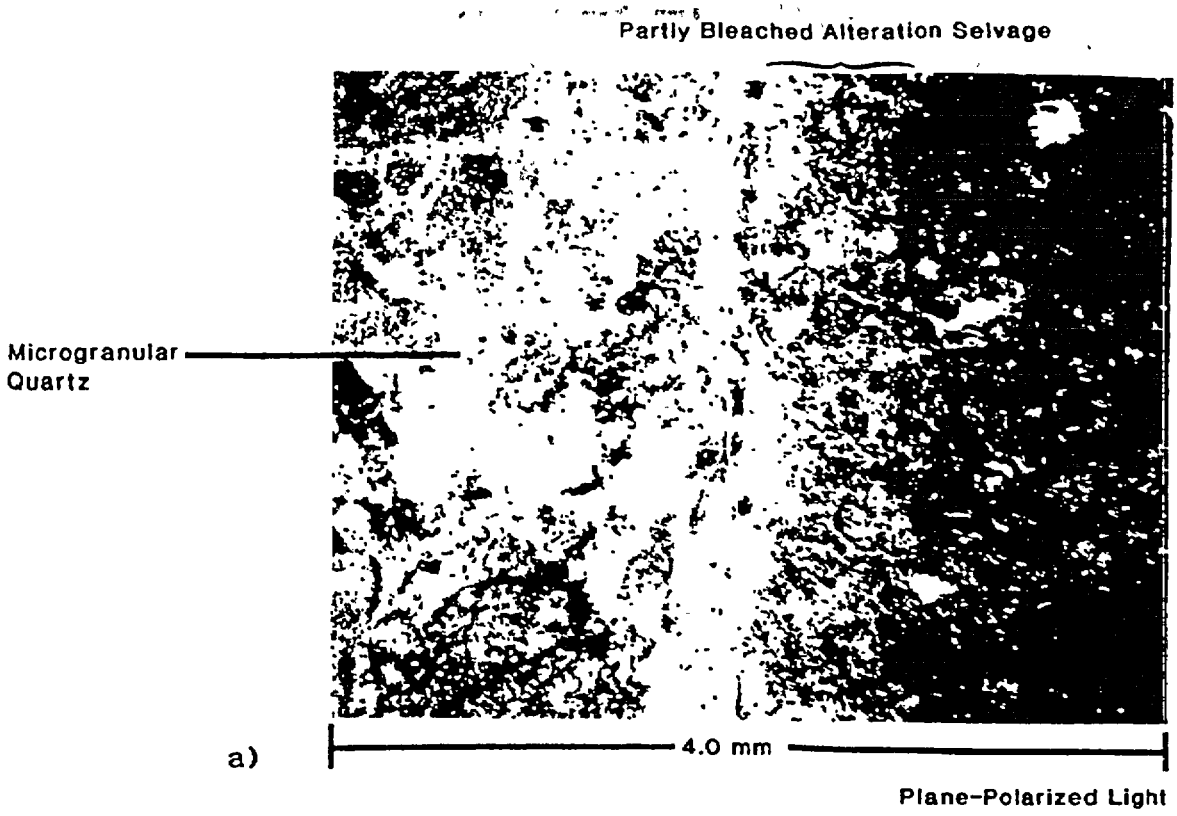
Partly Bleached Alteration Selvage
Microgranular Quartz
a)
4.0 mm
Plane-Polarized Light

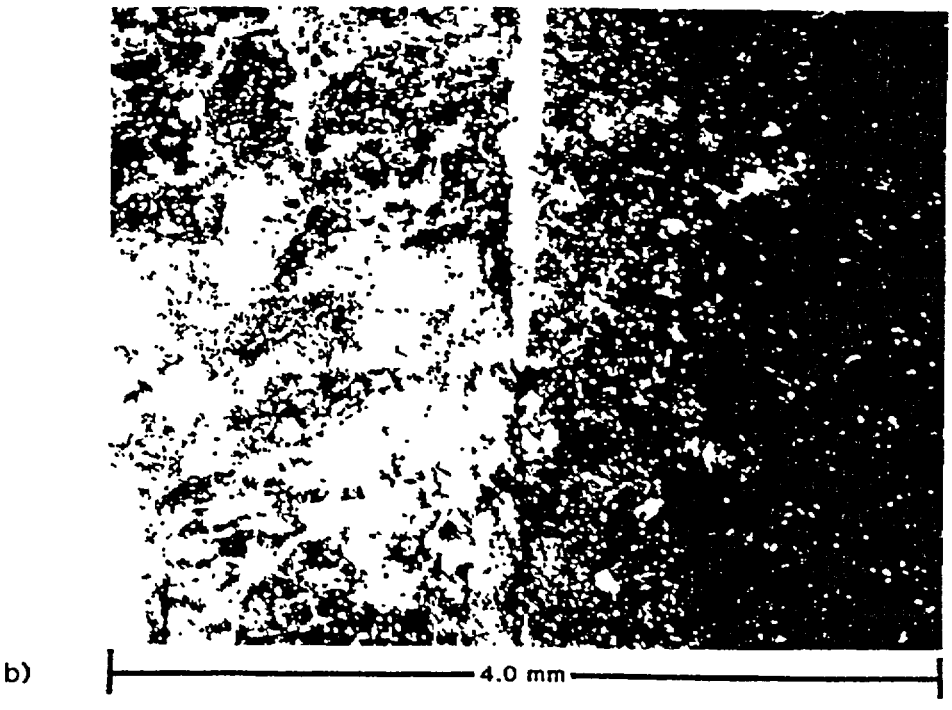
b)
4.0 mm
Crossed Nicols

Fig 17

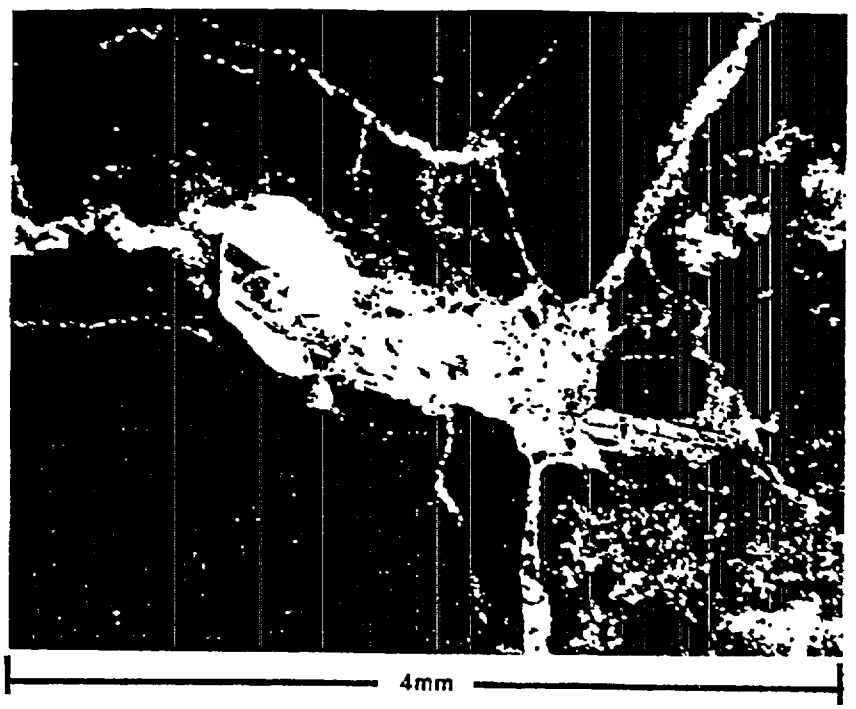

Fig 18

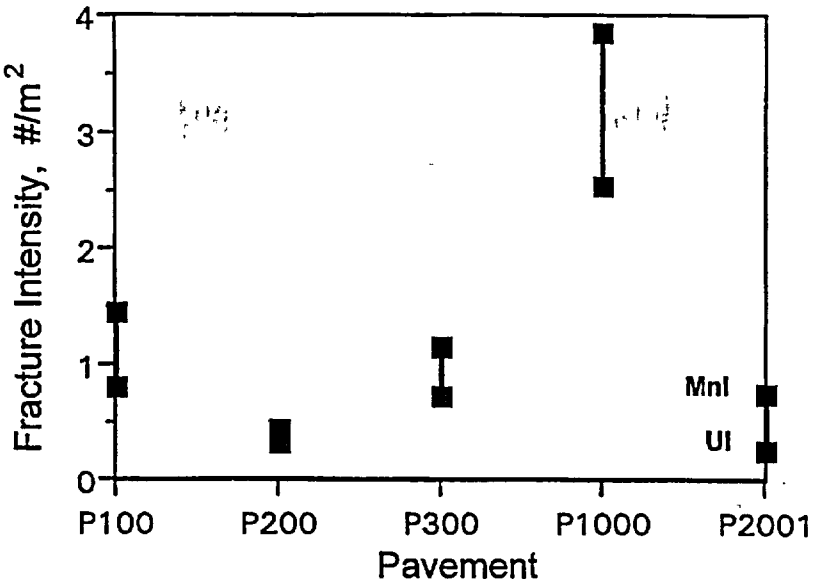
Fracture Intensity, #/m2
4
3
2
1
0
Mnl
Ul
P100
P200
P300
P1000
P2001
Pavement

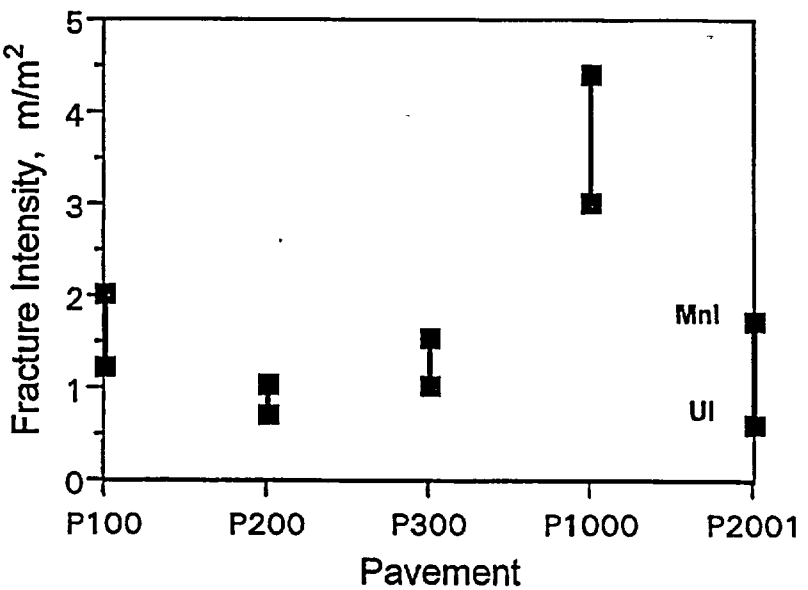
Fracture Intensity, m/m2
5
4
3
2
1
0
Mnl
Ul
P100
P200
P300
P1000
P2001
Pavement

Fig 19

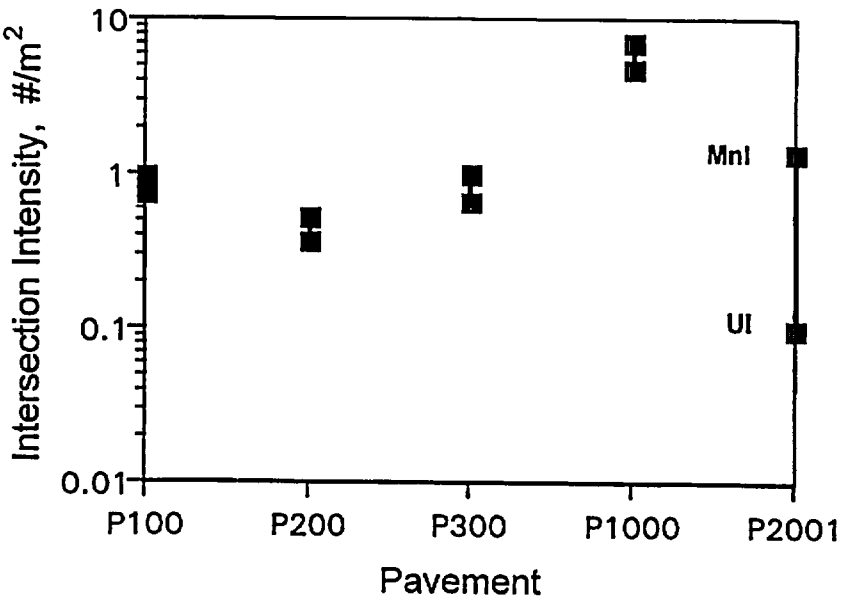
Intersection Intensity, #/m2
10
1
0.1
0.01
MnI
UI
P100
P200
P300
P1000
P2001
Pavement

Fig 20

U.S. DEPARTMENT OF THE INTERIOR
U.S. GEOLOGICAL SURVEY

Prepared in Cooperation with the
U.S. Department of Energy

PLATE 1.

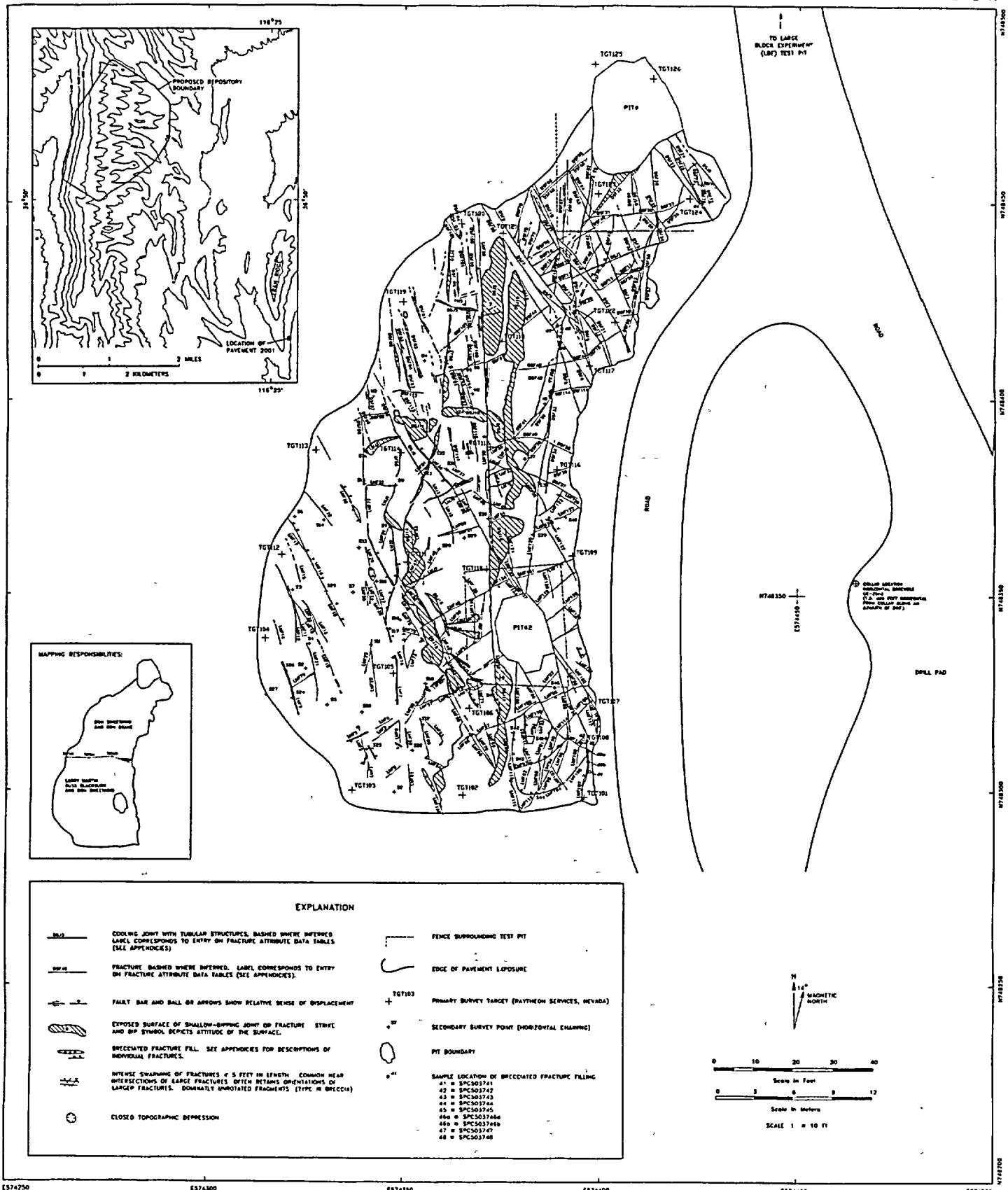

EXPLANATION

- COOLING JOINT WITH TUBULAR STRUCTURES, DASHED WHERE INFERRED. LABEL CORRESPONDS TO ENTRY ON FRACTURE ATTRIBUTE DATA TABLES (SEE APPENDICES)
- FRACTURE DASHED WHERE INFERRED. LABEL CORRESPONDS TO ENTRY ON FRACTURE ATTRIBUTE DATA TABLES (SEE APPENDICES).
- FAULT BAR AND BALL OR ARROWS SHOW RELATIVE SENSE OF DISPLACEMENT
- EXPOSED SURFACE OF SHALLOW-DIPPING JOINT OR FRACTURE. STRIKE AND DIP SYMBOL DEPICTS ATTITUDE OF THE SURFACE.
- BRECCIATED FRACTURE FILL. SEE APPENDICES FOR DESCRIPTIONS OF INDIVIDUAL FRACTURES.
- INTENSE SWARMING OF FRACTURES < 5 FEET IN LENGTH. COMMON NEAR INTERSECTIONS OF LARGE FRACTURES. OFTEN RETAINS ORIENTATIONS OF LARGER FRACTURES. DOMINATLY UNROTATED FRAGMENTS (TYPE IN BRECCIA)
- CLOSED TOPOGRAPHIC DEPRESSION
- FENCE SURROUNDING TEST PIT
- EDGE OF PAVEMENT EXPOSURE
- TGT103 PRIMARY SURVEY TARGET (RAYTHEON SERVICES, NEVADA)
- SECONDARY SURVEY POINT (HORIZONTAL ENHANCING)
- PIT BOUNDARY
- SAMPLE LOCATION OF BRECCIATED FRACTURE FILLING
  - 41 = SPC503741
  - 42 = SPC503742
  - 43 = SPC503743
  - 44 = SPC503744
  - 45 = SPC503745
  - 46a = SPC503746a
  - 46b = SPC503746b
  - 47 = SPC503747
  - 48 = SPC503748

N 14° MAGNETIC NORTH

0 10 20 30 40
Scale in Feet
0 3 6 9 12
Scale in Meters
SCALE 1 = 10 ft

Raytheon data for some areas provided by Raytheon Services, Nevada.
Nevada State Plane Coordinates in feet.

FRACTURE TRACE MAP, PAVEMENT P2001, FRAN RIDGE, YUCCA MOUNTAIN, NEVADA

Participant USGS
Database - USGS
Prepared - 2-DEC-94:14:59:26

Yucca Mountain Site Characterization Project
Planning and Control System (PACS)
Participant Planning Sheet (PSA03)

Inc. Dollars in Thousands (Unesc.)

P&S Account - 1.2.3.2.2.1.2 USGS J. Timothy Sullivan 12/8/94

P&S Account Title - Structural Features within the Site Area

PWBS Element Number - 1.2.3.2.2.1.2

PWBS Element Title - Structural Features within the Site Area

Baseline Start - 03-oct-1994
Baseline Finish - 28-jun-1996

QA - YES

	Fiscal Year Distribution											
	Prior	FY1995	FY1996	FY1997	FY1998	FY1999	FY2000	FY2001	FY2002	FY2003	FY2004	Future	At Complete
Annual Budget	0	2887	2418	0	0	0	0	0	0	0	0	0	5305

Statement of Work

Direct observation of geologic features in the field and recording of data on aerial photographs and in notebooks. Transfer field data onto a stable topographic base using a mechanical analytical plotter in the photogrammetry laboratory. Collect additional field data with assistance of completed map. Measure and analyze fracture characteristics (abundance, orientation, aperture, roughness, fracture-fill minerals) from uncleared outcrops to furnish the bulk of fracture data for this activity. Clear surficial material on pavements, map and photograph fractures, and record fracture characteristics (density, orientations, apertures, roughness, trace length, spatial distribution, degree of connectivity, fracture-filling minerals). Compile 2-D fracture network models from fracture trace maps and data set. Determine attitudes of fractures and faults by oriented core and paleomagnetic techniques. Integrate characterization of core fractures with surface studies. Analyze Borehole fracture by borehole video-camera and acoustic televiewer. Perform geologic mapping of the exploratory shaft facility (ESF) and drifts, including in situ fracture and geologic mapping and photogrammetric geologic mapping; perform prototype geologic experiments for studying the ESF which involve the development of methods for field data collection and photogrammetric mapping for the repository block at Yucca Mountain. Mark, survey and photograph shaft walls. Collect oriented samples. Map fracture roughness, aperture, direction of movement and lithostratigraphic features. Select and define structural and fracture domains with similar properties in exploratory shaft. Install sensors in shaft wall drillholes. Conduct VSP. Conduct laboratory analysis of core samples for seismic propagation effects.

QARD applies to this effort.

Deliverables will be reviewed and accepted in accordance with the YMSCO Procedure for acceptance of contract deliverables unless otherwise specified.

DELIVERABLES

Deliv ID	Description/Completion Criteria	Due Date
3GGF500M	LTR RPT: ENHANCEMENT OF SCOTT & BONK Criteria - This level 3 milestone will consist of a Letter Report summarizing the evaluation of the internal consistency of the 1:12,000 scale map Scott and Bonk (1984) and the data and interpretations from a photo lineament study for the central block of Yucca Mountain. This area was mapped at a scale of 1:12,000, but recent revisions in stratigraphy and the increased detail of scrutiny of stratigraphic and structural relations necessitates enhancement and possible verification of parts of the Scott and Bonk map. Data collected for this investigation will consist of (1) evaulation of map and cross section relations based on geometric consistency and compatibility with borehole data, and (2) map of dominant structures (1:12,000) and evaluation of lineaments identified on areal photographs and remote sensing images. This activity does not evaluate the stratigraphy and will provide only limited data on the amounts of separation on selected faults.;;This level 3 milestone will be met when a publication package segment has been submitted to the TPO in compliance with YMP-USGS-QMP-3.04 and the TPO has forwarded the information to DOE-YMSCO for concurrence and USGS Director's Office for approval.;;TEXT WAS TRUNCATED.	30-jun-1995

Inc. Dollars in Thousands (Unesc.)

0G32212 Structural Features within the Site Area (continued)

DELIVERABLES

Deliv ID	Description/Completion Criteria	Due Date
3GGF510M	LTR RPT: GEOMETRY & CONTINUITY - SUNDANCE FAULT Criteria - This Level 3 milestone will provide an analysis report of the Sundance Fault within the study area that includes a map, conclusions on the character of the fault, and recommendations for future study.;;This milestone will be met when a Letter Report package segment has been submitted to the TPO in compliance with YMP-USGS-QMP-3.04 and the TPO has forwarded the information to DOE-YMSCO for concurrence and USGS Director's Office for approval.	31-aug-1995
3GGF530M	RPT: STRUCT/STRAT OF THE ESF - NORTH RAMP Criteria - This Level 3 report will provide full-periphery maps, generalized cross-section of the North Ramp, and discussion of significant geologic and structural features. The report will provide an assessment of mapping techniques applied in study, and recommendations for future ESF mapping study technique. February 1, 1995 milestone will include data collected through November 1, 1994. Mapping data will be submitted to LRC and available upon request to the project office and the participants. This milestone will be met when a publication package segment has been submitted to the TPO in compliance with YMP-USGS-QMP-3.04 and the TPO has forwarded the information to DOE-YMSCO for concurrence and USGS Director's Office for approval.	31-jan-1995
3GGF540M	RPT: STRUCT/STRAT OF THE ESF - NORTH RAMP Criteria - This Level 3 report will provide full-periphery maps, updated generalized cross-section of the North Ramp, and discussion of significant geologic and structural features. The report will provide an assessment of mapping techniques applied in study, and recommendations for future ESF mappingstudy technique. The milestone will include data collected through April 1, 1995. Mapping data will also be submitted to LRC and available upon request to the project office and the pahrticipants. This milestone will be met when a publication package segment has been submitted to the TPO in compliance with YMP-USGS-QMP-3.04 and the TPO has forwarded the information to DOE-YMSCO for concurrence and USGS Director's Office for approval.	30-jun-1995
3GGF550M	LRT RPT: VERT CONT/FRAC CHAR PAINTBRUSH GRP Criteria - This level 3 Milestone will be met with a Letter Report containing maps, tabular fracture attributes, stereographic projections and histograms, overlays, a computer file of the fracture data, and a evaluation of significant textural features in the thin sections. The report will include the results and conclusions of the study and recommendations for further investigations.;;This milestone will be met when a Letter Report package has been submitted to the TPO in compliance with YMP-USGS-QMP-3.04 and the TPO has forwarded the information to DOE-YMSCO for concurrence and USGS Director's Office for approval.	31-aug-1995
3GGF560M	LETTER REPORT: PAVEMENT MAPPING AT FRAN RIDGE Criteria - This milestone will be met by a Letter Report, containing maps, data, conclusions, and recommendations for further work. Produced by detailed mapping of fractures and tabulation of fracture attributes at the Fran Ridge Pavement. The Letter Report shall have been completed in compliance with YMP-QMP-3.04.;;This milestone will be met when a publication package segment has been submitted to the	30-jun-1995

0G32212 Structural Features within the Site Area (continued)

DELIVERABLES

Deliv ID	Description/Completion Criteria	Due Date
	TPO in compliance with YMP-USGS-QMP-3.04 and the TPO has forwarded the information to DOE-YMSCO for concurrence and USGS Director's Office for approval.	

Approvals

Technical Reviewer 12/8/94 Date

QA Reviewer 12/8/94 Date